Electrochemical degradation and chemical aging of carbon felt electrodes in all-vanadium redox flow batteries

Inaugural-Dissertation
to obtain the academic degree
Doctor rerum naturalium (Dr. rer. nat.)

submitted to the Department of Biology, Chemistry and Pharmacy
of Freie Universität Berlin

by

Igor Derr

from Sosnowoborsk

Berlin, 2017

I hereby declare that the thesis submitted is my own unaided work. All direct or indirect sources used are acknowledged as references.

Igor Derr Berlin, 23.03.2017

Supervisor: Prof. Dr. Christina Roth

Second examiner: Prof. Dr. Peter Strasser

Date of the defense: 08.05.2017

Zusammenfassung

Vanadium Redox Flow Batterien sind eine vielversprechende Technologie für großtechnische Anwendungen. Einer der wichtigsten Vorteile ist die lange Lebensdauer des Systems. In der vorliegenden Dissertation wurde die dynamische und statische Degradation von Kohlenstoffvlieselektroden in Vanadium Redox Flow Batterien untersucht. Die Degradation äußert sich immer in einem Leistungsverlust des Systems. Dabei kamen sowohl elektrochemische als auch spektroskopische Messmethoden zum Einsatz. Drei unterschiedliche Degradationsprotokolle wurden entwickelt um sowohl dynamische (elektrochemische) Degradation als auch statische (chemische) Alterung reproduzierbar zu induzieren. Chemische Alterung bei Kontakt mit wässriger Schwefelsäure und gängigem Vanadiumelektrolyt trat immer auf und äußerte sich in einem Leistungseinbruch der negativen Halbzelle. Durch eine Erhöhung der Temperatur konnte eine höhere Alterungsgeschwindigkeit beobachtet werden, was auf eine chemische Reaktion schließen ließ. Die Auftragung der Alterungsgeschwindigkeit gegen die Zeit wies zwei Bereiche mit unterschiedlichen Geschwindigkeitskonstanten auf. Es wurde festgestellt, dass die ersten 5 Tage stets eine höhere Alterungsgeschwindigkeit zeigten als die darauffolgenden 6-24 Tage.

Die elektrochemische Degradation der Kohlenstoffelektroden wurde bei allen durchgeführten Zyklierungsexperimenten beobachtet. Die Degradationsgeschwindigkeit hing stark von den gewählten experimentellen Parametern, wie z.B. der maximalen Zellspannung (Abbruchspannung) und der Gesamtdauer des Versuchs, ab. Dabei wurde mittels elektrochemischer Impedanzspektroskopie und UI-Polarisationskurven festgestellt, dass eine höhere Abbruchspannung zu höheren Degradationsgeschwindigkeiten führt. Dabei war die Abhängigkeit der elektrochemischen Degradation von der Versuchsdauer stärker ausgeprägt im Vergleich zur Abhängigkeit von der Gesamtanzahl an Zyklen, die gemessen wurden. Dies lässt darauf schließen, dass ein Großteil der auftretenden Verluste durch chemische Alterung verursacht wurde. Alle Zyklierungsversuche wiesen ebenfalls zwei unterschiedliche Geschwindigkeiten bezüglich der Degradation auf, vergleichbar mit den Messungen der chemischen Alterung. Der Gesamtleistungseinbruch für jeweils 50 Zyklen lag, je nach Zyklierungsparametern, zwischen 60 %-75 %. Dieser Gesamtleistungseinbruch wurde in drei Hauptbestandteile unterteilt. Dabei konnten 10 %-55 % der Gesamtverluste auf die Degradation der Elektroden zurückgeführt werden. Der verbleibende Anteil konnte auf

Ohm‘sche Verluste und elektrolytabhängige Verluste zurückgeführt werden. Elektrolyt-bezogene Verluste sind z.B. die Selbstentladung, die durch das Wandern von Vanadium durch die Membran verursacht wird. Ein Ungleichgewicht zwischen den Halbzellen kann auch durch diverse parasitäre Reaktionen, wie die Wasserstoffevolution aus dem Elektrolyt und die CO_2-Entwicklung des Vlieses, hervorgerufen werden.

XPS-Messungen zeigten, dass die Kohlenstoffelektroden in beiden Halbzellen oxidieren. Diese Beobachtung ist signifikant, da das Vlies der negativen Halbzelle bei Potentialen unterhalb von 0.21 vs. NHE nicht oxidieren sollte, weil dies das Standardpotential für die C/CO_2 Reaktion ist. Der Gesamtanteil an Sauerstoffgruppen nahm laut XPS auf beiden Elektroden zu. Die Leistung der positiven Halbzelle wurde dadurch nur wenig beeinflusst, während die negative Halbzelle einen deutlichen Leistungseinbruch verzeichnete. Daraus folgte die Annahme, dass die negative Halbzellreaktion eine intramolekulare Reaktion ist, während die positive Halbzellreaktion ein reiner Elektronentransfer ist und daher keine Abhängigkeit von den Oberflächengruppen des Kohlenstoffs aufweist. Daher müsste die negative Halbzelle viel empfindlicher auf die Änderung der Oberflächengruppen reagieren. Um die unvermeidliche Oxidation der Kohlenstoffelektrode in der negativen Halbzelle zu verhindern wurde diese mit Bismut modifiziert. Eine Stabilisierung der Bismutpartikel auf dem Kohlenstoffvlies konnte jedoch nicht erreicht werden, stattdessen fand eine ständige Auflösung und sukzessive Abscheidung des Bismuts während des Zyklierens statt. Nichtsdestotrotz konnte der Leistungseinbruch, der durch die Oxidation der Elektrode in der negativen Halbzelle verursacht wurde, verhindert werden.

Abstract

All-vanadium redox flow batteries are a promising energy storage system for large scale applications. One of the most important advantage is supposed to be the life time of the system. In this thesis the dynamic and static degradation of carbon felt electrodes in all-vanadium redox flow batteries was investigated with electrochemical as well as spectroscopic techniques. The degradation expressed itself in form of an overall performance loss of the system. Three different degradation protocols were developed in order to induce reproducible electrochemical degradation (dynamic) and chemical aging (static). Chemical aging of the investigated carbon felt electrodes took place by mere contact with pure aqueous sulfuric acid as well as in standard vanadium electrolyte and was inevitable. Higher temperatures led to higher rates of degradation indicating a chemical reaction. The rate of degradation was time dependent and exhibited two regions with different rate constants. The first 5 days always showed a faster rate of degradation compared to the remaining 6-24 days.

Electrochemical degradation of the electrodes was found during all cycling experiments. The rate of degradation strongly depended on the cycling conditions such as the maximum cut-off voltage and the total time of the experiment. Higher cut-off voltages led to higher degradation of the electrode as determined by UI polarization curves and electrochemical impedance spectroscopy. In all experiments electrochemical degradation was more affected by the total duration of the experiment than the amount of cycles that were performed indicating a strong influence of chemical aging during the cycling experiments. All experiments exhibited two different rates of degradation, which were time dependent similar to the results from the chemical aging experiments. The overall performance loss for 50 cycles was estimated between 60 %-75 % depending on the cycling conditions. The overall losses were separated into three main contributions: The electrode degradation was accounted for 10 %-55 % of the overall performance loss, while the remaining losses were assigned to ohmic losses and to the imbalance of the electrolyte. The latter is caused by the cross-over of vanadium through the membrane as well as parasitic reactions, e.g. the hydrogen evolution reaction from the electrolyte or the CO_2 evolution from the felt.

XPS revealed an oxidation of the carbon felt electrodes after cycling in both half-cells. This was unexpected because the felt in the negative half-cell never exceeded 0.21 V vs. NHE and therefore it should not oxidize, since this is the standard potential for the C/CO_2 reaction. The overall amount of oxygen functional groups increased on both electrodes. However, the oxygen functional groups had a much stronger impact on the performance of the negative half-cell. This led us to the conclusion that the negative half-cell reaction follows an inner-sphere mechanism, while the positive half-cell reaction is assumed to follow an outer-sphere mechanism. Consequently this means that the negative half-cell is much more sensitive towards changes of the electrode surface. In order to prevent the oxidation of the negative half-cell, the electrode was modified with bismuth. The stabilization of the bismuth particles on the electrode could not be achieved, instead a dissolution followed by re-deposition during the cycling experiments was found. However, the modification successfully prevented the performance loss that was observed due to the oxidation of the electrode in the negative half-cell in previous experiments with pristine carbon felt electrodes.

List of Publications

Publications included in this thesis

I. Derr, M. Bruns, J. Langner, A. Fetyan, J. Melke, C. Roth, Degradation of all-vanadium redox flow batteries (VRFB) investigated by electrochemical impedance and X-ray photoelectron spectroscopy: Part 2 electrochemical degradation, J. Power Sources 325 (2016) 351–359, doi:10.1016/j.jpowsour.2016.06.040.

I. Derr, A. Fetyan, K. Schutjajew, C. Roth, Electrochemical analysis of the performance loss in all vanadium redox flow batteries using different cut-off voltages, Electrochim. Acta 224 (2017) 9–16, doi:10.1016/j.electacta.2016.12.043.

I. Derr, D. Przyrembel, J. Langner, J. Melke, M. Weinelt, C. Roth, Electroless chemical aging of all-Vanadium Redox Flow batteries (VRFB) investigated by Electrochemical Impedance and X-ray Photoelectron Spectroscopy, Electrochim. Acta (n.d.) (submitted on 03.02.17, in review).

Publications not included in this thesis

C. Brieger, J. Melke, N. van der Bosch, U. Reinholz, H. Riesemeier, A. Guilherme Buzanich, M.K. Kayarkatte, I. Derr, A. Schökel, C. Roth, A combined in-situ XAS–DRIFTS study unraveling adsorbate induced changes on the Pt nanoparticle structure, J. Catal. 339 (2016) 57–67, doi:10.1016/j.jcat.2016.03.034.

A. Fetyan, I. Derr, M.K. Kayarkatte, J. Langner, D. Bernsmeier, R. Kraehnert, C. Roth, Electrospun Carbon Nanofibers as Alternative Electrode Materials for Vanadium Redox Flow Batteries, ChemElectroChem 2 (2015) 2055–2060, doi:10.1002/celc.201500284.

G.A. El-Nagar, I. Derr, A. Fetyan, C. Roth, One-pot synthesis of a high performance chitosan-nickel oxyhydroxide nanocomposite for glucose fuel cell and electro-sensing applications, Appl. Catal. B Environ. 204 (2017) 185–199, doi:10.1016/j.apcatb.2016.11.031.

Abbreviations and Acronyms

AC	Alternating current
BDD	Boron doped diamond
BET	Brunauer–Emmett–Teller theory
C	Capacitor
CE	Current efficiency
CF	Carbon felt
CPE	Constant phase element
CTR	Charge transfer resistance
CV	Cyclic voltammetry
DLC	Double layer capacitance
DOS	Density of states
ECSA	Electrochemically active surface area
EDX	Energy dispersive X-ray spectroscopy
EE	Energy efficiency
EIS	Electrochemical impedance spectroscopy
GC	Glassy carbon
GDL	Gas diffusion layer
HER	Hydrogen evolution reaction
L	Inductor
NHE	Normal hydrogen electrode
OCP	Open circuit potential
OCV	Open circuit voltage
PAN	Polyacrylonitrile
PHES	Pumped hydroelectric energy storage
R_{ct}	Charge transfer resistance
RFB	Redox flow battery
RHE	Reversible hydrogen electrode
Ru	Contact resistance
SEI	Solid electrolyte interface

SEM	Scanning electron microscopy
SOC	State of charge
UHV	Ultra-high vacuum
VE	Voltage efficiency
VRFB	Vanadium redox flow battery
W	Warburg element
XPS	X-ray photoelectron spectroscopy
XRD	X-ray diffraction

Table of Contents

1. Introduction

At the beginning of the 21st century renewable energies are on the uprise. In Germany the proportion of renewable energy increased by 25 % to a total of 31 % in the year of 2015. For the years 2035 and 2050 the German government announced goals of 55 % and 80 % of energy generated from renewables, respectively [1]. With an increasing total percentage of renewable energies it is inevitable to store the energy in one way or another in order to maintain the supply during night hours. There are several ways to store electrical energy. Two examples for low capacity storages with high output energy and very fast response time are super-capacitors and flywheels. In the medium capacity storage range we can use electrochemical storage systems like the Li-ion battery, electrolyzer/fuel-cell-systems and redox flow batteries (RFB). For higher capacity storage ranges pumped hydroelectric energy storage (PHES) systems and also redox flow battery systems can be used [2–6]. All the mentioned systems will be needed in order to achieve 80 % energy supply from renewables, because they differ in response time and application limitations set by the climate and the environment. Also the costs of a system are always a critical factor. One of the most promising systems for the medium and high capacity storage range is the RFB. For a medium capacity storage range the Li-ion battery is cheaper in terms of $/kWh compared to RFB, but it becomes much more expensive if the life-time of both systems is considered ($/kWh/cycle) [2–5]. For high capacity storage systems the PHES is by far the cheapest, but it has a very slow response time and it needs specific environmental conditions, which limit its application. The most important advantages of the RFB are its flexibility towards the capacity/power ratio (similar to fuel-cells) and its long life-time, which is supposed to be 10,000 cycles or at least 10 years [2–5]. The life-time is expected to be very high, because no phase transitions take place during the charge/discharge process and the applied current densities are rather low compared to fuel-cells or Li-ion batteries. Low current densities are supposed to reduce the electrode degradation and parasitic reactions, which might be triggered by mass-transport limitations. In the past years a lot of effort was made to develop high surface electrodes by adding e.g. carbon black or carbon nanotubes to the carbon felt electrodes in order to increase the performance of the electrodes [7–17]. But only little effort was made to investigate the degradation of the carbon felts [18–21]. The manufacturers of VRFB systems promise life-times of 10 years and more. However,

according to the literature only little is known about the degradation mechanisms of the electrodes and the performance losses that are linked to them. The durability of the system is considered as one of its major advantages compared to other electrochemical storage systems. Therefore, the degradation of the electrodes needs to be investigated and understood in order to be prevented.

1.1. Redox flow batteries

Similar to fuel-cells the energy in a RFB can be stored outside of the electrochemical converter in two separate electrolyte tanks or it can also be stored in the electrochemical converter in the form of electro-deposited metal species similar to a Li-ion battery. In this thesis we will focus on a system, which stores the energy in two separate tanks. The volume of the tanks and the concentration of the electro-active species determine the capacity of the system. The power output can be tailored by varying the size and the amount of cells and cell-stacks as well as the applied current densities during operation. Different organic and inorganic electroactive species have been tested over the years [4]. The most prominent are the Fe/Cr system and the all-vanadium system. The Fe/Cr systems have been developed and used by the NASA in 1970-1980. Even though the costs of the Fe/Cr systems were low, they had the disadvantage of cross-contamination and poisoning because of the different elements in each half-cell [5]. The all-vanadium redox flow battery (VRFB) system was developed by Skyllas-Kazacos in the 1980s [22]. By using only one element as the electro-active species the poisoning from cross-contamination was prevented.

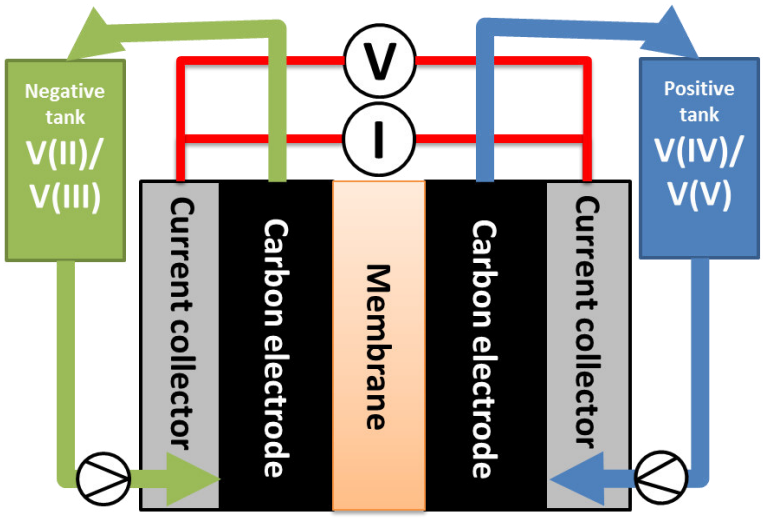

Figure 1: Schematic representation of an all-vanadium redox flow battery.

Introduction

The simplest VRFB system is shown in Figure 1. It consists of two electrolyte tanks, two pumps and one electrochemical converter (cell). The Cell consists of current collectors, electrodes, a separator and several gaskets. Broadly used materials for current collector plates are graphite, conductive polymer or glassy carbon. Carbon felts and carbon paper are used as electrodes. Different cation exchange membranes, anion exchange membranes or frits are used as separators. Several gasket materials like Viton, Teflon and other acid resistant polymers are employed in small scale systems.

During the discharge process the electrolytes are pressed through the carbon felt electrodes in both half-cells. Meanwhile the V(II) in the negative side is oxidized and the V(V) in the positive side is reduced. H_3O^+-ions are exchanged between the half-cells through the membrane in order to enable a current flow. The reaction equations of the VRFB are given in Equation 1 and Equation 2

Negative half-cell:

$E_0 = -0.26\,V\ vs.RHE$

$$V^{3+} + e^- \overset{charge\rightarrow}{\longleftrightarrow} V^{2+} \qquad \textbf{Equation 1}$$

Positive half-cell:

$E_0 = 1.0\,V\ vs.RHE$

$$VO^{2+} + 3\,H_2O \overset{charge\rightarrow}{\longleftrightarrow} e^- + VO_2^+ + 2\,H_3O^+ \qquad \textbf{Equation 2}$$

The electroactive species in a VRFB are V(II) and V(III) in the negative half-cell and V(IV) and V(V) are in the positive half-cell. The V(II) and V(III) species appear as solvated ions even in higher concentrated electrolyte solutions. The V(IV) and V(V) on the other hand are suspected to form oxides, dimers and complexes with sulfate [23,24]. In addition to 1-2 M vanadium the electrolyte also contains 2-5 M sulfuric acid and several different additives e.g. phosphoric acid, which are supposed to prevent the precipitation of the dissolved vanadium species (especially V(V)) at higher concentrations. The mechanism that was proposed for the positive half-cell is considered to be more complicated compared to the negative half-cell, because it involves a reaction with water [11]. However, the mechanism has not been verified by experiment so far. Also the nature of the half-cell reactions is not completely understood yet. We and Fink et al. [25] suggested an outer-sphere mechanism for the positive half-cell. In an outer-sphere mechanism the electron is passed from the electrode through the ligand-sphere to the metal atom as illustrated in Figure 2.

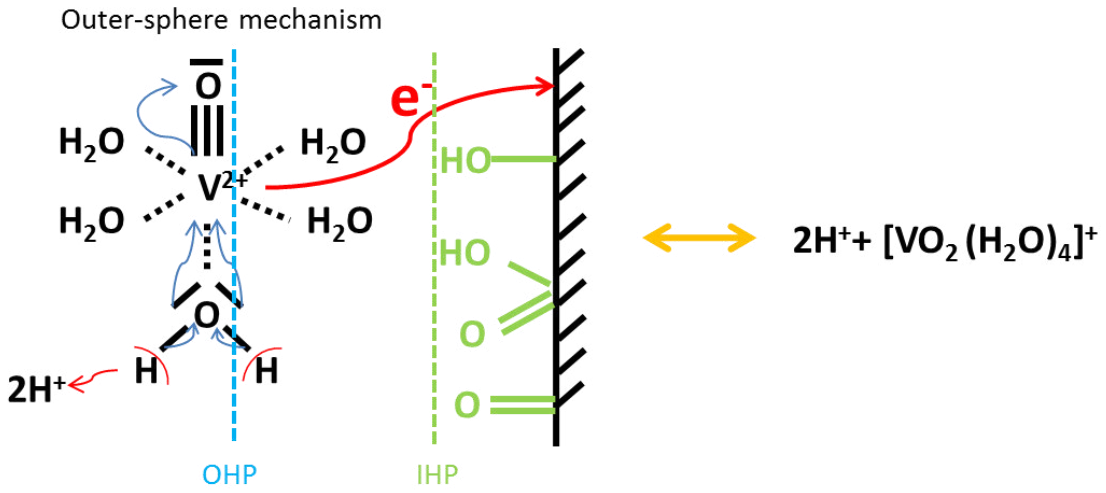

Figure 2: Schematic of a possible electron transfer route for an outer-sphere mechanism [V(IV) →V(V)]. OHP: outer Helmholtz plane, IHP: inner Helmholtz plane

The electron transfer is considered to be slower compared to the inner-sphere mechanism, where the electron is passed from the electrode over a mediator to the metal atom. In the inner-sphere mechanism the mediator is directly involved in the reaction [26–31]. In the case of an electrochemical reaction this mediator can be a surface functional group on the carbon electrode, as is shown in Figure 3, or a metal center of a catalyst cluster. This functional group can act as an adsorption site or even form a bond with the reactant in order to pass the electron.

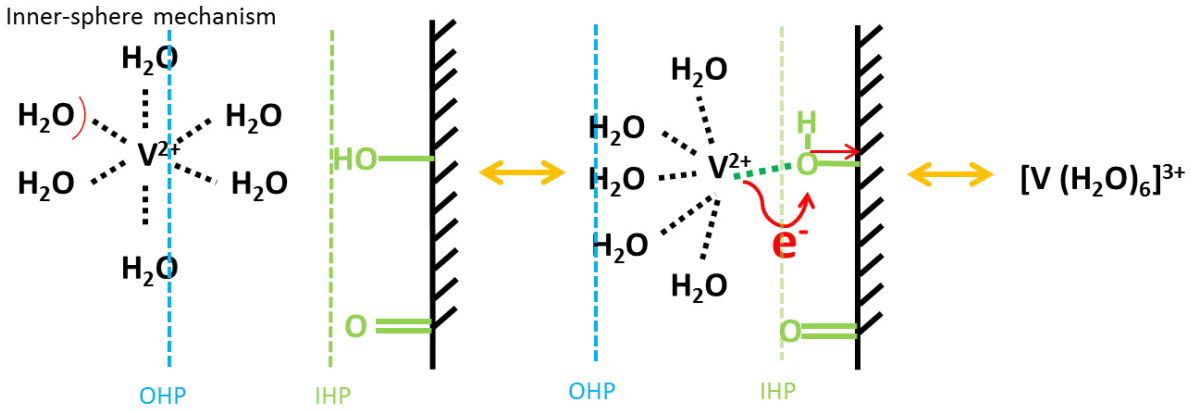

Figure 3: Schematic of a possible electron transfer route for an inner-sphere mechanism [V(II) →V(III)] . OHP: outer Helmholtz plane, IHP: inner Helmholtz plane

In contrast to that, an outer-sphere mechanism does not depend on specific active sites and the electron can be tunneled over a distance of up to 100 nm [31]. However, the electron transfer is only one of the processes that are necessary for a reaction to proceed smoothly.

An inner-sphere reaction can be rate limited by an adsorption step or a chemical reaction step. Therefore, the overall reaction rate of both mechanisms can be very similar, because the individual rate determining steps in each case can be different. In this work, we tried to differentiate between inner-sphere and outer-sphere mechanism by comparing the charge transfer resistances (kinetic properties) for different compositions and concentrations of oxygen functional groups on the carbon surface (physical properties).

With respect to the system design, two of the most popular cell designs are the so called flow-by design and the flow-through design. The flow-by design is very similar to a fuel-cell. Carbon paper or Gas diffusion layers (GDL) with several µm of thickness are used as the electrodes in both half-cells. The membrane can be e.g. a Nafion 117^{TM} by DuPont. The electrolyte is supplied through a flow-field that is implemented in the bipolar plates.

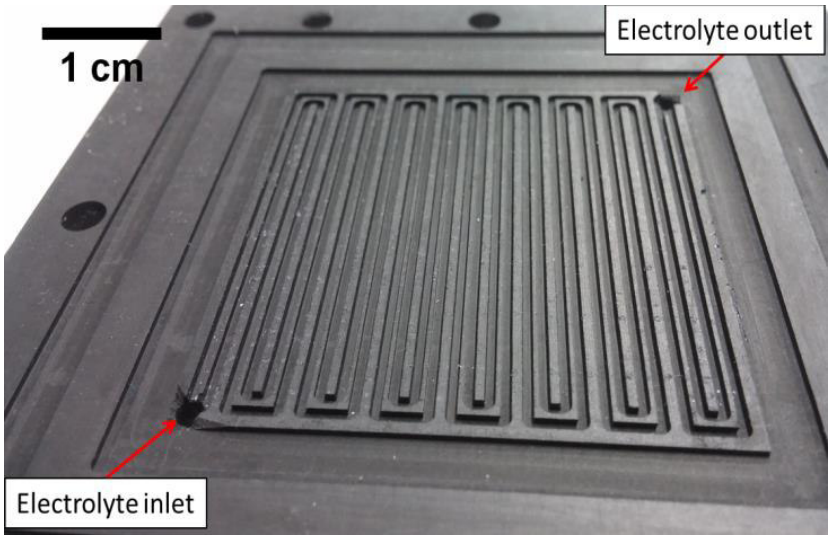

Figure 4: Flow-by geometry bipolar plate with a serpentine flow-field.

The serpentine pattern in Figure 4 is a popular example for flow-field geometries. From the engineering point of view the most difficult challenge is the flow-field design and the sealing of the cell-stacks. The flow-field determines the electrolyte distribution and therefore also the current/voltage distribution, which is crucial for larger cells and cell-stacks [32,33].

However, in this thesis we will focus on the more simple flow-through design, which is predominantly used in industry; an example of which is shown in Figure 5.

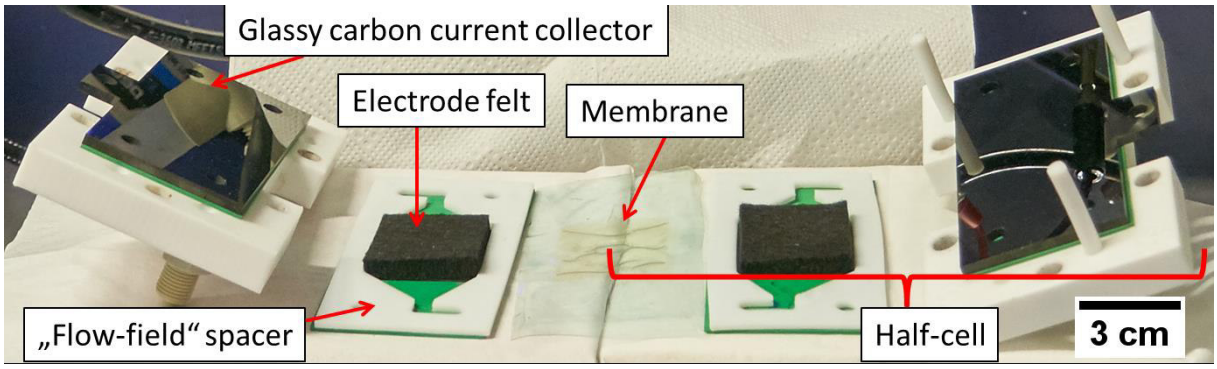

Figure 5: Flow-through cell with 6 mm thick carbon felt electrodes.

In a flow-through cell carbon felt electrodes with thicknesses of up to 6 mm and more are used. The separator material remains Nafion or similar cation or anion exchange membranes. The electrolyte is supplied by pressing the solution through the electrode felt. The performance of the cell strongly depends on the compression degree of the felt. Compression degrees between 20 %-50 % are used for different purposes [34,35]. With an increasing compression of the electrode felt the pressure drop increases [36]. This needs to be compensated by a higher pump rate in order to maintain sufficient mass-transport through the felt. A higher pump rate leads to a higher energy demand, which decreases the overall efficiency of the system. On the other hand, the contact resistance decreases with higher compression, which results in a better cell performance. The best operating conditions have to be screened individually for each system. However, from the chemical point of view the electrodes and the separators are the parts of interest for both cell designs.

The most common separator is the cation exchange membrane Nafion^{TM}. The membrane is a very important part of the system, because the cross-over of vanadium leads to self-discharge of the cell and also to an imbalance of the electrolyte, which results in irreversible performance losses [37–42]. That is why a lot of effort was dedicated to develop new membranes with high permeability for supporting electrolyte species like H_3O^+ or SO_4^{2-} and low permeability for vanadium [40,41,43–47].

In a regular charge/discharge operation the cell is cycled galvanostatically in a specific voltage window. The voltage is measured between both half-cells. The discharge process is usually terminated below a cell voltage of 1 V-0.8 V and the charge process proceeds up to 1.6 V-1.9 V. The maximum and the minimum cell voltage are called “cut-off voltage”, and are

used for terminating a charge or discharge process. The cut-off voltages are chosen based on the assumption that a certain voltage would lead to a specific parasitic reaction in one of the half-cells. At a cell voltage of 1.9 V an oxidation of the carbon electrode in the positive half-cell is expected as well as the formation of hydrogen in the negative half-cell [48–51]. Therefore, lower maximum cut-off voltages such as 1.6 V are preferred, even though the performance of the cell decreases significantly at higher current densities. This is compensated by increasing the number of cells in a stack in order to achieve sufficient energy values at lower current densities. The drawback is an increase of self-discharge and the overall cost of the system.

Higher current densities require more overpotential in order to achieve higher states of charge (SOC). The utilization of the full theoretical capacity of the employed electrolyte is therefore, crucial for the cost of the system. The energy efficiency (EE) of the system decreases with increasing current density and decreasing cut-off voltage. The energy efficiency is calculated from the current efficiency (CE) and the voltage efficiency (VE) as shown below in Equation 3 to Equation 5.

$$EE = VE * CE \qquad \textbf{Equation 3}$$

$$CE = \frac{\int I_{discharge}\, dt}{\int I_{charge}\, dt} \qquad \textbf{Equation 4}$$

$$VE = \frac{\int U_{discharge}\, dt}{\int U_{charge} dt} \qquad \textbf{Equation 5}$$

The CE strongly depends on the cross-over of vanadium and the occurrence of parasitic reactions. The cross-over of vanadium solely depends on permittivity of the membrane towards vanadium species, while parasitic reactions appear due to the selectivity of the electrode. Especially at higher current densities and in mass-transport limited regimes competing reactions, such as the HER, become favored compared to vanadium. This leads to self-discharge and an imbalance of the electrolyte. The VE depends on the overpotentials, which are necessary to perform the specific half-cell reactions and the cut-off voltages. Usually reported ranges for current efficiencies are between 90 %-99 %, while the voltage

efficiencies can be as low as 50 %. Overall energy efficiencies of 60 %-75 % have been reported so far [2–6]. At this point, the energy efficiency can only be improved by increasing the VE, which means by reducing the overpotentials that are required for the specific reactions.

1.2. Carbonaceous electrode material

The electrode material in VRFBs is carbon based. Depending on the cell design, the cell can be equipped with a carbon electrode in the form of a felt with thicknesses of several mm or in the form of a paper with only a few micrometers in thickness (GDL). The carbon fibers are produced from different precursor materials e.g. rayon or polyacrylonitrile (PAN) and woven into the final 3-D porous structure. The manufacturing process itself includes several stabilization and graphitization steps of the carbon fibers. During stabilization and graphitization the fibers are heated at temperatures between 200 °C-2000 °C in nitrogen and argon atmosphere. The properties of the carbon surface vary significantly depending on the precursor and the manufacturing conditions [7]. Before using a felt in a VRFB, it often needs to be conditioned or “activated”. This is either done by heat treating the carbon felt (CF) in air atmosphere for several hours at 300 °C-600 °C, boiling it in different mixtures of concentrated acids or applying high positive potentials to oxidize the carbon surface [52–57]. The activation of the felts has two beneficial effects. The first being the removal of aliphatic residues from the manufacturing process and the second being the introduction of defects in the form of different oxygen functional groups, such as -OH, -OOH, -O- and =O (or nitrogen in case of HNO_3 acid activation) on the carbon surface. Even though the mechanisms of the reactions in both half-cells are not known yet, the oxygen functional groups were found to enhance the performance of the cell significantly [16,58–60]. One of the reasons for the enhancement is the improved wettability of the carbon fibers, which leads to a larger electrochemically active surface area (ECSA). The second beneficial effect is the increased density of electronic states (DOS) around the Fermi level and an increase of charge carrier concentration inside the material [28–30,61,62]. The catalytic properties of the functional groups towards the electrochemical conversion of the different vanadium species are still being discussed.

1.3. Overpotentials and parasitic reactions in the VRFB

The total observed overpotential consists in contributions of ohmic, reaction and mass transport overpotential losses. The most dominant overpotentials are the ohmic overpotentials, which result from the conductivity of the membrane as well as the conductivity of the electrode and the current collector plates. For cells with Nafion^{TM} 117 membrane cell resistances of 1 to 2 Ω cm^2 were reported in the literature [20,63–65]. The contact resistance of the electrode can be varied with the compression degree of the felt or by adding binder materials. With an increasing compression degree the resistivity decreases, but the pressure losses increase, because the material becomes more dense.

The second major overpotential is the reaction overpotential, which depends on the electrode material. In the VRFB, carbon is commonly used as the electrode material in both half-cells. Therefore, the reaction overpotentials depend on the surface properties of the carbon fibers. Especially the surface functional groups, such as -OH, -OOH, -O- and =O determine the activity of the fibers towards different reactions. In the literature the functional groups are assigned to a catalytic enhancement in both half-cells [28,30,66,67]. However, recent studies revealed that the reaction in the positive half-cell might follow an outer-sphere mechanism, while the reaction in the negative half-cell follows an inner-sphere mechanism [28–30,66,68]. In an outer-sphere mechanism the solvation shell does not need to be broken or stripped off before the electron transfer [31]. Therefore, an outer-sphere reaction does not require functional groups on the carbon surface, which might act as a mediator during the electron transfer. Since graphite is a hydrophobic material, it is necessary to introduce functional groups on both electrodes in order to increase wettability and maximize the ECSA. The presence of defects on a graphitic carbon surface however also increases the reaction rates of several parasitic reactions, like the oxidation of carbon to CO and CO_2 [69]. Thermodynamically, the oxidation of carbon is possible at 0.21 V vs. normal hydrogen electrode (NHE), but it is kinetically hindered and therefore, it poses a competiting reaction with V(IV)/V(V) in the positive half-cell [69,70]. In the negative half-cell the standard potential of the V(II)/VIII) reaction is -0.26 V vs. NHE, which is in the thermodynamic region of the hydrogen evolution reaction (HER). Fortunately, the overpotential towards the HER on graphitic carbon is high and the vanadium reaction is therefore the preferred reaction [48]. In Figure 6 the thermodynamic potentials of the most important reactions are shown. The

curves indicate kinetic overpotentials and possible competition between two reactions in the same potential range.

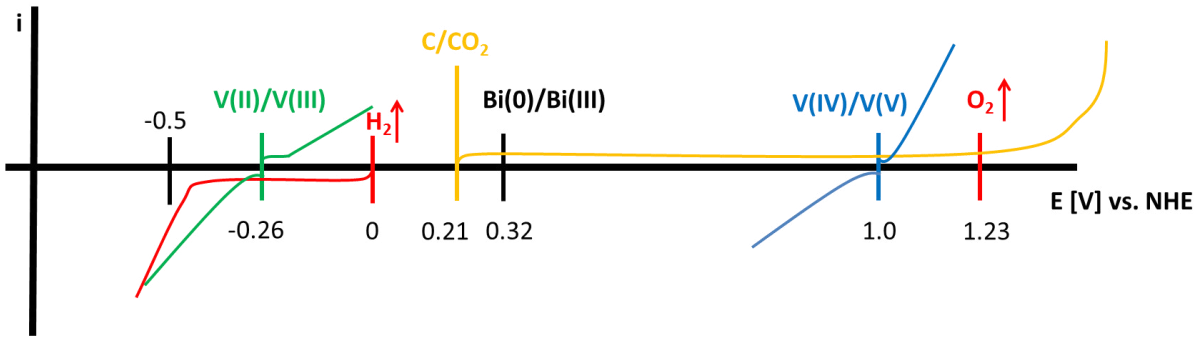

Figure 6: Theoretical standard potentials of the most important reactions in the VRFB [69–71]. The curves represent the approximate kinetic overpotentials that are required for the corresponding reaction on graphitic carbon.

But with increasing defects and operation temperature the HER becomes favored. The parasitic reactions do not only lead to an irreversible capacity loss, but also to an increase of the reaction overpotentials towards the vanadium reaction. In order to prevent parasitic reactions, the cut-off voltage of the cell is usually set between 0.9 V to 1.65 V. However, the half-cell potentials change dynamically with reactant concentration during charge/discharge. Therefore, an imbalanced electrolyte and degraded electrodes are more likely to favor parasitic reactions and to decrease the performance of the system irreversibly.

The mass-transport overpotentials are dominated by the diffusion coefficient of the vanadium ions in solution (~1 x 10^{-6} cm^2/s) and the convection, which is provided by the pumps. Increasing the pump rate results in a higher convection rate, but also leads to a higher energy consumption by the pumps. This decreases the overall efficiency of the system. For our system a convection rate of 50 mL min^{-1} was sufficient for the polarization curves that were measured at an SOC of 50 %. In Figure 7 an example of an UI-polarization curve and the corresponding power density is shown. The current did not increase upon an increase of the pump rate above 50 mL min^{-1}. At a certain pump rate the system becomes limited by the diffusion or a possible ad/desorption step of the vanadium. However, higher pump rates can be necessary at e.g. 10 % SOC or 90 % SOC in order to prevent parasitic reactions taking place during galvanostatic operation.

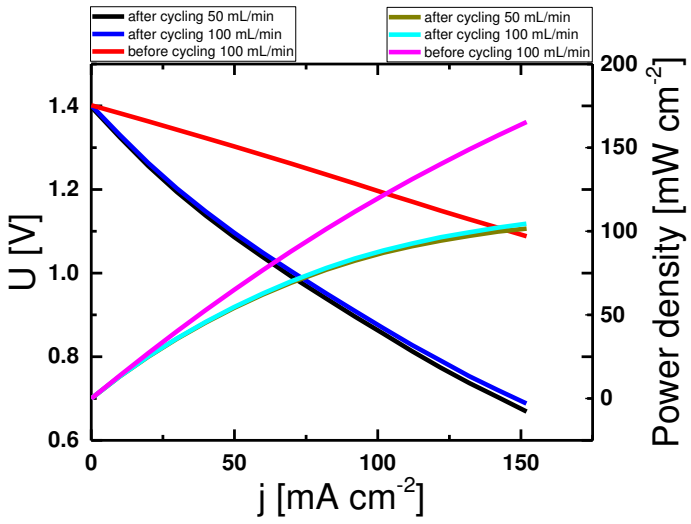

Figure 7: Example of a polarization curve and the corresponding power density before and after cycling at different pump rates.

The power density of the VRFB is low compared to fuel-cells [72] and li-ion batteries [73], which is one of the disadvantages of the system.

1.4. Thesis outline and research objective

This thesis is written in a cumulative way. The three published (and submitted) scientific manuscripts are supposed to give an insight into the results that were obtained within this Ph.D. project.

The main objectives were:

- Investigation of the overall performance losses
    - Develop reproducible degradation protocols
    - Define/measure the losses
    - Contribution separation: electrode vs. membrane vs. electrolyte overpotentials/losses
- Investigation of the electrode degradation
    - Find suitable electrochemical and physical measurement techniques
    - Investigate correlation between kinetic parameters and surface properties
- Improving the electrodes, preventing degradation by surface modification and operating parameters (cut-off)

The overall performance loss of the system ought to be separated into its individual contributions. The main focus was set on the electrodes. The objective of this work was to develop a reproducible degradation protocol for the VRFB and find suitable measurement techniques to reveal the change in performance over time as well as the change of the surface properties of the carbon electrodes.

Additional work (unpublished results) on the optimization of the electrodes by bismuth deposition will be presented in chapter 4.

2. Methods and techniques

2.1. Degradation protocols

The electrochemical degradation of the VRFB was achieved by galvanostatic cycling as well as in an accelerated cell-test with two-cells in series. The galvanostatic cycling was performed with 0.8 V-0.9 V as the cut-off voltage for the discharge process and 1.65 V-1.8 V for the charge process. The current densities were varied between 50 mA cm^{-2} to 100 mA cm^{-2}. In Figure 8 an example for one cycle with 1.8 V to 0.8 V cut-off voltages and 100 mA cm^{-2} is shown.

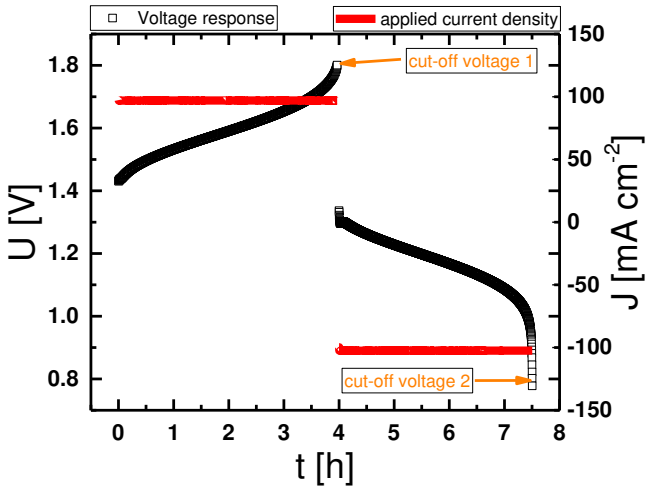

Figure 8: Exemplary cycle with 1.8 V to 0.8 V cut-off voltages and 100 mA cm^{-2}.

The cycling conditions determined the time/cycle and the overall length of the experiment. Cycling experiments of 5-30 days have been performed in order to investigate different performance reducing effects. The first experiments were performed under rather harsh conditions with a high cut-off voltage of 1.8 V and a high current density of 100 mA cm^{-2} in order to see, whether the system will show any loss of performance at all. Afterwards the cut-off voltage and the current densities were reduced to obtain more accurate results determining the origins of the performance loss.

2.2. Electrochemical measurements on 3-D carbon felt electrodes

Electrochemical measurements on bulky electrodes with 3-D pore structure and a large variety of different active sites, which lead to a non-uniform current/voltage distribution on

the surface, are difficult to perform with common techniques like cyclic voltammetry (CV). One significant problem is the mass-transport inside the felt, especially in the case of thick felts. In case of a three electrode setup, as shown in Figure 9, there is almost no convection through the felt even if a magnetic stirrer is used.

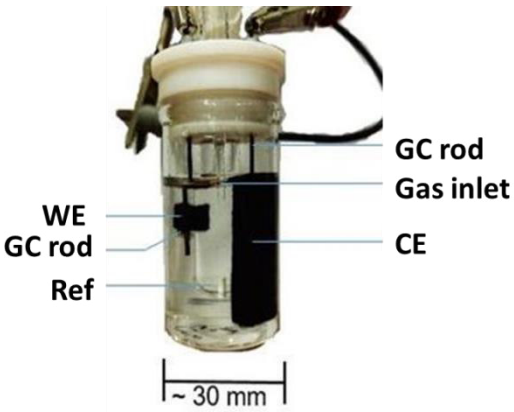

Figure 9: Three electrode setup with a carbon felt (CF) working electrode (WE), a CF counter electrode (CE) and a reference electrode (Ref). GC stands for glassy carbon.

Therefore, the volume of electrolyte inside the felt is exchanged only by diffusion during a normal CV measurement with 1 mV s^{-1}. Often reproducibility of consecutive cycles cannot be achieved, because the vanadium reactions are quasi irreversible and the initial concentration of the vanadium species inside the felt (c^{sur}) changes with every cycle and deviates from the bulk concentration (c^{bulk}). A second source of error is the uncertainty in the actual electrochemically active surface area (ECSA). Even though it is possible to calculate the physical surface area of the fibers or to measure BET (Brunauer–Emmett–Teller theory), it is not possible to estimate the exact ECSA because of the complicated correlations between the functional groups, the wettability, the DOS and the catalytic activity. One popular method to estimate the ECSA for different systems is the correlation of the double layer capacitance (DLC) to the active surface area. This method might work for polished metal electrodes with excess of free electrons at the electrode/electrolyte interface. Highly oriented graphitic structures on the other hand have a low concentration of free charge carriers inside the bulk material compared to a metal. In case of a spherical, graphitic fiber with a large surface area exposed to the electrolyte, the DLC could be limited by the free electrons in the electrode instead of the ECSA or the adsorbed ions. This would result in an underestimation of the ECSA. An overestimation of the ECSA could occur if a highly oxidized fiber is used. The functional groups enhance the DLC of the material, because they can be

polarized similar to an adsorbed ion. However, the sp^3-hybridized carbon surface insulates the electrode and decreases the ECSA. If we now take into account that the concentration of functional groups may change dynamically upon each charge and discharge cycle, the estimation of the ECSA by DLC measurements becomes very inaccurate.

The uncertainty in the ECSA and the reactant concentration at the electrode surface compared to the bulk solution make it difficult to estimate reliable kinetic parameters, like the exchange current density (j_0) from the Butler-Volmer equation in Equation 6 [74]. The exchange current density is a very popular parameter, which is usually derived from the Tafel-plot and used to compare the reaction rate of different catalysts. It is also an indicator for the overpotential that is required by the catalyst to perform the reaction.

$$j = j_0 \left[\frac{c_{ox}^{sur}}{c_{ox}^{bulk}} * \exp\left(\frac{\alpha z F * (V - V_{eq})}{R_{gas} * T} \right) - \frac{c_{red}^{sur}}{c_{red}^{bulk}} * \exp\left(\frac{-(1-\alpha) * z F * (V - V_{eq})}{R_{gas} * T} \right) \right] \quad \textbf{Equation 6}$$

j: $current\ density$

j_0: $exchange\ current\ density$

c_{ox}^{sur}: $concentration\ of\ oxidant\ at\ the\ electrode\ surface$

c_{ox}^{bulk}: $concentration\ of\ oxidant\ in\ bulk\ solution$

c_{red}^{sur}: $concentration\ of\ reductant\ at\ the\ electrode\ surface$

c_{red}^{bulk}: $concentration\ of\ reductant\ in\ bulk\ solution$

α: $transfer\ coefficient$

z: $number\ of\ electrons$

F: $Faraday\ constant$

V: $applied\ potential$

V_{eq}: $equilibrium\ potential$

R_{gas}: $gas\ constant$

T: $absolute\ temperature$

One popular approach to compare two different electrodes with each other is the analysis of specific parameters, which are obtained by cyclic voltammetry measurements. A typical dE/dt-input signal and the corresponding results for each half-cell are shown in Figure 10.

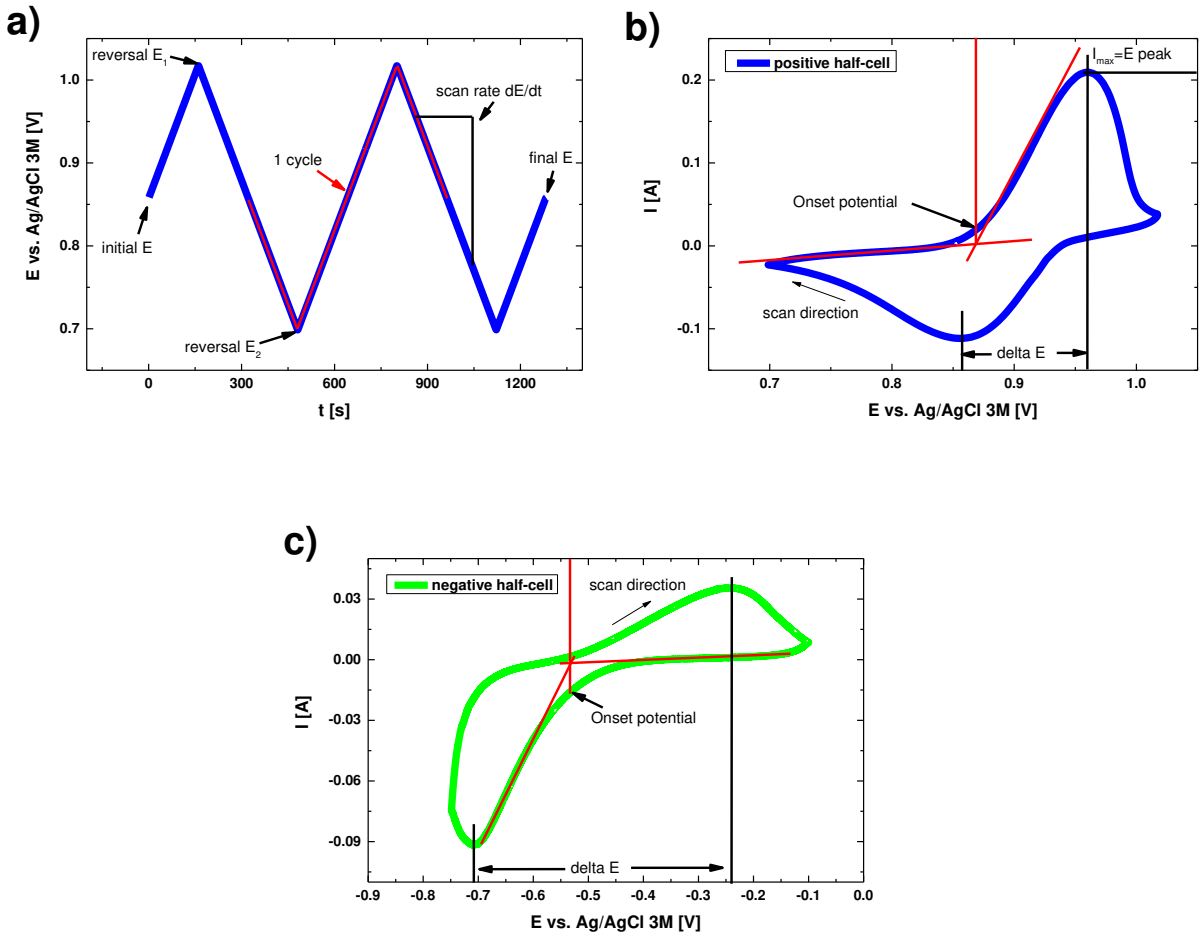

Figure 10: Exemplary cyclic voltammetry (CV) input signal and resulting voltammograms.

- **a) Significant input parameters such as the scan rate.**
- **b) CV of the positive half-cell with 1 mV s^{-1} and the analysis of the significant parameters.**
- **c) CV of the negative half-cell with 1 mV s^{-1}.**

The evaluation of CV results usually includes the current maximum (I_{max}) of the peak, the potential of the peak (E_{peak}), the onset potential and in case of a reversible or quasi irreversible reaction also the peak separation (ΔE). The current maximum and the peak position strongly depend on the ECSA and also on the mass-transport and diffusion [9]. Therefore, it is not recommended to draw conclusions from these two parameters, because they may be misleading due to mass-transport limitations and unknown ECSA. Since the peak separation is estimated from the peak positions, it should also not be used for the analysis of the reversibility of a redox couple [67]. The only parameter that should be independent of ECSA and mass-transport is the onset potential. The onset potential region is solely controlled by the kinetic overpotentials, which depend on the catalytic properties of the electrode material.

Using CV for the study of long-term stability is a routine approach. Different cycling conditions were reported for long-term CV measurements. The scan rate is usually chosen between 100 mV s^{-1} to 1 mV s^{-1} for several 100 cycles [75]. However, in our case this is rather difficult because of various reasons. As mentioned before, the vanadium reaction is a quasi-irreversible reaction. In addition to that we work with highly porous electrodes without any convection, which means that mass-transport is ensured only by diffusion. In case of porous electrodes the mass-transport inside the pores (3-dimensional diffusion) is different compared to the outer surface of the electrode (2-dimensional diffusion) as was described by Friedl et al. [67]. This has an impact on the reversibility (i.e. peak position) and the peak current in a CV measurement. One advantage of working with redox couples that change the color of the electrolyte upon oxidation or reduction is the visualization of reversibility. During a long-term CV the initial concentration of the electrolyte changes with every cycle due to irreversibility of the reaction and diffusion issues. This can be observed directly via a change of electrolyte color in diluted vanadium solution. E.g. starting with a blue solution (V(IV) appears blue in aqueous electrolyte), which turns greenish (V(V) appears yellow in aqueous electrolyte) after 10 CV cycles. At this point the initial conditions that were present during the first cycle are not valid anymore and the specific CV parameters will differ, simply because the concentration of the electrolyte changes. This leads to a change of the peak positions and maximum peak currents. The results could be misinterpreted by overestimation of possible electrode degradation.

A more promising approach for the application of CV measurements was designed in this work. Two flow-cells were equipped in series. One flow-cell was used for charging of the electrolyte and maintaining the SOC (compensating cell). The second flow-cell was used for electrochemical analysis of the carbon felt electrodes (“active cell”).

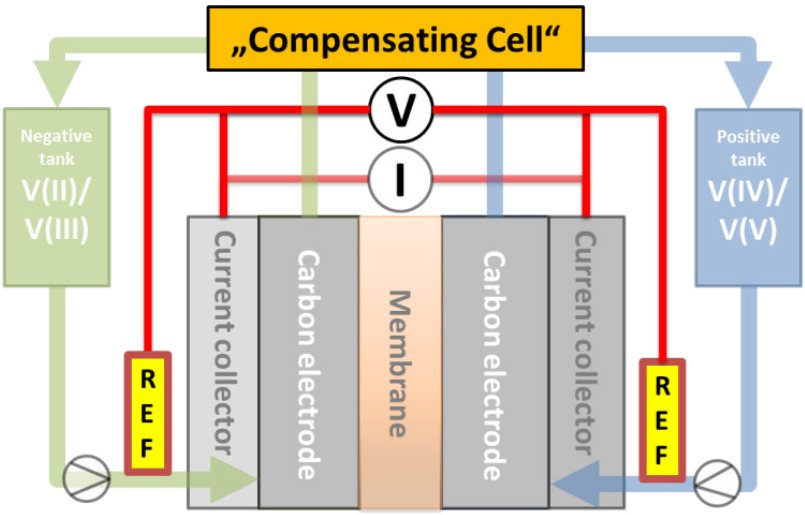

Figure 11: Schematic setup of a flow-cell with a reference electrode at the inlet. GC: Glassy Carbon current collector, WE: working electrode felt, ME: Membrane and CE: counter electrode felt. The second flow cell is positioned in series to compensate the accumulation of one species due to irreversibility of the redox couple.

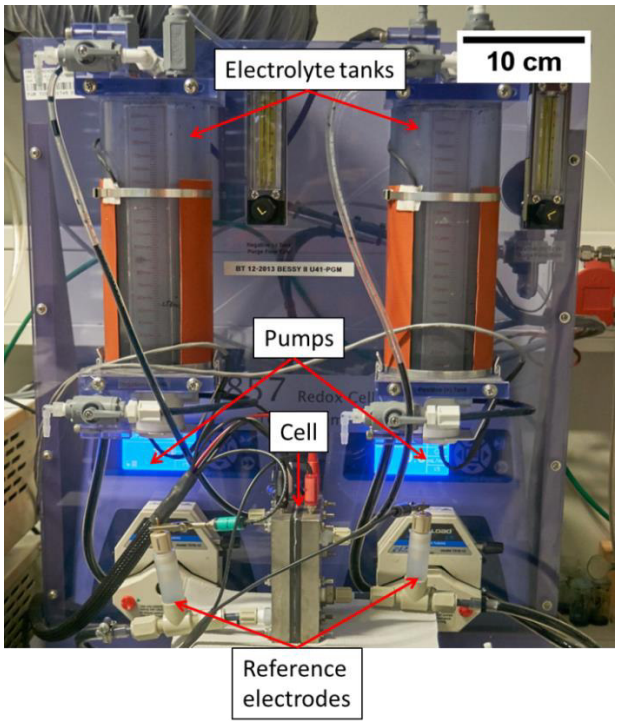

Figure 12: Scribner Associates Inc. testbench with a flow cell and a reference electrode at each inlet.

In order to perform half-cell measurements reference electrodes were implemented at the inlet of each half-cell. In Figure 11 and Figure 12 the setup with the reference electrodes at the inlets of the cell is shown. The second flow cell (compensating cell) in Figure 11 is positioned in series after the active cell. This type of setup has several advantages compared to a regular 3-electrode setup in a beaker. The compensating cell is used to maintain the

initial state of charge, which might deviate due to quasi irreversibility of different redox reactions in the active cell. The convection can now be ensured by the pumps, which force the electrolyte through the felt. The compression degree of the felt and the distances between all electrodes are kept constant, which is important for the comparison of two different electrodes, because these parameters also have an impact on the measured parameters. Since, the diffusion layer is still present the analysis by CV remains difficult. One alternative to CV is the electrochemical impedance spectroscopy (EIS). During a potentiostatic EIS measurement an AC voltage ($V_{(t)}$) with an amplitude (V_A) of e.g. 10 mV is applied at a certain potential (e.g. OCP) over a certain frequency range ($\omega = 2\pi ft$) (Equation 7). This input signal yields a current response ($I_{(t)}$) with an amplitude (I_A) and a phase shift (ϕ) (Equation 8). The connection between the voltage input and the current response is depicted in Figure 13 for a single frequency. The correlation of voltage input and responding current can be expressed in an absolute impedance ($Z_A=|Z|$) and the phase shift (Equation 9).

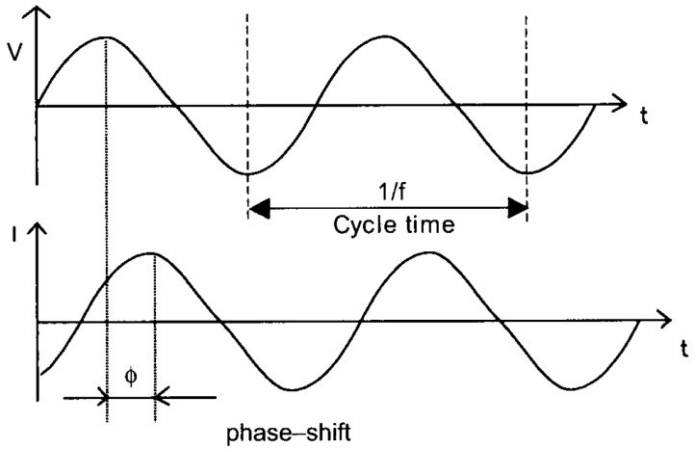

Figure 13: Sinusoidal voltage input and current response at a single frequency during electrochemical impedance spectroscopy (EIS) [74].

$$V_{(t)} = V_A * \sin(2\pi ft) = V_A * \sin(\omega t) \qquad \textbf{Equation 7}$$

$$I_{(t)} = I_A * \sin(\omega t + \varphi) \qquad \textbf{Equation 8}$$

$$Z = \frac{V_{(t)}}{I_{(t)}} = \frac{V_A * \sin(\omega t)}{I_A * \sin(\omega t + \varphi)} = Z_A * \frac{\sin(\omega t)}{\sin(\omega t + \varphi)} \qquad \textbf{Equation 9}$$

One standard way of representing impedance data is the Nyquist plot shown in Figure 14. The real (Z_{real}) and imaginary ($-Z_{im}$) parts can be calculated by applying Equation 10.

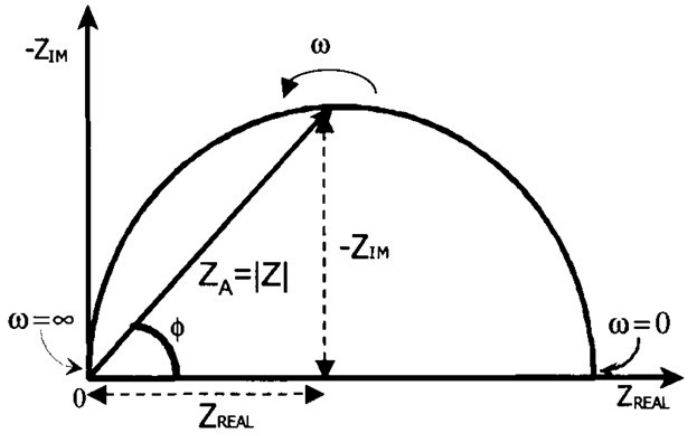

Figure 14: Impedance data represented as a Nyquist plot [74].

$$Z = \frac{V}{I} = Z_A * e^{j\varphi} = Z_A * (\cos(\varphi) + j * \sin(\varphi)) = Z_{real} + j * Z_{im}$$ **Equation 10**

A phase shift of 0 ° represents ohmic behavior (Z_{real}) and a phase shift of -90 ° corresponds to pure capacitive behavior (Z_{im}). Even though the Nyquist plot contains a lot of information it is quite difficult to correlate the frequency dependence of the system without additional information. Therefore, the Bode plot (Figure 15) is used as an additional source of information to analyze impedance data.

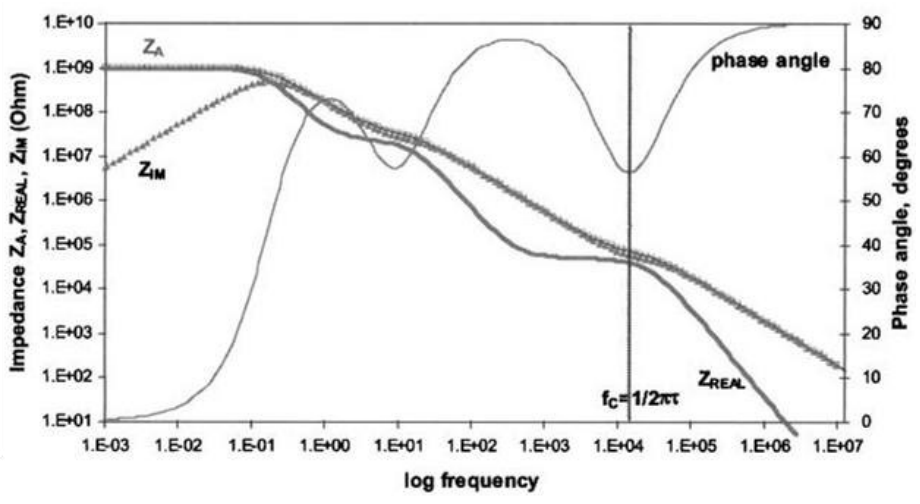

Figure 15: Impedance data represented as a Bode plot [74].

The Bode plot usually depicts the frequency dependence of the phase shift and the magnitude of the impedance (|Z|). In some cases the representation of the Z_{real} and Z_{im} can also be helpful for the estimation of the characteristic relaxation frequency (f_c) of a time constant (R|C). The relaxation frequency allows us to make assumptions on what type of process takes place, because certain processes are observed in particular frequency ranges [74]. For an electrochemical experiment with a redox couple in conductive aqueous electrolyte, the high frequency range (MHz-kHz) is usually dominated by ohmic resistance, polarization processes and diffusion related processes. The faradaic reaction can be observed in the medium frequency range (Hz-mHz). The low frequency range (mHz-µHz) is dominated by diffusion and mass-transport limitations.

In order to evaluate the impedance data a physical model has to be applied. A simple model contains inductive (L), resistive (R) and capacitive (C) elements to describe the impedance data. For a pure resistor the magnitude is |Z|=R, for a pure capacitor the magnitude depends on the frequency $|Z|=(\omega C)^{-1}$. In case of a parallel R|C circuit the impedance can be calculated with Equation 11 and Equation 12.

$$Z_{real\,(\omega)} = \frac{R}{1 + (\omega RC)^2} \qquad \textbf{Equation 11}$$

$$Z_{im\,(\omega)} = -\frac{\omega R^2 C}{1 + (\omega RC)^2} \qquad \textbf{Equation 12}$$

EIS has several advantages over CV. Since the measurements are conducted with an AC voltage and an amplitude of 10 mV at OCP, the concentration of the electrolyte inside the felt does not change as quickly as it does in a CV ($\rightarrow c^{sur} \approx c^{bulk}$). Also a small exciting signal of 5-10 mV allows to neglect degradation due to electrochemical stress of the electrode. Therefore, it is possible to investigate degradation that was induced by chemical (static) aging, which might appear due to mere contact with electrolyte without inducing electrochemical stress.

For our system, the frequency range is set between 1 MHz to 10 mHz for a precise measurement or 1 Hz for a fast measurement. With a fast measurement information about the charge transfer resistance (CTR, R_{ct}) and the contact resistance (Ru) can be obtained. The CTR is proportional to the inverse exchange current density (j_0) (Equation 13). These kinds of

measurements can be applied during cycling, which allows to monitor the development of the CTR and the Ru after each charge and discharge cycle. A single frequency (1 kHz-10 kHz) measurement can also be applied during a charge or discharge process to estimate the contact resistance throughout the whole time.

$$R_{ct} = \frac{R_{gas} * T}{z * F * j_0} \Rightarrow j_0 \sim \frac{1}{R_{ct}} \qquad \textbf{Equation 13}$$

However, every technique has its pitfalls and challenges. EIS is a very sensitive technique that needs equilibrium conditions in order to obtain reliable results at each frequency and to reduce the signal to noise ratio. Another downside is that the data has to be described with a physical model. This is done by fitting the data to an electrical circuit (as shown in Figure 16), which consists of inductor (L), resistors (R) and capacitors (C) in an ideal case.

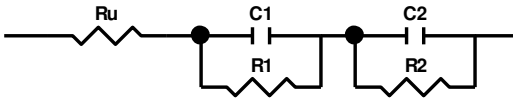

Element	Freedom	Value
Ru	Free(+)	1
C1	Free(+)	1E-05
R1	Free(+)	1
C2	Free(+)	0.1
R2	Free(+)	2

Figure 16: Example of a simple electrical circuit used for simulating and fitting EIS data. R: ideal resistor with Ru as the high frequency contact resistance and C: ideal capacitor.

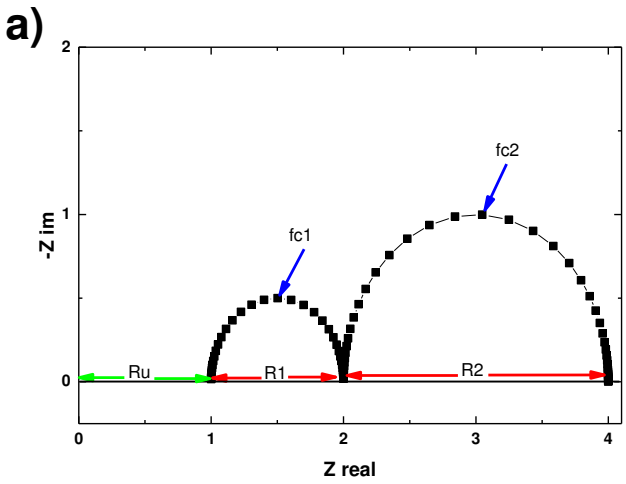

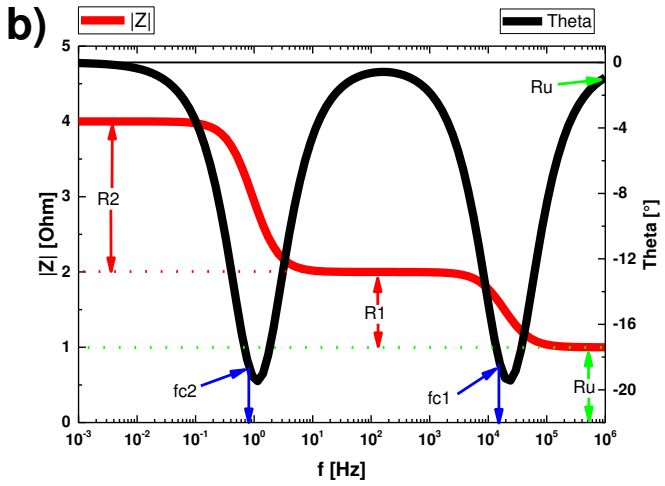

Figure 17: Nyquist (a)) and Bode (b)) plot of the simulation of the circuit that is shown in Figure 16. Ru: high frequency contact resistance, fc: characteristic relaxation frequency.

In Figure 17, a simulation of the circuit in Figure 16 is shown. Both plots clearly depict two separate processes, which are also called time constants (τ). In the Nyquist plot, these time constants are represented by a semicircle, while in the Bode plot they are represented by the minima of the phase shift and an increase of the magnitude. The first time constant appears at a characteristic frequency of 15 kHz and the second one at 0.75 Hz. As mentioned before, the frequency range allows to make assumptions on the nature of the process. In this case e.g. the first time constant could be a substrate polarization or pore diffusion and the second could be a charge transfer resistance.

However, as the system deviates from ideal behavior, more complicated electrical circuits have to be implemented. For a porous carbon felt with several active sites, which exhibit different activities towards the desired reaction, the current and voltage distribution on the electrode is not uniform due to non-uniform kinetics. Therefore, constant phase elements (CPE) have to be implemented instead of ideal capacitors to describe the distributed capacitive behavior. Also the mass-transport limited frequency region strongly depends on the electrode structure, which is why Warburg (W) elements are used to describe complex diffusion in porous materials. More variables have to be assigned, as the circuits become more complicated. These additional variables are a source of error for large circuits in case all variables are allowed to take any value (not constrained fitting). One example of such a circuit is shown in Figure 18.

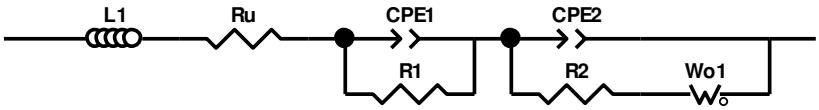

Element	Freedom	Value
L1	Free(+)	1E-07
Ru	Free(+)	1
CPE1-T	Free(+)	1E-05
CPE1-P	Free(+)	0.7
R1	Free(+)	1
CPE2-T	Free(+)	0.1
CPE2-P	Free(+)	0.75
R2	Free(+)	2
Wo1-R	Free(+)	2
Wo1-T	Free(+)	50
Wo1-P	Free(+)	0.3

Figure 18: Example of a more complicated electrical circuit, which could be used to fit data from a VRFB.

The circuit in Figure 18 is commonly used to describe two consecutive processes, which can appear during one EIS measurement in a real system. The inductive element (L) often needs to be implemented in case of large electrodes. Large electrodes tend to respond with high capacitive currents at high frequencies. These high currents can cause inductive interference in the cables of the potentiostat. In Figure 19 the circuit from Figure 18 was simulated with very similar parameters compared to Figure 16. However, the resulting Nyquist and the Bode plot became much more complicated and it is not so easy to analyze them anymore.

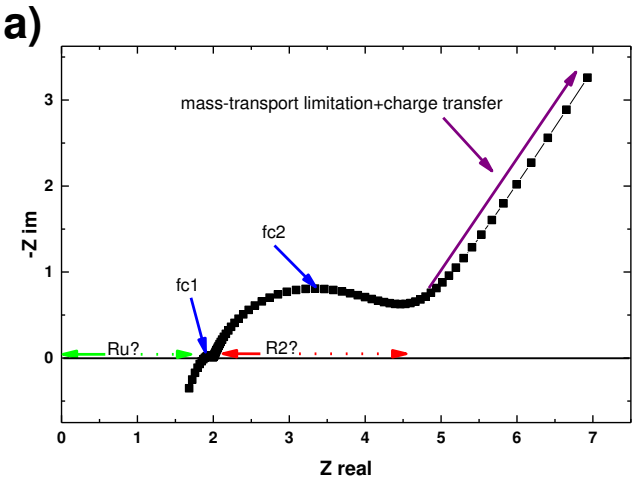

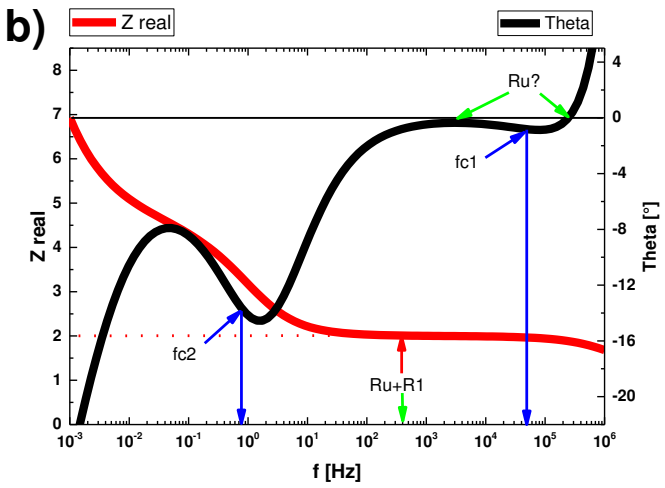

Figure 19: Nyquist (a)) and Bode (b)) plot of the simulation of the circuit that is shown in Figure 18.

If this was measured data instead of simulated data, then all parameters would be unknown and fitting a model to the measured data would be the only way to determine absolute values. For any type of fitting you need starting parameters. The more accurate the starting parameters, the better the fit. Therefore, it is necessary to know as much as possible about the system before measuring. E.g. does a value of 2 Ω make sense for the contact resistance (Ru) or is it too high? With a large amount of elements in the circuit it is possible to fit almost anything, but the accuracy and the physical meaning of the model will be lost. One way to increase accuracy of the fit is an experimental design in which one parameter (e.g. T, DC voltage, concentration,…) can be varied in a controlled way. Afterwards the resulting spectra (trend) can be correlated to certain processes. The consistency of the measured data is often verified by Kramers-Kronig calculation [74]. However, Kramer-Kronig has its limitations, which is why experimental methods are often used to verify the consistency of the data [76]. The linearity can be assured by running a CV measurement prior to EIS to estimate an appropriate DC voltage and an AC voltage. Otherwise the variation of the AC voltage can be used for the linearity check. The stability of the system can be checked by repeating the experiment under the same conditions.

Using EIS it is possible to unravel different processes, which appear prior or after a charge transfer like e.g. adsorption, diffusion or polarization. These are usually not visible in CV experiments because the whole reaction appears as just one peak. EIS is used in all fields of electrochemistry. Often it is implemented to understand the processes that appear before and after the charge-transfer. In Li-ion batteries the formation of the solid electrolyte

interface (SEI) and the diffusion through the SEI can be studied with EIS [77]. In fuel-cells EIS is used to investigate the adsorption and desorption processes on the cathode side [78]. In corrosion studies EIS is used to determine the health of the protecting coating of a substrate [79].

For complicated systems, like energy storage systems, the difficult part of EIS is to assign a time constant to a specific process, especially for a not well known system. This needs a lot of experimental work, but at the end one can differentiate between the appearing processes and their overall contribution to the performance losses of the system. This is very handy for a dynamic system with several different electroactive species in corrosive electrolyte, such as the VRFB.

2.3. Spectroscopic measurements of the carbon felt electrodes

The carbon felts that are used for electrochemical applications can have different properties. For the VRFB, graphitic carbon with ~5 at % surface functional groups exhibits the best performance during cell tests [80,81]. However, the spectroscopic analysis of carbon, especially with surface functional groups such as C=O and C-OH, is a difficult task. Several techniques are used to characterize the crystallinity, the particle size and the functionalization of the surface with different elements like oxygen or nitrogen. The penetration depth of each technique determines which properties of the carbon fiber can be analyzed. Raman spectroscopy has a penetration depth of ~50 μm, which is why it has been applied to investigate the bulk structure of carbon fibers. In particular, the D/G ratio is often used for the characterization of different carbon materials. The D/G ratio is an indicator for the graphitization degree of a sample. However, since the penetration depth is very high it is difficult to estimate the properties of just the surface layers. For the investigation of the surface layer, more sensitive techniques have to be used.

One popular technique to analyze surface properties of carbon materials is X-ray photoelectron spectroscopy (XPS). The penetration depth in carbon is ~5 nm, which allows to draw conclusions concerning the elemental composition of the surface layer. The sp^2/sp^3 hybridization ratio and the characteristic binding energies of e.g. C1s or O1s bonds are the most prominent way of analyzing surface layer compositions and concentrations of functional groups. Unfortunately, XPS requires ultra-high vacuum (UHV) conditions, which

makes it impossible to perform in-situ studies. Ex-situ XPS is therefore the most common technique used for the characterization of carbon surfaces, even though the processes in between electrochemical measurement and XPS measurement remain unknown. Of course, the sample transfer might be the source of artefacts.

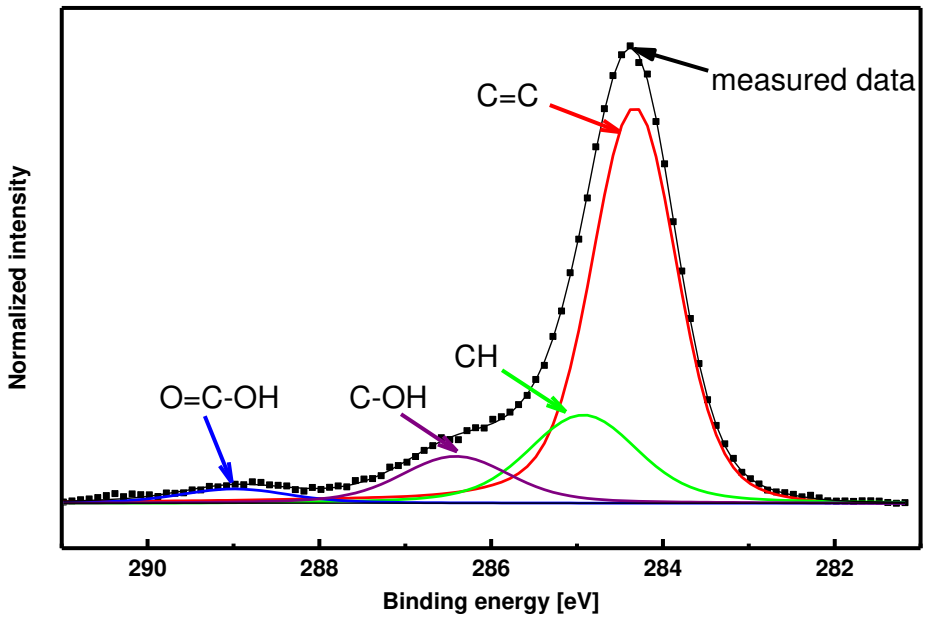

Figure 20: Example of a XP spectrum taken from chapter 3.1 Degradation of all-vanadium redox flow batteries (VRFB) investigated by electrochemical impedance and X-ray photoelectron spectroscopy: Part 2 electrochemical degradation.

In Figure 20 an example of a XP spectrum is shown. The black dotted curve represents the measured data. The binding energy region is that of the carbon 1s orbital. The spectrum is fitted with 4 different contributions namely the C=C sp^2-hybridized binding energy, the C-C sp^3-hybridized binding energy, the C-OH and the O=C-OH binding energy. The X-ray beam hits the sample and excites electrons from the core orbitals of the carbon atoms. These electrons have a characteristic kinetic energy when they leave the solid material and hit the detector. The binding energy of the electrons in the 1s orbital depends on the surrounding of the carbon atom and the bonds that are present (e.g C-C or C-O). Therefore, a specific binding energy can be assigned to a certain bond (or element). The quantification of different bond types is performed by quantifying the intensity of the corresponding energy and comparing them to one another [82]. In our example, the C1s energy with the highest count rate is that of sp^2-hybridized carbon, which is to be expected for a graphitic fiber.

The surface morphology of bulk samples can be studied with scanning electron microscopy (SEM). The penetration depth can be adjusted by the accelerating voltage of the electron beam. However, this technique is not capable of detecting surface functional groups and is therefore used in combination with XPS.

3. Discussion of the scientific manuscripts included in this thesis

The results of this thesis are presented in the following scientific manuscripts. Performance losses due to electrochemical degradation of the carbon felt electrodes were investigated in a flow-through test cell in chapter 3.1. EIS has been used among others to reveal the impact of chemical aging in chapter 3.2 and XPS and SEM measurements revealed changes of the carbon surface with respect to degradation. The overall losses of a VRFB system have been investigated with respect to the maximum cut-off voltage in chapter 3.3. In the last part of this work the electrode inside the negative half-cell was modified in order to reduce losses appearing due to electrode degradation (additional topic, chapter 4).

3.1. Degradation of all-vanadium redox flow batteries (VRFB) investigated by electrochemical impedance and X-ray photoelectron spectroscopy: Part 2 electrochemical degradation

3.1.1. Motivation

The durability of the VRFB system is the major key to its future success. But after the first literature search on the degradation of VRFB or stability tests of electrode material only a few scientific manuscripts were available. The degradation tests usually involved fast CV cycling or charge/discharge operation of small amounts of electrolyte in a static cell (no pumping). Applying these methods, one charge/discharge process or CV cycle can be performed in less than 1 min yielding results for more than 100 cycles in a short period of time. The obtained results were more or less conclusive and claiming that the degradation phenomena are negligibly small.

3.1.2. Description and Novelties

In the first experiments we intended to mimic realistic conditions for our cycling experiment and introduced reference electrodes at each inlet of the cell. The obtained cycling results were different from which was published before. The degradation of the system caused a performance loss of approximately 65 % after only 50 charge/discharge cycles. The

reference electrodes allowed us to monitor characteristic parameters with EIS during cycling. The development of the CTR revealed two regions with different degradation rates. The first 5 days (15 cycles) of the cycling experiment exhibited a stronger performance loss compared to the remaining time (cycles). Afterwards, the cycled electrodes were examined by EIS, XPS and SEM in order to determine which half-cell underwent the strongest degradation during the cycling experiment. EIS was measured inside the test cell against one of the implemented reference electrodes at specific states of charge. The negative half-cell was found to be the performance limiting half-cell after 50 cycles. The positive half-cell on the other hand did not show any significant performance loss. The SEM images showed heavily damaged carbon fibers in the negative half-cell. The XPS results revealed an oxidation of both electrodes. That was an unexpected finding, because the felt inside the negative half-cell was expected to undergo a reduction of the surface functional groups, as the potentials of the negative half-cell remained lower than -0.12 V vs. NHE at all times. The applied potential should prevent an oxidation of the carbon fibers. Therefore, we first believed that the oxidation of the negative felt might appear due to oxidation in air in between the cycling experiment and the ex-situ XPS measurement. A second cycling experiment was conducted to investigate, whether the felt in the negative half-cell loses activity due to a reduction of surface functional groups. The second experiment began like the first one with 50 charge/discharge cycles. After the 50^{th} cycle the polarity of the cell was reversed for 5 cycles. During these 5 cycles the felt in the original negative half-cell should be re-oxidized in case it was reduced during the first 50 cycles. Afterwards, 10 additional cycles in the original polarity were recorded. The reversal of polarity did not yield any recovery of the cell performance according to input/output energy values. This indicates that the electrode in the negative half-cell was oxidized during normal operation mode, which should not appear according to the thermodynamics of carbon oxidation. Besides the degradation of the electrode, the imbalance of the electrolyte was estimated to be one of the dominant sources for the loss of performance. According to SEM images the fibers of the negative electrode were damaged much stronger compared to the positive electrode. One assumption was that a cut-off voltage of 1.8 V led to very high negative potentials in the negative half-cell, which led to hydrogen evolution during the charge process. These findings led to the work that is presented in the following manuscripts.

3.2. Electroless chemical aging of all-Vanadium Redox Flow batteries (VRFB) investigated by Electrochemical Impedance and X-ray Photoelectron Spectroscopy

3.2.1. Motivation

In the first manuscript, we discussed that the carbon electrode in the negative half-cell was oxidized during normal cycling operation. There are at least two effects that can cause an oxidation of carbon. The first one would be the electrochemical stress that is applied by galvanostatic cycling. The second one is a static aging that appears due to a chemical reaction (chemical aging) induced by mere contact with the acidic electrolyte. Thermodynamically, the oxidation of carbon is expected to take place at potentials of +0.2 V vs. NHE and higher. Therefore, we conducted experiments simulating static aging to investigate the origin of the inevitable oxidation of the negative electrode that takes place during cycling.

3.2.2. Description and Novelties

This manuscript consists of two parts. In the first part, we conducted 3-electrode measurements in a beaker with three different electrolytes and at two different temperatures. The electrodes were immersed in the corresponding electrolyte at a fixed temperature for 8-30 days. EIS measurements were performed in an electrolyte of the same composition but at room temperature every 24 h. In the second part, the experiment was repeated at standard conditions in a regular test cell with a 2-cells in series setup and reference electrodes at the inlet. The electrode was not removed during the 8 day measurement. Therefore, it had no direct contact to air atmosphere in between measurements because the electrolyte tanks were purged with nitrogen.

Since any kind of electrochemical stress needed to be prevented, we used the second cell for charging and maintaining the state of charge over 8-12 days. EIS was very useful in order to obtain results without electrochemically stressing the electrodes, which would apply for CV or polarization curve measurements. The electrodes from the second experiment were further examined with ex-situ XPS.

Chemical aging was found to take place in pure 2 M sulfuric acid and in presence of vanadium at different oxidation states. Increasing the temperature led to a stronger

decrease of the double layer capacitance in case of the pure sulfuric acid measurements. The same behavior was observed for diluted vanadium in sulfuric acid. In presence of vanadium aging could be detected by comparing the development of the charge transfer resistance over time (24 h). In case of a concentrated vanadium solution (in sulfuric acid) a temperature dependence could not be observed. It seems that the vanadium is also involved in the aging process of the carbon. All measurements revealed two regions with different slopes for the rate of aging. During the first 5 days the electrode seems to undergo a much stronger aging compared to the remaining time. The correlation of the CTRs of the chemical aging experiment compared to the electrochemical degradation experiment revealed, that the performance loss during the first several days might be caused by chemical aging. Therefore, the overall degradation is not necessarily cycle dependent but rather time dependent.

The second experiment in the test cell confirmed the results that were obtained in the 3-electrode setup in a beaker. Both electrodes from the second experiment were used as samples for ex-situ XPS measurements. The electrode in the negative half-cell was oxidized causing a decrease of sp^2-hybridized carbon and a large increase of –OH and –OOH groups. XPS revealed a stronger oxidation of the electrode inside the positive half-cell. But as was shown in 3.1, this did not affect the performance of the positive half-cell. The conclusion of both manuscripts is that the positive half-cell is dominated by an outer-sphere mechanism, while the negative half-cell follows an inner-sphere mechanism. The inner-sphere mechanism strongly depends on the functional groups. The increase of –OH and –OOH seems to have a negative effect on the reaction rate of the negative half-cell. As a result of the oxidation, the sp^3-hybridized carbon content increased. According to XPS the amount of –C=O groups as well as sp^2-hybridized carbon decreased during the chemical aging experiment. Therefore, it is not clear, if the insulation of the carbon surface by –OH and –OOH formation or the decrease of –C=O groups is the major factor for the change in reaction rate. However, these effects appear simultaneously and cause a decrease of ECSA. Therefore, it is inevitable to modify the electrode in the negative half-cell to maintain its activity.

3.3. Electrochemical analysis of the performance loss in all vanadium redox flow batteries using different cut-off voltages

3.3.1. Motivation

The cut-off voltage is one of the most important parameters for the performance of the VRFB especially at higher current densities (e.g. 100 mA cm^{-2}). The higher the cut-off voltage, the better the performance, but with a higher cut-off voltage a higher rate of degradation can be assumed. Therefore, the long-term performance should be more stable with moderate current densities. Manufacturers of commercial VRFB systems use cut-off voltages between 1.6 V-1.7 V in order to prevent degradation and hydrogen evolution. Using only 1.6 V as the cut-off voltage leads to low maximum states of charge at sufficient current densities, which unnecessarily increases the cost of the system.

The results of both previous manuscripts show that the rate of degradation does not solely depend on electrochemical stress. Therefore, we performed two long-term experiments with different maximum cut-off voltages in order to investigate the degradation rate, the occurrence of possible parasitic reactions and the overall performance of the system as well as the loss of performance over time.

3.3.2. Description and Novelties

Two cycling experiments were performed under identical conditions. The only parameter that was varied was the maximum cut-off voltage. The half-cell potentials were monitored during cycling as well as the CTRs. Polarization curves and CTRs were recorded in fresh electrolyte before and after cycling. This enabled us to separate the performance loss caused by an imbalance of the electrolyte from the performance loss that appears due to electrode degradation. The results of both cell-tests were comparable to the results in chapter 3.1. The half-cell potential of the negative half-cell was independent of the maximum cut-off voltage. The positive half-cell on the other hand showed higher potentials with increasing cut-off voltage. The dynamic change of the potential, especially during the first several days was revealed by half-cell potential monitoring. These results are in agreement with our chemical aging experiments.

The imbalance of the electrolyte was made visible by comparing the SOCs that were calculated from the cell voltage (OCV) to the SOCs that were calculated from the potentials

of the negative half-cell (OCP). For the higher cut-off voltage the negative half-cell was rate limiting, while at 1.65 V the positive half-cell became rate limiting.

The electrode degradation was investigated with half-cell polarization curves and compared to the full-cell polarization curves. The half-cell polarization curves revealed a high increase of kinetic overpotentials at the negative half-cell, while the positive half-cell was almost unaffected by the oxidation of the electrode. EIS measurements during the cell tests showed the development of the CTR, which increased stronger for the experiment with 1.8 V cut-off voltage. This indicates a stronger degradation of the system for higher cut-off voltages, but the overall performance of the system was still better with 1.8 V compared to 1.65 V. However, we could show that degradation appears even at lower cut-off voltages and that the risk of hydrogen evolution cannot be estimated from the maximum cell voltage, because the half-cell potentials adjust dynamically to the requirements of the system. Comparing both experiments the risk of hydrogen evolution was approximately the same, because the potential of the negative half-cell remained identical.

4. Modification of the electrode in the negative side (paper draft)

4.1. Motivation

In the previous manuscripts we describe the performance loss and the inevitable oxidation of the carbon electrodes. In order to maintain performance it is necessary to modify the electrode in the negative half-cell. We should either prevent a further oxidation of the carbon fibers to maintain active sites or replace the active sites by a different catalyst similar to fuel-cell electrode assemblies. For an acidic electrolyte non-noble metals usually do not perform well. Noble metals tend to evolve hydrogen and increase the cost of the system. Therefore, we tried to modify the felts with “cheap” metals that have a high overpotential towards hydrogen evolution and are stable in acidic solutions. The first experiments were performed with lead that was deposited chemically and electrochemically on the carbon felt. The standard potential of led is -0.13 V vs. NHE, which is why it was not possible to stabilize it on the electrode, since the potentials during cycling can become as positive as 0.2 V vs. NHE. In a different approach we used antimony, which was not suitable because the vanadium reaction was inhibited.

For the third approach we chose bismuth, because it has similar properties to lead but a higher standard potential. The modification with bismuth was previously reported in the literature as a way to inhibit hydrogen evolution [58,75,83,84]. It was also implemented in the positive half-cell [85]. Most of the studies relied on CV analysis of carbon felt electrodes. It was not clear whether the performance increases due to an increased surface area or due to a catalytic effect of bismuth. However, most important was that it does not inhibit the vanadium reaction and, therefore, can be used for further stability tests.

4.2. Experimental

The bismuth was electrochemically deposited from an acidic solution (50 mM $BiNO_3$) inside the test cell. The flow rate during the deposition was set to 100 mL min^{-1}. The deposition was performed with 50 mA cm^{-2} pulses. The pulse duration was 1 s and the time between pulses was also 1 s. The deposition was stopped after a charge of 350 C was transferred. This is equal to approximately 50 wt% of bismuth compared to the felt mass (felt mass = 487 mg).

Modification of the electrode in the negative side

Afterwards the modified felt was implemented in the negative half-cell. Before the cycling experiment the electrolyte was charged with a different cell to a SOC of 50 % to avoid Bi-oxidation during the initial charge cycle. 50 cycles were performed with 100 mA cm^{-2} and 100 mL min^{-2} with a cut-off voltage between 0.8 V-1.8 V. After the 50^{th} cycle the electrolyte was exchanged and 2 additional cycles were recorded. Polarization curves and EIS were recorded before and after cycling in fresh electrolyte with a SOC of 50 %. The modified felt was examined with SEM, EDX and XRD before and after cycling to characterize the aging effects in more detail.

4.3. Results and discussion

The deposition of bismuth was performed in the test cell that was also used for regular cycling because the convection through the felt could be controlled by the pump rate. Previous depositions in beaker set-up yielded unsatisfying results concerning the bismuth content inside the felt, as is shown in Figure 21. The deposition took place only at the outer surface of the felt, even with large pulse pauses of 10 s and more to allow for better mass-transport of the Bi^{3+} into the felt.

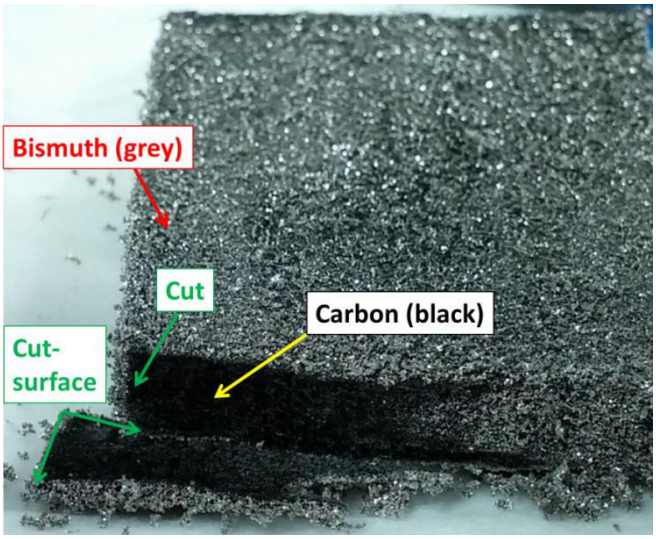

Figure 21: Bismuth (grey particles) deposited with a pulse technique in a 3-electrode beaker set-up. The theoretically deposited amount of Bi was 50 wt%.

The deposition in the test cell also led to a non-uniform distribution of the bismuth. The membrane side of the electrode was the preferred deposition site compared to the current collector side. This might be due to lower ionic resistances at the membrane side, which allowed higher current densities. This experiment gave furthermore an insight in where the

vanadium reaction might take place preferentially, especially at higher current densities. A 2-dimensional non-uniform current/voltage distribution has been reported by Clement et al. and Becker et al. [32,33]. We observed a preferred deposition of bismuth on the membrane side, which also indicates a non-uniform current/voltage distribution from the current collector to the membrane. Combining these findings with previously reported results we suggest a 3-dimensional non-uniform current/voltage distribution for thick electrodes. Electrochemical stress and possible degradation that comes with it most likely varies with the current/voltage distribution on the electrode. Therefore, thinner electrodes might be a better choice in order to decrease ohmic resistances and the cell-stack volume.

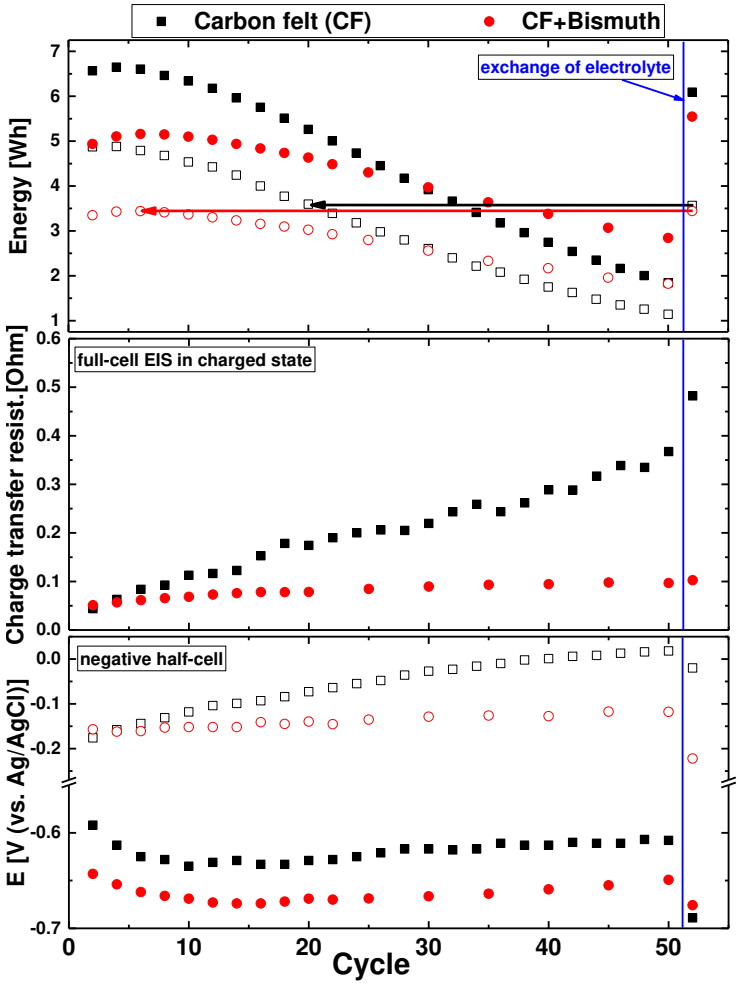

Figure 22: Input and output energy, CTR and max. half-cell potentials of the negative half-cell for the cycling experiment with the bismuth electrode. The black squares represent data from the experiment that was presented in 3.3 as a comparison for the bismuth modified felt (red). The current density and the flow rate of the experiments are different. Therefore, only the development of the curves can be compared.

Modification of the electrode in the negative side

In Figure 22, the analysis of the cycling experiment with the modified bismuth electrode in the negative half-cell is shown. The ohmic resistance decreased by ~0.5 Ω cm^2 compared to regular carbon felt (CF). The overall energy output decreased by 47 % after 50 cycles, but after exchanging the electrolyte, it could be completely recovered compared to the regular CF electrode. The energy efficiency remained at ~65 %. For the unmodified electrode, the energy efficiency decreased by 15 % after 50 cycles. The CTR in the fully charged cell increased slightly during the first 10 cycles and remained constant for the remaining amount of cycles. The maximum potentials that were recorded show a similar development for the charge process compared to the unmodified electrode. The discharge process on the other hand exhibits a much more stable potential development for the modified electrode. This shows that the overpotentials did not increase as significantly as they did for unmodified CF.

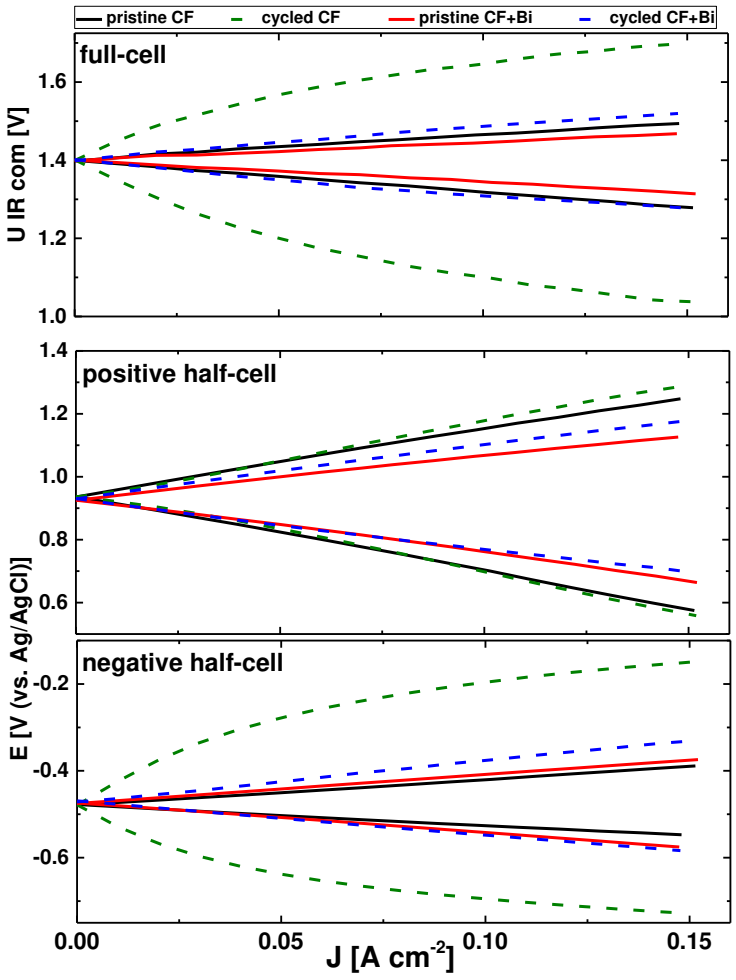

Figure 23: Polarization curves before and after cycling in fresh electrolyte. The experiment with the bismuth electrode is shown in red and blue. Black and green represent the experiment from 3.3 with 1.8 V cut-off voltage.

Modification of the electrode in the negative side

In Figure 23 the polarization curves for both experiments are shown. The modified electrode does not show any significant performance loss in the full-cell UI. A slight increase of the overpotentials can be observed for the charge process of the positive half-cell and the discharge process of the negative half-cell. In comparison, the unmodified CF showed a large increase of the overpotential for both the charge and the discharge process of the negative half-cell.

The degradation of the electrode was found to be negligibly small compared to the unmodified CF. The reason for the performance loss with the modified electrode remains the imbalance of the electrolyte that is caused by the cross-over of vanadium through the membrane and possible oxidation of the vanadium with oxygen. However, these losses could be controlled either by an anion exchange membrane, which does not let the vanadium ions pass, or a better cell management monitoring and "replenishing" the electrolyte in-situ.

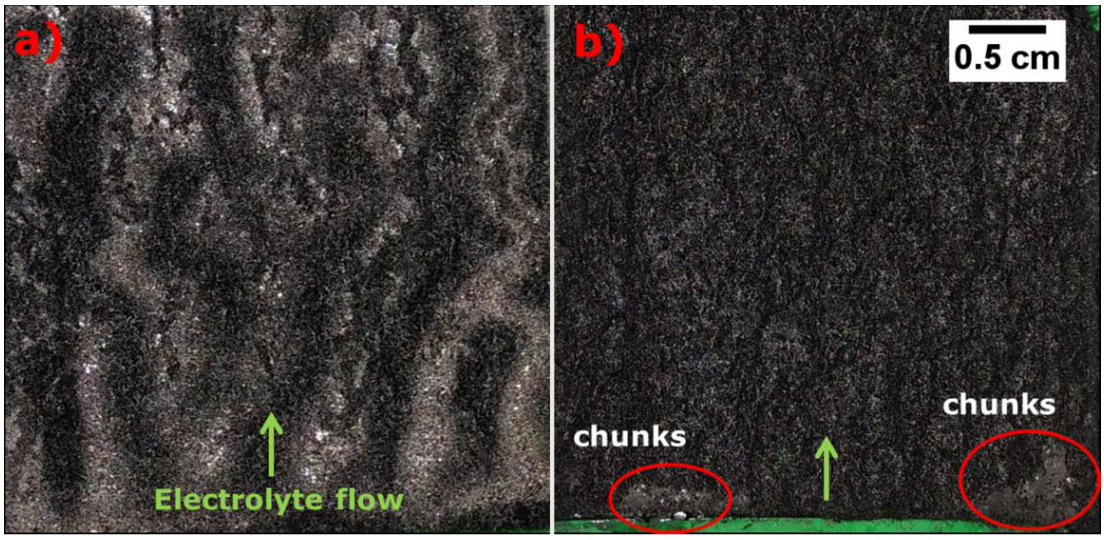

Figure 24: Pictures of the membrane side of the modified felt before cycling a) and after cycling b).

In Figure 24, the bismuth modified felt is shown before and after cycling for 50 cycles. The grey metallic color in Figure 24 a) indicates the deposited bismuth on the membrane side of the felt. The distribution of the Bi was not ideally homogeneous, but the amount seemed sufficient. After 50 cycles a large amount of the bismuth was found at the edge of the electrode (electrolyte inlet). The surface of the membrane side does not show a significant grey color anymore. This means that bismuth is being dissolved and redeposited during cycling.

Modification of the electrode in the negative side

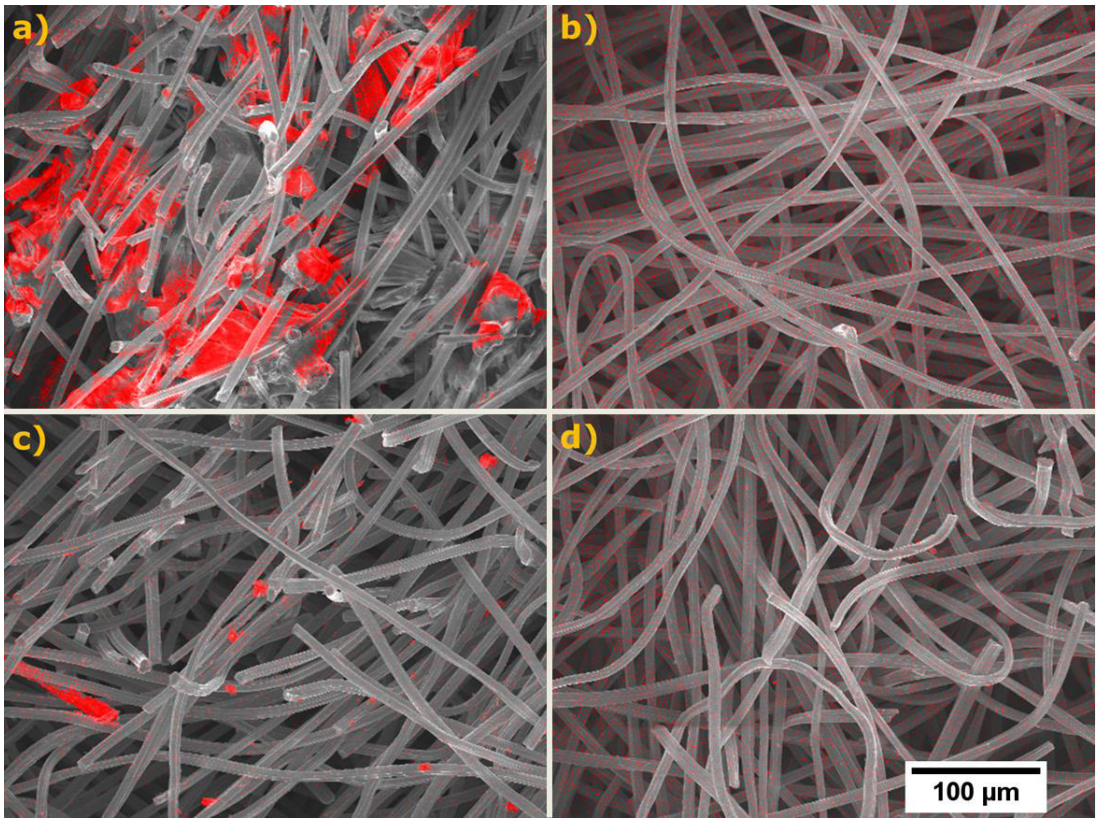

Figure 25: EDX mapping of the Bi modified felt before and after cycling for 50 cycles.

- **a) Membrane side before cycling.**
- **b) Membrane side after 50 cycles.**
- **c) Current collector side before cycling.**
- **d) Current collector after 50 cycles.**

In Figure 25, EDX mappings of the modified bismuth felt are shown before and after cycling. Before cycling the concentration on the membrane side is clearly higher compared to the current collector side. Large agglomerates were formed at the membrane side during deposition. After cycling, these agglomerates dissolved and redeposited, which led to a more homogeneous distribution and a smaller size of the particles throughout the whole felt except for the edges at the inlet of the cell. The edge of the electrode is shown in Figure 26. It is the first part that comes in contact with fresh electrolyte containing dissolved bismuth species. Therefore, large agglomerates are formed at this position. This might lead to an increase of the pressure drop due to blockage of pores, which would increase the energy demand that is required for the pumps. This would result in a lower overall efficiency of the system.

Modification of the electrode in the negative side

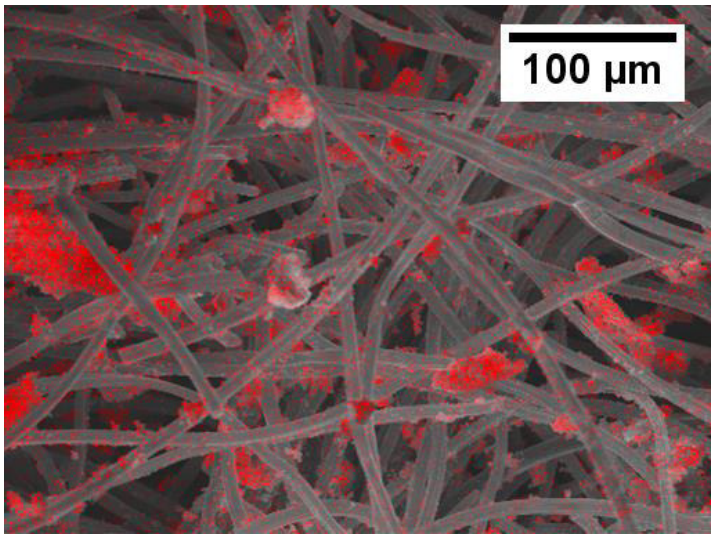

Figure 26: EDX mapping of the edge site of the Bi modified electrode after 50 cycles. The red dots represent Bi particles.

In Figure 27, XRD patterns of the Bi modified electrode are shown. Although noisy, before cycling, the pattern reveals more than just elemental bismuth. Several different complex compounds were detected but not specified due to the comparatively poor signal-to-noise ratio. After cycling, the XRD pattern changes towards more distinct reflections attributed to elemental bismuth as the dominant species.

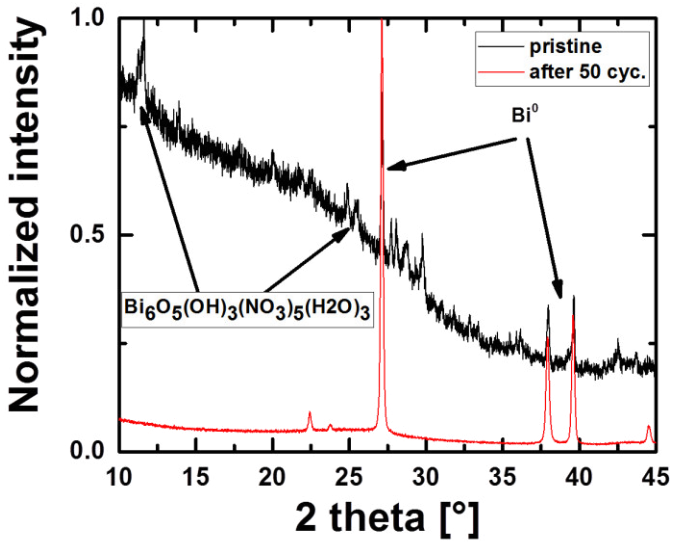

Figure 27: XRD pattern of the Bi modified electrode before and after cycling.

The experiments with bismuth modified electrodes have shown that it is possible to prevent the degradation of the negative electrode. However, it is not clear yet, how the bismuth is involved in the reaction process. David J. Suarez et al. have proposed a mechanism that

depicts Bi as a catalyst for the vanadium reaction [75]. Hereby bismuth forms BiH_x, which interacts with vanadium and enhances the performance of the electrode, while it inhibits the hydrogen evolution reaction. But it has not been confirmed yet. We observed a dissolution and a redeposition of the bismuth during our experiment. It is not clear, whether the carbon electrode is oxidized during the experiment. Also the preferred sites for the redeposition are not known. It is possible that the Bi particles preferentially deposit on specific functional groups, which inhibit the vanadium reaction. Therefore, the bismuth would not catalyze the reaction, but protect the fibers from further oxidation, which would lead to a stable sp^2/sp^3 ratio of the carbon surface.

4.4. Conclusion

The modification of the negative electrode with bismuth enhanced the stability of the electrode and prevented performance loss due to degradation of the negative half-cell. The overall performance was completely recovered after exchanging the electrolyte. The origin of the enhancement is not known so far. It is possible that bismuth catalyzes the reaction or simply protects the fibers from oxidation. Further experiments are required to understand the role of bismuth.

5. Conclusion and future work

The first objective of this thesis was to find a way to determine degradation phenomena in the carbon felts with a reproducible protocol. This was achieved with two different protocols. The first protocol was applied in a two-cells in series set-up, where one cell was used for maintaining the state of charge, while the other cell was held at a constant current or potential to simulate a charge or discharge process over a certain period of time. The second and more important protocol consisted of cycling operations with a specific set of parameters. A reference electrode was implemented at each inlet of the operating cell in order to determine the contributions of different processes to the overall performance loss of the system. These reference electrodes allowed us to monitor the performance of each half-cell over time and develop a third protocol for the investigation of chemical aging of the electrodes. Electrochemical impedance spectroscopy studies were carried out during cycling as well as during our chemical aging experiments to monitor the development of the charge-transfer resistance and the ohmic resistance.

The degradation of the electrodes strongly depends on the cycling conditions. The overall performance loss after 50 cycles was found to be 60 % to 75 % for the output energy. 10 % to 55 % of the overall losses were assigned to the electrode degradation in different experiments. The remaining losses were assigned to the imbalance of electrolyte and ohmic losses. The overall performance loss does not seem to depend on the amount of cycles but rather on the total duration of the experiment, which indicates that the degradation process is not purely dependent on electrochemical stress. Using EIS it was possible to differentiate between the performance loss of the full-cell and both half-cells. It turned out that the full-cell performance becomes limited by the performance of the negative half-cell after a certain amount of cycles. The positive half-cell, on the other hand, did not show any significant performance loss at all. The XPS analysis revealed an oxidation of the electrodes in both half-cells, which was unexpected because the oxidation of the negative half-cell should not be possible due to the potentials that are applied to it during cycling. However, the oxidation of both electrodes seemed to have a much larger impact on the performance of the negative half-cell. An attempt to recover the performance of the negative half-cell by changing the polarity of the cell after a certain amount of cycles was not successful.

A further investigation of the chemical aging that was assumed to take place during cycling was conducted in two different types of set-up. Using a common beaker set-up it was possible to investigate a large amount of electrode felts after soaking them in different electrolyte and storing them at particular temperatures. Measurements in pure sulfuric acid revealed that the double layer capacitance decreased by 40 %-60 % after only 12 days of mere contact with electrolyte. Increasing the temperature during the storage in electrolyte led to higher aging rates of the felts. This increase of the aging rate with increasing temperature indicates a chemical reaction. The experiments in pure sulfuric acid were followed up with experiments in diluted and concentrated V(III) solution, which also contained sulfuric acid to investigate the role of vanadium. In case of vanadium the charge transfer resistance of the V(III) oxidation was used as an indicator for the aging of the electrode. The rate of aging was found to be not only dependent on the sulfuric acid but also on the concentration of vanadium. For the diluted vanadium solution the development of the aging rates is very similar to what was obtained from pure sulfuric acid. But in concentrated vanadium solution the aging rate of the samples that were stored at room temperature was higher compared to the samples that were stored at 40 °C. This might be due to a reaction of the felt with the vanadium. However, all experiments showed a decrease of the initial aging rate after 5 days. A decrease of the degradation rate after 4-6 days was also observed during all cycling experiments, indicating that the degradation initially might be dominated by chemical aging. The results obtained in the beaker set-up were then reproduced in a VRFB test cell under the same conditions that were used for cycling. The electrodes from the second experiments were analyzed with XPS. The findings were similar to the results from the cycling experiment stating that both felts were oxidized during the chemical aging experiment. According to the XP spectra the amount of oxygen functional groups increased on both felts. The amount of sp^3-hybridized carbon increased stronger than the amount of the additional functional groups. It is possible that a CO or CO_2 evolution took place, which resulted in an insulated, sp^3-hybridized carbon surface. Therefore, the increase of the charge transfer resistance can be explained by a loss of ECSA and an insulation of the carbon surface.

Since the chemical aging seemed to be inevitable on carbon electrodes, it is important to understand and prevent the electrochemical degradation and possible parasitic reactions. This is often done by decreasing the maximum cut-off voltage. We found that a higher cut-

off voltage leads to a higher rate of degradation, but this is not visible in the overall performance of the system during the first 50 cycles, because the cell with higher cut-off voltage performs much better compared to lower maximum cut-off voltage. Therefore, longer cycling experiments should be conducted, because they might give a more accurate estimation of the degradation rates, which then would also be visible in the overall performance of the cell.

In the last part of this thesis the electrode inside the negative half-cell was modified with bismuth in order to prevent the inevitable degradation of the carbon, which was one dominant factor for the overall performance loss during cycling operations with pure carbon felt electrodes. The first results revealed that it was possible to prevent electrode degradation and recover almost 100 % of the initial performance after 50 cycles by exchanging the electrolyte. The charge transfer resistance of the full-cell remained almost constant after a slight increase during the first 10 cycles. However, the bismuth was dissolved and redeposited during cycling, which led to an accumulation of bismuth at the inlet of the cell. This might lead to a blockage of the inlet and increase the pressure losses in the system. Therefore, further experiments are required to stabilize the bismuth particles on the carbon surface and investigate the role of bismuth in the vanadium reaction.

The mechanism of the V(II)/V(III) reaction most likely follows an inner-sphere mechanism, because the performance strongly depends on oxygen functional groups. Judging by the chemical aging experiment it is the C=O that catalyzes the reaction. The positive half-cell on the other hand is more complicated. The reaction rate does not seem to be influenced by additional oxygen functional groups, which indicates an outer-sphere mechanism. But the V(IV) and V(V) species both have at least one oxygen atom bound to it. This oxygen atom might act as the mediator in the reaction with the sp^2-hybridized carbon. This has to be investigated in order to understand the nature of the process. One possible way to do that is the implementation of boron doped diamond (BDD) electrodes. These electrodes have a surface that consists of either H- or O- terminated carbon atoms. Therefore, an adsorption of electroactive species from electrolyte is unlikely, which would inhibit any kind of inner-sphere reaction.

In the future, a further investigation of the role of bismuth in the negative half-cell should be conducted. More fundamental experiments on glassy carbon could give an insight into the

catalytic properties towards the V(II)/V(III) reaction. Also the distribution of bismuth inside the felt and the stabilization of the bismuth particles need to be addressed before it can be implemented in commercial large scale storage systems.

Acknowledgments

I would like to thank Michael Bruns from the KIT Karlsruhe and Daniel Przyrembel from the FU Berlin, who provided access to much needed XPS and helped with the interpretation of the results.

Literature

[1] https://www.bmwi.de/DE/Themen/Energie/Erneuerbare-Energien/erneuerbare-energien-auf-einen-blick.html, (14.11.16), (2016).

[2] P. Alotto, M. Guarnieri, F. Moro, Redox flow batteries for the storage of renewable energy: A review, Renew. Sustain. Energy Rev. 29 (2014) 325–335. doi:10.1016/j.rser.2013.08.001.

[3] G. Kear, A.A. Shah, F.C. Walsh, Development of the all-vanadium redox flow battery for energy storage: a review of technological, financial and policy aspects, Int. J. Energy Res. 36 (2012) 1105–1120. doi:10.1002/er.1863.

[4] G.L. Soloveichik, Flow Batteries: Current Status and Trends, Chem. Rev. 115 (2015) 11533–11558. doi:10.1021/cr500720t.

[5] A.Z. Weber, M.M. Mench, J.P. Meyers, P.N. Ross, J.T. Gostick, Q. Liu, Redox flow batteries: a review, J. Appl. Electrochem. 41 (2011) 1137–1164. doi:10.1007/s10800-011-0348-2.

[6] C. Ponce de León, A. Frías-Ferrer, J. González-García, D.A. Szánto, F.C. Walsh, Redox flow cells for energy conversion, J. Power Sources. 160 (2006) 716–732. doi:10.1016/j.jpowsour.2006.02.095.

[7] J. Langner, M. Bruns, D. Dixon, A. Nefedov, C. Wöll, F. Scheiba, H. Ehrenberg, C. Roth, J. Melke, Surface properties and graphitization of polyacrylonitrile based fiber electrodes affecting the negative half-cell reaction in vanadium redox flow batteries, J. Power Sources. 321 (2016) 210–218. doi:10.1016/j.jpowsour.2016.04.128.

[8] G. Wei, C. Jia, J. Liu, C. Yan, Carbon felt supported carbon nanotubes catalysts composite electrode for vanadium redox flow battery application, J. Power Sources. 220 (2012) 185–192. doi:10.1016/j.jpowsour.2012.07.081.

[9] J. Friedl, C.M. Bauer, A. Rinaldi, U. Stimming, Electron transfer kinetics of the – Reaction on multi-walled carbon nanotubes, Carbon. 63 (2013) 228–239. doi:10.1016/j.carbon.2013.06.076.

[10] M. Steimecke, S. Rümmler, N.-F. Schuhmacher, T. Lindenberg, M. Hartmann, M. Bron, A comparative Study of Functionalized High-Purity Carbon Nanotubes towards the V(IV)/V(V) Redox Reaction using Cyclic Voltammetry and Scanning Electrochemical Microscopy, Electroanalysis. (2016) n/a-n/a. doi:10.1002/elan.201600614.

[11] K.J. Kim, M.-S. Park, Y.-J. Kim, J.H. Kim, S.X. Dou, M. Skyllas-Kazacos, A technology review of electrodes and reaction mechanisms in vanadium redox flow batteries, J. Mater. Chem. A. 3 (2015) 16913–16933. doi:10.1039/C5TA02613J.

[12] A. Fetyan, I. Derr, M.K. Kayarkatte, J. Langner, D. Bernsmeier, R. Kraehnert, C. Roth, Electrospun Carbon Nanofibers as Alternative Electrode Materials for Vanadium Redox Flow Batteries, ChemElectroChem. 2 (2015) 2055–2060. doi:10.1002/celc.201500284.

[13] J. Ryu, M. Park, J. Cho, Catalytic Effects of B/N-co-Doped Porous Carbon Incorporated with Ketjenblack Nanoparticles for All-Vanadium Redox Flow Batteries, J. Electrochem. Soc. 163 (2016) A5144–A5149. doi:10.1149/2.0191601jes.

[14] L. Shi, S. Liu, Z. He, H. Yuan, J. Shen, Synthesis of boron and nitrogen co-doped carbon nanofiber as efficient metal-free electrocatalyst for the VO2+/VO2+ Redox Reaction, Electrochimica Acta. 178 (2015) 748–757. doi:10.1016/j.electacta.2015.08.026.

[15] H.Q. Zhu, Y.M. Zhang, L. Yue, W.S. Li, G.L. Li, D. Shu, H.Y. Chen, Graphite–carbon nanotube composite electrodes for all vanadium redox flow battery, J. Power Sources. 184 (2008) 637–640. doi:10.1016/j.jpowsour.2008.04.016.

[16] M.P. Manahan, Q.H. Liu, M.L. Gross, M.M. Mench, Carbon nanoporous layer for reaction location management and performance enhancement in all-vanadium redox flow batteries, J. Power Sources. 222 (2013) 498–502. doi:10.1016/j.jpowsour.2012.08.097.

[17] M. Park, Y. Jung, J. Kim, H. il Lee, J. Cho, Synergistic Effect of Carbon Nanofiber/Nanotube Composite Catalyst on Carbon Felt Electrode for High-Performance All-Vanadium Redox Flow Battery, Nano Lett. 13 (2013) 4833–4839. doi:10.1021/nl402566s.

[18] G. Merei, S. Adler, D. Magnor, D.U. Sauer, Multi-physics Model for the Aging Prediction of a Vanadium Redox Flow Battery System, Electrochimica Acta. 174 (2015) 945–954. doi:10.1016/j.electacta.2015.06.046.

[19] R. Jervis, L.D. Brown, T.P. Neville, J. Millichamp, D.P. Finegan, T.M.M. Heenan, D.J.L. Brett, P.R. Shearing, Design of a miniature flow cell for in situ x-ray imaging of redox flow batteries, J. Phys. Appl. Phys. 49 (2016) 434002. doi:10.1088/0022-3727/49/43/434002.

[20] A.M. Pezeshki, R.L. Sacci, G.M. Veith, T.A. Zawodzinski, M.M. Mench, The Cell-in-Series Method: A Technique for Accelerated Electrode Degradation in Redox Flow Batteries, J. Electrochem. Soc. 163 (2016) A5202–A5210. doi:10.1149/2.0251601jes.

[21] J.N. Noack, L. Vorhauser, K. Pinkwart, J. Tuebke, Aging Studies of Vanadium Redox Flow Batteries, ECS Trans. 33 (2011) 3–9. doi:10.1149/1.3589916.

[22] M. Skyllas-Kazacos, M. Rychcik, R.G. Robins, A.G. Fane, M.A. Green, New All-Vanadium Redox Flow Cell, J. Electrochem. Soc. 133 (1986) 1057–1058. doi:10.1149/1.2108706.

[23] M. Gattrell, J. Park, B. MacDougall, J. Apte, S. McCarthy, C.W. Wu, Study of the Mechanism of the Vanadium 4+/5+ Redox Reaction in Acidic Solutions, ResearchGate. 151 (2004). doi:10.1149/1.1630594.

[24] W. Wang, X. Fan, J. Liu, C. Yan, C. Zeng, A novel mechanism for the oxidation reaction of VO2+ on a graphite electrode in acidic solutions, J. Power Sources. 261 (2014) 212–220. doi:10.1016/j.jpowsour.2014.03.053.

[25] H. Fink, J. Friedl, U. Stimming, Composition of the Electrode Determines Which Half-Cell's Rate Constant is Higher in a Vanadium Flow Battery, J. Phys. Chem. C. 120 (2016) 15893–15901. doi:10.1021/acs.jpcc.5b12098.

[26] H. Taube, H. Myers, R.L. Rich, Observations on the mechanism of electron transfer in solution, J. Am. Chem. Soc. 75 (1953) 4118–4119. doi:10.1021/ja01112a546.

[27] D.E. Richardson, H. Taube, Mixed-valence molecules: Electronic delocalization and stabilization, Coord. Chem. Rev. 60 (1984) 107–129. doi:10.1016/0010-8545(84)85063-8.

[28] P. Chen, M.A. Fryling, R.L. McCreery, Electron Transfer Kinetics at Modified Carbon Electrode Surfaces: The Role of Specific Surface Sites, Anal. Chem. 67 (1995) 3115–3122. doi:10.1021/ac00114a004.

[29] K.K. Cline, M.T. McDermott, R.L. McCreery, Anomalously Slow Electron Transfer at Ordered Graphite Electrodes: Influence of Electronic Factors and Reactive Sites, J. Phys. Chem. 98 (1994) 5314–5319. doi:10.1021/j100071a023.

[30] R.L.M. Peihong Chen, Control of Electron Transfer Kinetics at Glassy Carbon Electrodes by Specific Surface Modification, Anal. Chem. 68 (1996). doi:10.1021/ac960492r.

[31] Richard C. Alkire, Philip N. Bartlett, Jacek Lipkowski, Electrochemistry of Carbon Electrodes, Wiley, 2015.

[32] M. Becker, N. Bredemeyer, N. Tenhumberg, T. Turek, Polarization curve measurements combined with potential probe sensing for determining current density

distribution in vanadium redox-flow batteries, J. Power Sources. 307 (2016) 826–833. doi:10.1016/j.jpowsour.2016.01.011.

[33] J.T. Clement, D.S. Aaron, M.M. Mench, In Situ Localized Current Distribution Measurements in All-Vanadium Redox Flow Batteries, J. Electrochem. Soc. 163 (2016) A5220–A5228. doi:10.1149/2.0241601jes.

[34] S.-K. Park, J. Shim, J.H. Yang, C.-S. Jin, B.S. Lee, Y.-S. Lee, K.-H. Shin, J.-D. Jeon, The influence of compressed carbon felt electrodes on the performance of a vanadium redox flow battery, Electrochimica Acta. 116 (2014) 447–452. doi:10.1016/j.electacta.2013.11.073.

[35] T.-C. Chang, J.-P. Zhang, Y.-K. Fuh, Electrical, mechanical and morphological properties of compressed carbon felt electrodes in vanadium redox flow battery, J. Power Sources. 245 (2014) 66–75. doi:10.1016/j.jpowsour.2013.06.018.

[36] A. Tang, J. Bao, M. Skyllas-Kazacos, Studies on pressure losses and flow rate optimization in vanadium redox flow battery, J. Power Sources. 248 (2014) 154–162. doi:10.1016/j.jpowsour.2013.09.071.

[37] K. Ngamsai, A. Arpornwichanop, Analysis and measurement of the electrolyte imbalance in a vanadium redox flow battery, J. Power Sources. 282 (2015) 534–543. doi:10.1016/j.jpowsour.2015.01.188.

[38] N. Roznyatovskaya, T. Herr, M. Küttinger, M. Fühl, J. Noack, K. Pinkwart, J. Tübke, Detection of capacity imbalance in vanadium electrolyte and its electrochemical regeneration for all-vanadium redox-flow batteries, J. Power Sources. 302 (2016) 79–83. doi:10.1016/j.jpowsour.2015.10.021.

[39] K. Oh, S. Won, H. Ju, A comparative study of species migration and diffusion mechanisms in all-vanadium redox flow batteries, Electrochimica Acta. (2015). doi:10.1016/j.electacta.2015.03.012.

[40] C. Sun, J. Chen, H. Zhang, X. Han, Q. Luo, Investigations on transfer of water and vanadium ions across Nafion membrane in an operating vanadium redox flow battery, J. Power Sources. 195 (2010) 890–897. doi:10.1016/j.jpowsour.2009.08.041.

[41] T. Sukkar, M. Skyllas-Kazacos, Water transfer behaviour across cation exchange membranes in the vanadium redox battery, J. Membr. Sci. 222 (2003) 235–247. doi:10.1016/S0376-7388(03)00309-0.

[42] X.-G. Yang, Q. Ye, P. Cheng, T.S. Zhao, Effects of the electric field on ion crossover in vanadium redox flow batteries, Appl. Energy. 145 (2015) 306–319. doi:10.1016/j.apenergy.2015.02.038.

[43] Y. Ashraf Gandomi, D.S. Aaron, M.M. Mench, Coupled Membrane Transport Parameters for Ionic Species in All-Vanadium Redox Flow Batteries, Electrochimica Acta. 218 (2016) 174–190. doi:10.1016/j.electacta.2016.09.087.

[44] X. Huang, Y. Pu, Y. Zhou, Y. Zhang, H. Zhang, In-situ and ex-situ degradation of sulfonated polyimide membrane for vanadium redox flow battery application, J. Membr. Sci. (2016). doi:10.1016/j.memsci.2016.09.053.

[45] J.-K. Jang, T.-H. Kim, S.J. Yoon, J.Y. Lee, J.-C. Lee, Y.T. Hong, Highly proton conductive, dense polybenzimidazole membranes with low permeability to vanadium and enhanced H2SO4 absorption capability for use in vanadium redox flow batteries, J. Mater. Chem. A. 4 (2016) 14342–14355. doi:10.1039/C6TA05080H.

[46] X. Li, A.R. dos Santos, M. Drache, X. Ke, U. Gohs, T. Turek, M. Becker, U. Kunz, S. Beuermann, Polymer electrolyte membranes prepared by pre-irradiation induced graft copolymerization on ETFE for vanadium redox flow battery applications, J. Membr. Sci. (2016). doi:10.1016/j.memsci.2016.10.053.

[47] L. Yu, F. Lin, L. Xu, J. Xi, A recast Nafion/graphene oxide composite membrane for advanced vanadium redox flow batteries, RSC Adv. 6 (2016) 3756–3763. doi:10.1039/C5RA24317C.

[48] F. Chen, J. Liu, H. Chen, C. Yan, Study on Hydrogen Evolution Reaction at a Graphite Electrode in the All-Vanadium Redox Flow Battery, Int. J. Electrochem. Sci. 7 (2012).

[49] R. Schweiss, A. Pritzl, C. Meiser, Parasitic Hydrogen Evolution at Different Carbon Fiber Electrodes in Vanadium Redox Flow Batteries, J. Electrochem. Soc. 163 (2016) A2089–A2094. doi:10.1149/2.1281609jes.

[50] A.A. Shah, H. Al-Fetlawi, F.C. Walsh, Dynamic modelling of hydrogen evolution effects in the all-vanadium redox flow battery, Electrochimica Acta. 55 (2010) 1125–1139. doi:10.1016/j.electacta.2009.10.022.

[51] C.-N. Sun, F.M. Delnick, L. Baggetto, G.M. Veith, T.A. Zawodzinski, Hydrogen evolution at the negative electrode of the all-vanadium redox flow batteries, J. Power Sources. 248 (2014) 560–564. doi:10.1016/j.jpowsour.2013.09.125.

[52] W. Zhang, J. Xi, Z. Li, H. Zhou, L. Liu, Z. Wu, X. Qiu, Electrochemical activation of graphite felt electrode for VO2+/VO2+ redox couple application, Electrochimica Acta. 89 (2013) 429–435. doi:10.1016/j.electacta.2012.11.072.

[53] B. Sun, M. Skyllas-Kazacos, Chemical modification of graphite electrode materials for vanadium redox flow battery application—part II. Acid treatments, Electrochimica Acta. 37 (1992) 2459–2465. doi:10.1016/0013-4686(92)87084-D.

[54] B. Sun, M. Skyllas-Kazacos, Modification of graphite electrode materials for vanadium redox flow battery application—I. Thermal treatment, Electrochimica Acta. 37 (1992) 1253–1260. doi:10.1016/0013-4686(92)85064-R.

[55] Y.-R. Shin, S.-M. Jung, I.-Y. Jeon, J.-B. Baek, The oxidation mechanism of highly ordered pyrolytic graphite in a nitric acid/sulfuric acid mixture, Carbon. 52 (2013) 493–498. doi:10.1016/j.carbon.2012.10.001.

[56] T.J. Rabbow, M. Trampert, P. Pokorny, P. Binder, A.H. Whitehead, Variability within a single type of polyacrylonitrile-based graphite felt after thermal treatment. Part I: physical properties, Electrochimica Acta. 173 (2015) 17–23. doi:10.1016/j.electacta.2015.05.020.

[57] T.J. Rabbow, M. Trampert, P. Pokorny, P. Binder, A.H. Whitehead, Variability within a single type of polyacrylonitrile-based graphite felt after thermal treatment. Part II: chemical properties, Electrochimica Acta. 173 (2015) 24–30. doi:10.1016/j.electacta.2015.05.058.

[58] T. Liu, X. Li, H. Nie, C. Xu, H. Zhang, Investigation on the effect of catalyst on the electrochemical performance of carbon felt and graphite felt for vanadium flow batteries, J. Power Sources. 286 (2015) 73–81. doi:10.1016/j.jpowsour.2015.03.148.

[59] A.J. Pak, E. Paek, G.S. Hwang, Impact of Graphene Edges on Enhancing the Performance of Electrochemical Double Layer Capacitors, J. Phys. Chem. C. 118 (2014) 21770–21777. doi:10.1021/jp504458z.

[60] Yuqing Huang, Qi Deng, Xiongwei Wu, Shuangyin Wang, N, O Co-doped carbon felt for high-performance all-vanadium redox flow battery, International Journal of Hydrogen Energy. (2016) 1–9. doi:10.1016/j.ijhydene.2016.04.004.

[61] H. Gerischer, An interpretation of the double layer capacity of graphite electrodes in relation to the density of states at the Fermi level, J. Phys. Chem. 89 (1985) 4249–4251. doi:10.1021/j100266a020.

[62] H. Gerischer, R. McIntyre, D. Scherson, W. Storck, Density of the electronic states of graphite: derivation from differential capacitance measurements, J. Phys. Chem. 91 (1987) 1930–1935. doi:10.1021/j100291a049.

[63] S. Rudolph, U. Schröder, I.M. Bayanov, S. Hage-Packhäuser, “Unexpected” behaviour of the internal resistance of a vanadium redox flow battery, J. Power Sources. 306 (2016) 394–401. doi:10.1016/j.jpowsour.2015.11.107.

[64] K.H. Kim, B.G. Kim, D.G. Lee, Development of carbon composite bipolar plate (BP) for vanadium redox flow battery (VRFB), Compos. Struct. 109 (2014) 253–259. doi:10.1016/j.compstruct.2013.11.002.

[65] E. Agar, C.R. Dennison, K.W. Knehr, E.C. Kumbur, Identification of performance limiting electrode using asymmetric cell configuration in vanadium redox flow batteries, J. Power Sources. 225 (2013) 89–94. doi:10.1016/j.jpowsour.2012.10.016.

[66] C.A. McDermott, K.R. Kneten, R.L. McCreery, Electron transfer kineticss of aquated Fe +3/+2 , Eu +3/+2 , and V +3/+2 at carbon electrodes: inner sphere catalysis by surface oxides, J. Electrochem. Soc. 140. (1993).

[67] J. Friedl, U. Stimming, Determining Electron Transfer Kinetics at Porous Electrodes, Electrochimica Acta. 227 (2017) 235–245. doi:10.1016/j.electacta.2017.01.010.

[68] J. Melke, P. Jakes, J. Langner, L. Riekehr, U. Kunz, Z. Zhao-Karger, A. Nefedov, H. Sezen, C. Wöll, H. Ehrenberg, C. Roth, Carbon materials for the positive electrode in all-vanadium redox flow batteries, Carbon. 78 (2014) 220–230. doi:10.1016/j.carbon.2014.06.075.

[69] H. Liu, Q. Xu, C. Yan, Y. Qiao, Corrosion behavior of a positive graphite electrode in vanadium redox flow battery, Electrochimica Acta. 56 (2011) 8783–8790. doi:10.1016/j.electacta.2011.07.083.

[70] J.-G. Oh, W.H. Lee, H. Kim, The inhibition of electrochemical carbon corrosion in polymer electrolyte membrane fuel cells using iridium nanodendrites, Int. J. Hydrog. Energy. 37 (2012) 2455–2461. doi:10.1016/j.ijhydene.2011.10.072.

[71] A.J. Bard, R. Parsons, J. Jordan, Standard Potentials in Aqueous Solution, CRC Press, 1985.

[72] S. Litster, G. McLean, PEM fuel cell electrodes, J. Power Sources. 130 (2004) 61–76. doi:10.1016/j.jpowsour.2003.12.055.

[73] P. Sehrawat, C. Julien, S.S. Islam, Carbon nanotubes in Li-ion batteries: A review, Mater. Sci. Eng. B. 213 (2016) 12–40. doi:10.1016/j.mseb.2016.06.013.

[74] V.F. Lvovich, Impedance Spectroscopy: Applications to Electrochemical and Dielectric Phenomena, Wiley, 2012.

[75] D.J. Suárez, Z. González, C. Blanco, M. Granda, R. Menéndez, R. Santamaría, Graphite felt modified with bismuth nanoparticles as negative electrode in a vanadium redox flow battery, ChemSusChem. 7 (2014) 914–918. doi:10.1002/cssc.201301045.

[76] D. Johnson, ZViewTM Tutorial - Kramers-Kronig Transformations, (n.d.).

[77] Li Wang, Jishi Zhao, Xiangming He, *, Jian Gao, Jianjun Li, Chunrong Wan, Changyin Jiang, Electrochemical Impedance Spectroscopy (EIS) Study of LiNi 1/3 Co 1/3 Mn 1/3 O 2 for Li-ion Batteries, Int. J. Electrochem. Sci. 7 (2012) 345–353.

[78] Xiao-Zi Riny Yuan, Electrochemical Impedance Spectroscopy in PEM Fuel Cells, Springer, 2010.

[79] Z. Brytan, J. Niagaj, L. Reiman, Corrosion studies using potentiodynamic and EIS electrochemical techniques of welded lean duplex stainless steel UNS S82441, Appl. Surf. Sci. 388, Part A (2016) 160–168. doi:10.1016/j.apsusc.2016.01.260.

[80] A. Di Blasi, O. Di Blasi, N. Briguglio, A.S. Aricò, D. Sebastián, M.J. Lázaro, G. Monforte, V. Antonucci, Investigation of several graphite-based electrodes for vanadium redox flow cell, J. Power Sources. 227 (2013) 15–23. doi:10.1016/j.jpowsour.2012.10.098.

[81] J. Langner, M. Bruns, D. Dixon, A. Nefedov, C. Wöll, F. Scheiba, H. Ehrenberg, C. Roth, J. Melke, Surface properties and graphitization of polyacrylonitrile based fiber electrodes affecting the negative half-cell reaction in vanadium redox flow batteries, J. Power Sources. 321 (2016) 210–218. doi:10.1016/j.jpowsour.2016.04.128.

[82] J. Michael Hollas, Modern Spectroscopy, 4th ed., Wiley, 2003.

[83] B. Li, M. Gu, Z. Nie, Y. Shao, Q. Luo, X. Wei, X. Li, J. Xiao, C. Wang, V. Sprenkle, W. Wang, Bismuth Nanoparticle Decorating Graphite Felt as a High-Performance Electrode for an All-Vanadium Redox Flow Battery, Nano Lett. 13 (2013) 1330–1335. doi:10.1021/nl400223v.

[84] G. Wei, X. Fan, J. Liu, C. Yan, Electrospun carbon nanofibers/electrocatalyst hybrids as asymmetric electrodes for vanadium redox flow battery, J. Power Sources. 281 (2015) 1–6. doi:10.1016/j.jpowsour.2015.01.161.

[85] Z. González, A. Sánchez, C. Blanco, M. Granda, R. Menéndez, R. Santamaría, Enhanced performance of a Bi-modified graphite felt as the positive electrode of a vanadium redox flow battery, Electrochem. Commun. 13 (2011) 1379–1382. doi:10.1016/j.elecom.2011.08.017.

Included publications reprints (with permission)

Degradation of all-vanadium redox flow batteries (VRFB) investigated by electrochemical impedance and X-ray photoelectron spectroscopy: Part 2 electrochemical degradation

Abstract

Electrochemical degradation (ED) of carbon felt electrodes was investigated by cycling of a flow through all-vanadium redox flow battery (VRFB) and conducting half-cell measurements with two reference electrodes inside the test bench. ED was detected using half-cell and full-cell electrochemical impedance spectroscopy (EIS) at different states of charge (SOC). Reversing the polarity of the battery to recover cell performance was performed with little success. Renewing the electrolyte after a certain amount of cycles restored the capacity of the battery. X-ray photoelectron spectroscopy (XPS) reveals that the amount of surface functional increases by more than a factor of 3 for the negative side as well as for the positive side. Scanning electron microscope (SEM) images show a peeling of the fiber surface after cycling the felts, which leads to a loss of electrochemically active surface area (ECSA). Long term cycling shows that ED has a stronger impact on the negative half-cell [V(II)/V(III)] than the positive half-cell [V(IV)/V(V)] and that the negative half-cell is the rate-determining half-cell for the VRFB.

Reference:

I. Derr, M. Bruns, J. Langner, A. Fetyan, J. Melke, C. Roth, Degradation of all-vanadium redox flow batteries (VRFB) investigated by electrochemical impedance and X-ray photoelectron spectroscopy: Part 2 electrochemical degradation, J. Power Sources 325 (2016) 351–359, doi:10.1016/j.jpowsour.2016.06.040.

https://doi.org/10.1016/j.jpowsour.2016.06.040

Electroless chemical aging of all-Vanadium Redox Flow batteries (VRFB) investigated by Electrochemical Impedance and X-ray Photoelectron Spectroscopy

Igor Derr[1*], Daniel Przyrembel[2], Jakob Schweer[1], Abdulmonem Fetyan[1], Joachim Langner[3], Julia Melke[1], Martin Weinelt[2], Christina Roth[1]

[1] *Institute for Chemistry and Biochemistry, Freie Universität Berlin, Takustr. 3, D-14195 Berlin*

[2] *Institute for Experimental Physics, Freie Universität Berlin, Arnimallee 14, 14195 Berlin*

[3] *Institute for Applied Materials (IAM), Karlsruhe Institute of Technology (KIT), Hermann-von-Helmholtz-Platz 1, D-76344 Eggenstein*

* Corresponding author. E-mail: igor.derr@fu-berlin.de ; Phone: +49-30-838-65297. *Manuscript has been submitted to Electrochimica Acta.*

Keywords: Vanadium, VRFB, aging, EIS, XPS, carbon electrode

Abstract

Electroless chemical aging of commercially available, porous carbon felt electrodes for the all-vanadium redox flow battery (VRFB) was investigated by full-cell and half-cell measurements in a beaker and a cell with flow-through geometry at different states of charge and different temperatures. Changes in the charge transfer resistance and the double layer capacitance due to chemical aging were determined by electrochemical impedance spectroscopy (EIS) and correlated with ex-situ X-ray photoelectron spectroscopy (XPS). EIS measurements revealed that the aging of the carbon electrodes was dependent on the temperature for low vanadium concentration and independent of the temperature for high vanadium concentration. This indicates that the electroless aging of the electrodes happens due to a chemical reaction with the sulfuric acid and with the vanadium. XPS measurements revealed that after 8 days of mere contact with electrolyte the amount of surface functional groups on the carbon felt electrodes increased by factors of 1.5 to 1.8 and that the conducting sp^2-hybridized layer was diminished by a factor of 2 or more. Furthermore, the negative half-cell [V(II)/V(III)] is more strongly affected by chemical aging than the positive half-cell [V(IV)/V(V)]. Electroless aging was found to be inevitable for the used carbon felts.

Introduction

Redox flow batteries (RFBs) are a very promising technology for the storage of only intermittently available, excess renewable energy. The largest advantage compared to other energy storage

systems like Li-ion batteries is the storage of energy in an aqueous electrolyte [1]. The capacity of a RFB system only depends on the volume and concentration of its electrolyte, whereas the power output depends on the size and the amount of cells used for the conversion of different electroactive species. RFBs are supposed to have a very long lifetime of more than 10,000 cycles or 10 years. Because the electrical energy is being stored in the aqueous electrolyte, no phase transitions are involved which could be incomplete and lead to irreversible losses. The electrodes for flow-through geometry usually are porous carbon felts with a large surface area. In most cases these felts are activated chemically or thermally, which increases their wettability [2,3] and oxidizes unwanted residues from the manufacturing process [4]. Carbon is the most prominent electrode material because it is cheap and more corrosion-resistant compared to stainless steel or other non-noble metals that would be suitable for large-scale applications [5]. Another significant advantage of carbon is the high overpotential towards the hydrogen evolution reaction (HER) which is one possible side reaction in the negative half-cell [6,7]. The electrolyte usually contains 2-5 mol/L of sulfuric acid which will oxidize the carbon felts chemically without applying a current or voltage [3]. This effect is inevitable and will be referred to as chemical aging (CA). However, so far literature on the aging of VRFBs is scarce and the effects that cause performance loss in RFBs are still being discussed [8,9]. Nevertheless, any change of the carbon felt surface might induce a change in the performance. One possible factor might be the coverage of oxygen functional groups on the electrode, which can either increase due to oxidation or decrease due to reduction of the carbon surface [10]. Moreover, also changes in the sp^2/sp^3 ratio of the carbon surface were observed to affect the charge transfer at the positive half-cell [11].

In this work we studied the electroless aging of the carbon felt electrodes by soaking them in electrolyte for a defined period of time at a certain temperature. In order to investigate the possible static performance degradation of the electrode, membrane, and electrolyte we introduced a protocol including electrochemical impedance spectroscopy (EIS) measurements for the full-cell and both half-cells. EIS measurements are used to monitor changes in the contact resistance (R_u), double layer capacitance and charge transfer resistance (CTR, R_{ct}) [12]. One of the largest advantages of EIS compared to the more readily applied cyclic voltammetry is the low current/voltage that is applied during the measurement, so that side reactions like the HER can be neglected. Additionally, ex-situ X-ray photoelectron spectroscopy (XPS) was used to reveal changes of the carbon felt surface with respect to the amount of functional groups over time. The obtained results can be used to understand the processes, which occur when the carbon felts are brought into prolonged contact with the acidic electrolytes, and help in developing more stable electrode materials for VRFBs.

Experimental

Chemical aging experiment

The first experiments were performed in a small electrochemical cell (Figure 1 b)) with a three-electrode setup and an electrolyte volume of 16 mL. Both the working (5x5x6 mm^3) and the counter electrode (25x10x6 mm^3) were GFA6 carbon felts (SGL Carbon, Germany). The carbon felt (CF) was heat-treated for 25 h at 400 °C in air atmosphere. The reference electrode was a saturated calomel electrode (SCE) with 220 mV vs. a standard hydrogen electrode (SHE).

<u>Beaker experiments</u>

18 samples have been investigated with electrochemical impedance spectroscopy (EIS) under different aging conditions. In each case at least three samples were measured under the same conditions. In the first measuring series the CF's were immersed in pure 2 M H_2SO_4 at room temperature and 40 °C for 10 to 30 days. Each day EIS measurements were conducted in fresh, pure 2 M H_2SO_4 at room temperature. In the second and third measuring series the electrolytes were 0.16 M V(III) with 2 M H_2SO_4 and 1.6 M V(III) with 2 M H_2SO_4 instead of pure H_2SO_4. Therefore the EIS measurements were conducted in the respective electrolyte solution at room temperature. The vanadium electrolyte was purchased from GfE (Germany) and initially consisted of 2 M H_2SO_4, 0.05 M H_3PO_4 and 1.6 M V(III)/V(IV) with an oxidation state of +3.5. The V(III) solution was prepared by charging the 1.6 M vanadium electrolyte with a 50 cm^2 flow by cell in a Scribner 857 test bench (Scribner Associates Inc., USA). The V(III) electrolyte was kept under argon and nitrogen atmosphere during the measurements in order to prevent oxidation of V(III) to V(IV). EIS measurements were performed with an AC voltage of 10 mV in a frequency range between 100 kHz and 10 mHz. The DC voltage was set to 0 V vs. SCE for the measurements in pure H_2SO_4 to ensure that the maximum double layer capacitance can be accessed in the low-frequency region. For the V(III) containing electrolytes the DC voltage was set to -0.4 V vs. SCE because at this potential only a slow reduction of V(III) can be expected.

Flow cell experiment

For the second experiment the VRFB test bench, Scribner 857, was used to operate a Micro flow cell® (Electrocell, Denmark) with a flow-through design and a cation exchange membrane in series with a 50 cm^2 flow cell with a flow-by geometry equipped with an anion exchange membrane as shown in Figure 1 a). The cation exchange membrane was a Nafion® 117 membrane by DuPont that was used as received. The chemical aging (CA) was determined for the Micro flow cell® whereas the charging of the electrolyte was done using the large flow-by cell. The latter was needed to maintain the state of charge (SOC) throughout the experiment without electrochemically stressing the electrodes in the Micro flow cell®. Two different types of membrane (anion and cation exchange) were used to minimize concentration gradients and prevent an imbalance of water between both half-cells. As electrolyte for each side 100 mL commercially available GfE electrolyte were used. The positive and negative electrolyte tanks contained a magnetic stirrer and were purged with 30 mL/min nitrogen throughout the experiment. Furthermore, two Ag/AgCl (3 M KCl, 215 mV vs. SHE) reference electrodes (Metrohm) were positioned at the inlet of the Micro flow cell® forming a Luggin capillary-like setup with the current-collector plate (glassy carbon) as described by Langner et al. [13]. EIS measurements were conducted against the Ag/AgCl reference electrodes with either a Gamry 600 or a Gamry 3000 potentiostat.

The Micro flow cell® was equipped with carbon felts, GFA6 (SGL Carbon SE), which had been activated thermally at 400° C for 25 h in air atmosphere. The 10 cm^2 (sample: C1000) felts were mounted in the cell (20%-30% compression rate [14,15]). Glassy carbon Sigradur G current collectors by Hochtemperatur-Werkstoffe GmbH were used for optimal electrochemical stability and a leakage-free setup. As gasket materials Teflon and Viton were used.

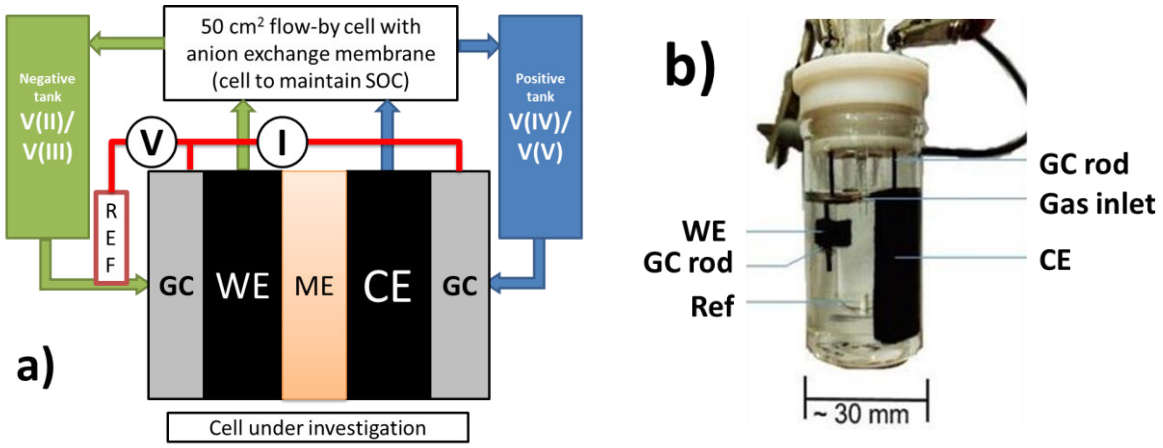

Figure 1. Schematic of both setups that were used.

a) Schematic of the setup with two cells in series. REF: Ag/AgCl reference electrodes, GC: glassy carbon current collector plates, WE: working electrode (carbon felt electrode), CE: counter electrode (carbon felt electrode) and ME: Nafion® 117 membrane. The operating cell (below) had a 10 cm^2 electrode surface area. The second cell (above, 50 cm^2) was used for charging and discharging procedures before every half-cell measurement in the operating cell.

b) Three-electrode setup with carbon felt working (WE) and counter (CE) electrode. The reference (Ref) electrode was a SCE with 230 mV vs. SHE. The carbon felts were pulled over glassy carbon (GC) rods.

The electrolyte was initially charged to a SOC of 50 % (1.4 V open circuit voltage (OCV) [16]) and was kept in the system for 8 days. Each day the SOC had to be adjusted with the large flow-by cell due to self-discharge (crossover of Vanadium). Every 24 h for 8 days throughout the experiment, EIS measurements have been carried out. An AC voltage of 10 mV was applied with a frequency range between 100 kHz to 10 mHz. The DC voltage was set to 0 mV (vs. the OCP of the Ref) in general. In addition to the EIS measurements also XPS measurements were carried out on three kinds of samples: The electrode felt after heat treatment in air (C1000) and felts from the positive (C1000 p) and negative (C1000 n) half-cell after chemical aging for 8 days as described above.

Table 1 gives an overview of the chemical aging experiment and the used samples.

Table 1. Nomenclature for the chemical aging experiments (CA).

Sample name	Description
H_2SO_4-Tx	Experiment in pure H_2SO_4 with 0.25 cm^2 electrode, for the corresponding temperature (Tx).
0.16M-Tx	Experiment in 0.16 M V(III) and 2 M H_2SO_4 with 0.25 cm^2 electrode, for the corresponding temperature (Tx).
1.6M-Tx	Experiment in 1.6 M V(III) and 2 M H_2SO_4 with 0.25 cm^2 electrode, for the corresponding temperature (Tx).
C1000 d	Experiment in 1.6 M V(III) and 2 M H_2SO_4 with 10 cm^2 electrodes in SOC 50 % solution at room temperature, for the corresponding day (d).
C1000 p	Sample from the positive half-cell
C1000 n	Sample from the negative half-cell

The EIS data were fitted with the equivalent circuits shown in Figure 2. R_U is the solution/contact resistance, CPE_{DL} and R_{ct} stand for the double layer capacitance and the charge transfer resistance (CTR) of the faradaic arc in the medium-frequency region. The Warburg part W_o describes the mass

transport limited diffusion effects in the low-frequency region. Constant phase elements (CPE) were used for fitting the capacitive parts instead of ideal capacitors, because the penetration depth of the voltage and the current response vary due to the porosity and the inhomogeneity of the carbon felt, which results in non-ideal semi-circles. The capacitance was calculated from the CPE parameters [17,18].

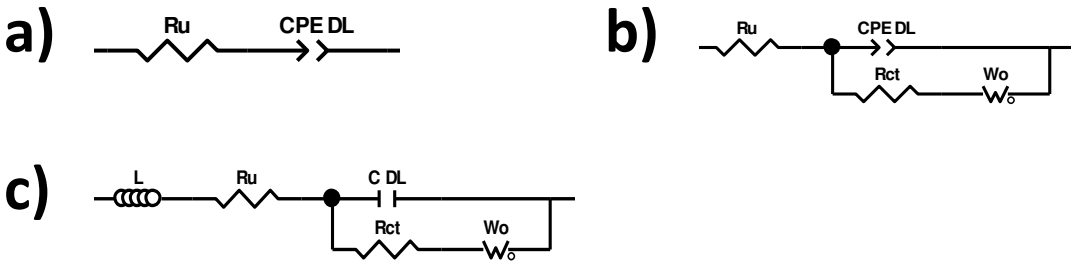

Figure 2. Electrical circuits used for fitting the data in Figure 3 and Figure 4.

- **a) Circuit used for estimating the double layer capacitance in Figure 3 a) . R_u: contact resistance, CPE_{DL}: double layer capacitance.**
- **b) Circuit used for estimating the charge transfer resistance in Figure 3 b). R_u: contact resistance, CPE_{DL}: double layer capacitance, R_{ct}: charge transfer resistance, W_0: Warburg diffusion.**
- **c) Circuit used for estimating the charge transfer resistance in Figure 4 a). L: inductance R_u: contact resistance, C_{DL}: Double layer capacitance, R_{ct}: charge transfer resistance, W_0: Warburg diffusion.**

XPS measurements

XPS measurements were carried out in an ultrahigh vacuum (UHV) apparatus (base pressure during measurements below $3 \cdot 10^{-10}$ mbar). The setup comprised an all-mu-metal chamber fitted with a monochromatized Al-$K_{\alpha l}$ X-ray source (VG Scienta MX 650; 1486.7 eV, line focus of ca. 3 x 8 mm^2) along with a high-resolution electron analyzer (VG Scienta SES-200 u), allowing for a spectral resolution below 300 meV, and a quick-load lock with a sample garage for fast sample changes *in vacuo*. The binding energies were referenced to an Au(111) sample (Au $4f_{7/2}$ peak at 83.96 eV [19] with a FWHM of 0.48 eV) and are correct within 50 meV. The samples were mounted on molybdenum sample holders (SPECS SH 2/12) using UHV-compatible double-sided adhesive carbon tape (Plano GmbH) providing a sufficiently high electrical conductivity to make additional charge compensation unnecessary. Sample pieces from the electrode felts with dimensions of 10x10x2 mm^3 were cut after rinsing them with copious amounts of DI water and letting them dry thoroughly in air atmosphere before the transfer into UHV. Measurements were carried out with the X-ray source operating with an excitation power of 450 W (15 KV, 30 mA). The samples were positioned for perpendicular take-off geometry. Spectra were recorded in constant analysis energy (CAE) mode with an analyzer pass energy of 200 eV and a curved entrance slit of 0.2 mm width to achieve high resolution along with a large signal-to-noise ratio. Beside survey spectra to check the overall sample composition, detailed spectra have been measured of the most intense peaks for the elements of interest, carbon (C 1s) and oxygen (O 1s), and of sulfur (S 2p). O 1s and S 2p spectra were evaluated using backgrounds of the Shirley type [20]. For the C 1s spectra Tougaard-type backgrounds [21] were employed to account for and preserve the shake-up peak structure present in the long inelastic loss tail on the high-binding-energy side [22]. The spectra were decomposed using symmetric Voigt-profile peaks, only the C 1s signal intensity ascribed to graphite-like sp^2 hybridized carbon species was fitted using an asymmetric pseudo-Voigt profile [23].

Results and discussion

Electrochemical analysis

In Figure 3 a) the double layer capacitances (DLC) of the felts that were kept in 2 M sulfuric acid at room temperature and 40 °C for 12-30 days are shown. The data were fitted with the equivalent circuit shown in Figure 2 a). The initial capacitance differs for each sample because the heat-treatment of the felts was performed on different days and therefore the initial surface properties might vary due to differing air atmosphere conditions. The capacitance was normalized to the mass of the felt, which was between 11-13 mg.

The exposure of the felt to the sulfuric acid led to a decrease of the double layer capacitance for both temperatures. Both experiments exhibited two regions with different slopes for the linear decrease of the capacitance. It seems that the electroless aging of the felts took place at a faster rate during the first 5 days. After the 5th day the slope decreased. The overall decrease of the capacitance for the samples at room temperature and 40 °C was ~40 % and ~60 %, respectively after 12 days. The sample that was kept at room temperature was measured again after an exposure time of 30 days. The capacitance fade was ~60 % compared to the first day of the experiment. The sample that was kept at 40 °C aged at a faster rate according to the slopes and the capacitance fade after 12 days. These results show that a chemical reaction takes place on the carbon surface.

In Figure 3 b) the felts were exposed to 0.16 M V(III) with 2 M sulfuric acid at room temperature and 40 °C for 12 days. The charge transfer resistance (CTR) towards the V(III) reduction was measured each 24 h. The EIS data were fitted with the circuit shown in Figure 2 b). The charge transfer resistances showed similar (but inverse) behavior as the capacitance measurements in Figure 3 a). The charge transfer resistance increased with time. The plot can be divided into two regions with different slopes. The first 5 days exhibit a higher slope for both temperatures compared to the remaining 7 days. The CTRs of the room temperature samples did not increase significantly after 5 days. The overall increase of the CTRs was ~85 % and a factor of ~4 for the room temperature and 40 °C samples, respectively after 12 days. The aging rate again was promoted by an elevated temperature indicating a chemical reaction.

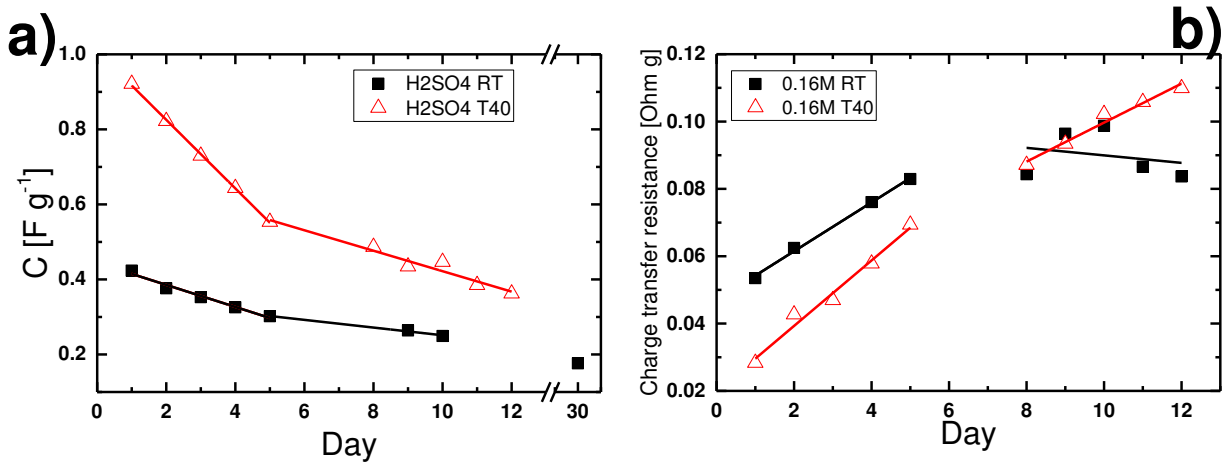

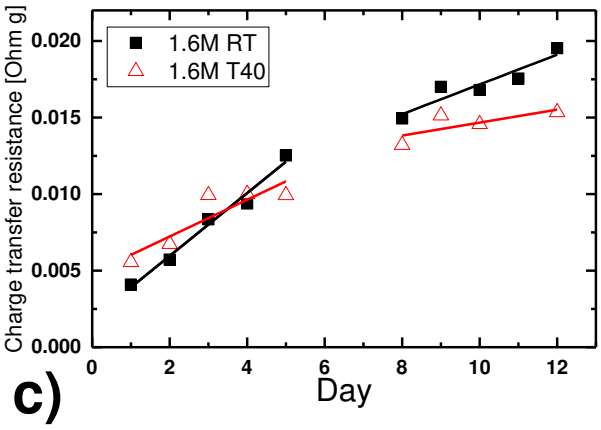

Figure 3. Double layer capacitance and charge transfer resistance plots of the chemical aging experiments at different temperatures. The values have been normalized to the mass of the felts.

- **a) Normalized double layer capacitance for the chemical aging (CA) experiment in pure, 2 M H_2SO_4 at room temperature (RT) and 40 °C (T40) for the corresponding day.**
- **b) Normalized charge transfer resistance for the chemical aging (CA) experiment in 0.16 M V(III) with 2 M H_2SO_4 at room temperature (RT) and 40 °C (T40) for the corresponding day.**
- **c) Normalized charge transfer resistance for the chemical aging (CA) experiment in 1.6 M V(III) with 2 M H_2SO_4 at room temperature (RT) and 40 °C (T40) for the corresponding day.**

In Figure 3 c) the CTRs of the felts exposed to 1.6 M V(III) with 2 M sulfuric acid for 12 days are shown. The CTRs increased with time for both samples. Again the plot is divided into two regions with different slopes. The first 5 days exhibit a higher rate of aging compared to the remaining 7 days. But in this case the sample at 40 °C showed a slower aging rate compared to the room temperature sample. For the 1.6 M V(III) electrolyte the estimation of the CTRs was more difficult, because of the polarization of the electrode and the GC substrate in the high-frequency region. The high-frequency time constant was much more dominant compared to the CTR arc. Therefore, the CTRs had a higher overall error. Nevertheless, the development of all 6 samples that were measured (not shown here) showed similar behavior comparing the different temperatures. The CTRs increased by a factor of ~3.1-4.8 and ~2.0-2.8 for the sample at room temperature and 40 °C, respectively after 12 days. This indicates that not only the sulfuric acid participates in the alteration of the carbon surface, but also the vanadium itself.

The electroless aging of the CFs did not only depend on the temperature, but also on the concentration of the V(III) species. The capacitance of the felts decreased with increasing temperature in pure, 2 M sulfuric acid. For lower concentration of V(III) the CTRs towards V(III) reduction reaction increased with temperature. At higher V(III) concentrations the aging rate at room temperature was higher compared to the samples at 40 °C. All experiments exhibit a degradation of the carbon felt indicating a chemical reaction of the carbon felt with both the sulfuric acid as well as the vanadium. The role of vanadium is not clear yet. If a V(III) solution is stored under nitrogen atmosphere the OCP will still change towards more positive potentials with time. This indicates the formation of V(IV). Either this happens due to an oxidation with oxygen, which diffuses into the sealed sample container or it could be possible that a comproportionation reaction of V(III) takes place. This would lead to the formation of V(II) and V(IV). V(II) is a strong reducing agent, which is e.g. capable of reducing H_3O^+ to hydrogen [24] or cause a reduction of the carbon surface.

The experimental conditions in a beaker do not exactly correspond to conditions that would be found in a flow cell. It is also not possible to monitor and control the concentration of different vanadium species. Therefore, a second experiment at room temperature with a setup according to Figure 1 a) was performed. Two separate cells were used in series. In the first cell the chemical aging experiment was performed, while the second cell was used to charge the electrolyte and maintain the state of charge (SOC) throughout the experiment. The advantages of using a flow cell are the constant compression rate, a continuous contact between the GC substrate and the felt and a precise control of the electrolyte concentration, since the system is closed and filled with nitrogen.

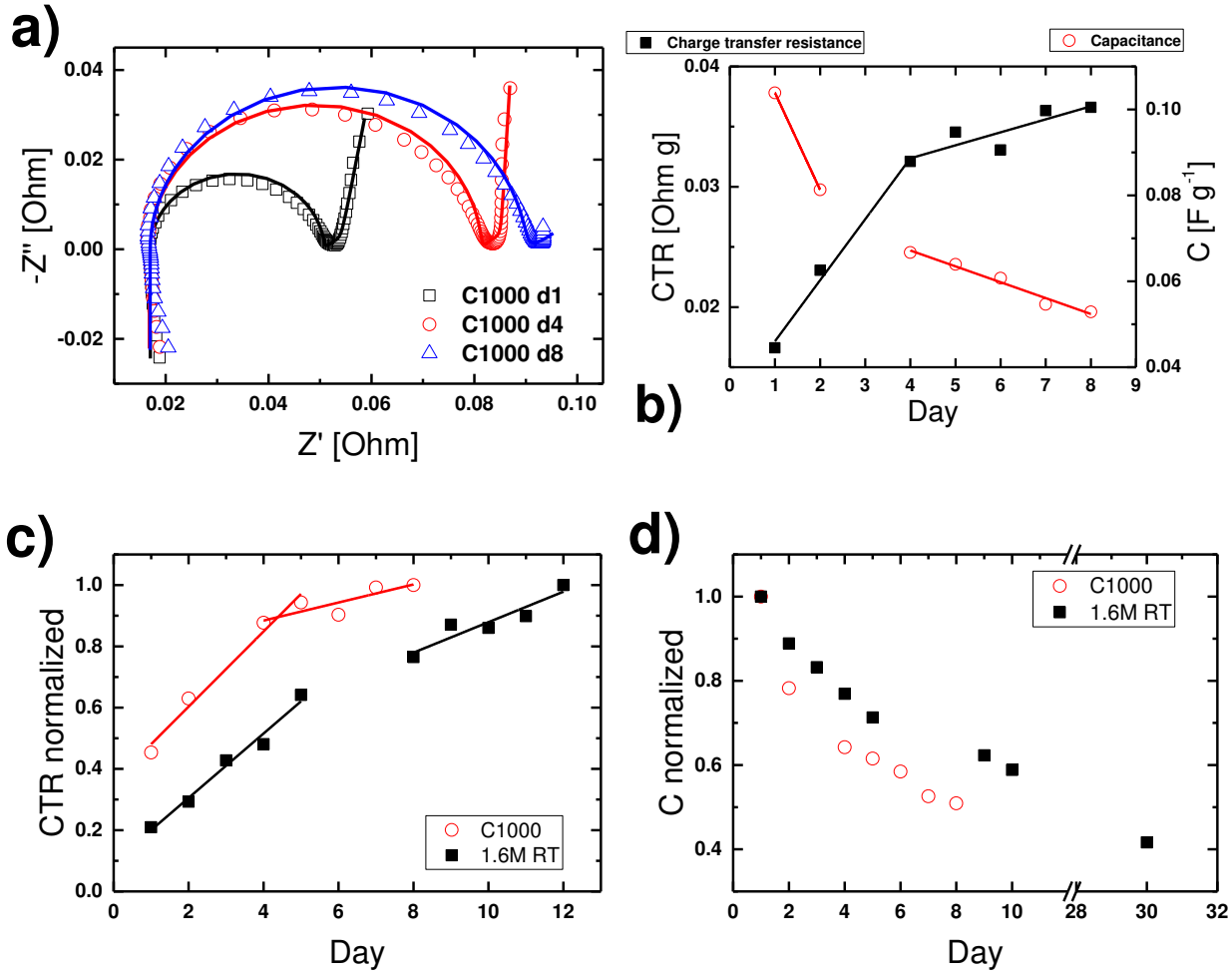

Figure 4. Second chemical aging experiment with 10 cm^2 electrodes (C1000), at room temperature in a flow-through cell. The electrolyte was 1.6 M vanadium and 2 M sulfuric acid at a SOC of 50 %. A second cell was used for charging and maintaining the SOC (Figure 1 a)).

- **a) Nyquist plots of C1000 sample (10 cm^2) recorded as a function of time, dots: recorded data, solid lines: associated fits.**
- **b) Fitting results of C1000 for the charge transfer resistance and the double layer capacitance. The values were normalized to the electrode mass.**
- **c) The charge transfer resistance of the first experiment at room temperature and 1.6 M vanadium (Figure 3 c)) normalized to 1 and compared to the normalized CTR of the second experiment (C1000).**
- **d) Double layer capacitance of the first experiment at room temperature and pure sulfuric acid (Figure 3 a)) normalized to 1 and compared to the normalized DLC of the second experiment (C1000)..**

The second chemical aging experiment was performed with 10 cm^2 electrodes (C1000) at a SOC of 50 % in a flow-through cell (see Figure 1 a)). In Figure 4 a) Nyquist plots of the first, fourth and eighth day are shown. The CTR increased from 16 mΩ g on the first day to 36 mΩ g on the eighth day. The

data were fitted with the equivalent circuit shown in Figure 2 c). For this experiment an ideal capacitor (C_{DL}) could be used to describe the capacitive part of the faradaic arc, because the semi-circle was almost ideal (CPE alpha parameter > 0.95). The Nyquist plots show a high-frequency inductive contribution followed by a semi-circle that represents the faradaic process and a low-frequency tail which appears due to diffusion effects. The inductive part did not appear for the smaller samples in Figure 3, because for smaller electrode size the current response is much lower compared to the 10 cm^2 electrodes.

In Figure 4 b) the calculated values for the CTR and the DLC are shown for 8 days. As the CTR increased from 16 mΩ g to 36 mΩ g, the DLC decreased from 103 mF g^{-1} to 53 mF g^{-1}. The increase of the CTR was similar to the first experiment (Figure 3). After 4 days of mere contact with electrolyte the CTR has increased by almost a factor of 2. After the 4^{th} day the aging rate decreased significantly until the 8^{th} day.

In Figure 4 c) the charge transfer resistances of the first experiment at room temperature and 1.6 M V(III) (Figure 3 c)) were normalized and compared to the normalized CTRs of the second experiment in the flow cell. The first 5 days exhibit almost identical aging rates even though the absolute values vary. After the 5^{th} day the aging rate decreased for both experiments. The variation of the total values is ascribed to different heat-treatment dates and different setups. The initial felt properties may vary due to different air atmosphere conditions during heat treatment. Also the compression and contact of the felt vary due to the setup.

In Figure 4 d) the double layer capacitance of the first experiment at room temperature and 2 M sulfuric acid (Figure 3 a)) were normalized and compared to the normalized DLCs of the second experiment in the flow cell. The DLC in the flow cell showed a more pronounced exponential decay after 8 days already, while the DLC in pure sulfuric acid decreased slower. This implies the participation of the vanadium in the aging process, which was also observed for the experiments in Figure 3 c).

A decreasing DLC can be explained by a loss of electrochemically active surface area (ECSA), a decrease of the density of states (DOS) [25,26], or a change of electrolyte composition [27]. A decrease in the ECSA can occur due to a loss of oxygen functional groups as they oxidize to gaseous CO or CO_2 leaving behind non-conductive sp^3-hybridized carbon on the surface of the felt. This leads to a decreased wettability and reduced conductivity of the carbon surface. A loss of functional groups would also cause a decrease of the DOS [28]. Because H_2SO_4 is able to oxidize the carbon surface, there should be more functional groups after the experiment. If this argument holds, then the DOS should not be the limiting factor, since it increases with additional functional groups. The additional functional groups would lead to an increase of the DLC [29]. In our experiment, a decrease of the DLC was observed indicating either decreases of the ECSA due to CO and CO_2 evolution or changes of the electrolyte composition. The effect of the electrolyte on the DLC can be neglected for the measurements in Figure 3 a) because it was pure sulfuric acid. However, for the measurements in the flow-cell, the effect of the electrolyte cannot be neglected because the electrolyte also contained vanadium. The imbalance of the electrolyte does not only affect the vanadium concentration in the half-cells but also the H_3O^+ concentration, which changes during charge operation due to the reaction of V(III) to V(IV) and V(IV) to V(V) in the positive half-cell. The imbalance of the electrolyte had an impact on the DLC, but was not the dominant contribution, since the samples in Figure 3 a)

exhibited a similar trend in the DLC decay. Therefore, the changes of the CF surface properties were the dominant contribution.

The overall DLCs were larger for the smaller samples. The difference of the electrode size and setups resulted in a CTR that was in general smaller by a factor of 10 for C1000 compared to the small samples in Figure 3, even though the geometric surface area and mass differed by a factor of ~40. The influence of the geometric surface area on the CTR has been reported by Friedl et al. [30]. The relationship between mass/geometric size and DLC or R_{ct}^{-1} should be linear. The overall impedance of C1000 samples in the flow cell was higher than that of the small samples (Figure 3 a-c) if all values are normalized to the mass. The reasons for this are the differences of the electrode size to the ECSA ratio, the setup conditions and different electrolyte concentrations. E.g. if the electrode in the flow cell is compressed by ~30 % than this might lead to a lower DLC compared to the uncompressed felt in the 3-electrode setup. All EIS fitting results can be found in Table 2.

Table 2. Fitting results for the EIS data in Figure 3 and Figure 4. The calculated values have an error of ±20 %.

	H_2SO_4 RT	H_2SO_4 T40	C1000	0.16M RT	0.16M T40	1.6M RT	1.6M T40	C1000
Day	C [mF g^{-1}]	C [mF g^{-1}]	C [mF g^{-1}]	CTR [mΩ g]	CTR [mΩ g]	CTR [mΩ g]	CTR [mΩ g]	CTR [mΩ g]
1	423.6	921.3	103.9	53.5	28.3	4.1	5.6	16.6
2	376.5	822.2	81.3	62.4	42.7	5.7	6.7	23.1
3	352.6	729.6			46.9	8.4	9.9	
4	325.8	643.7	66.7	76.1	57.8	9.4	10.0	32.1
5	302.1	553.4	63.9	82.9	69.4	12.5	9.9	34.5
6			60.7					33.1
7			54.6					36.3
8		486.6	52.9	84.4	87.1	14.9	13.2	36.6
9	264.0	434.5		96.4	93.4	17.0	15.1	
10	249.3	446.8		98.8	102.2	16.8	14.6	
11		385.1		86.6	105.8	17.6		
12		362.3		83.7	109.9	19.5	15.3	
30	176.4							

XPS analysis

From XP survey spectra (see supporting online material) the elemental composition of the samples was obtained. As expected the pristine felt after heat treatment in air (C1000) consisted of only carbon and oxygen species. The samples from the two felts used in the positive (C1000 p) and negative half-cells (C1000 n) contained in addition small amounts of sulfur and vanadium species. Further constituents, especially phosphorus species, have not been observed. Carbon, oxygen and sulfur signals of the spectra have been investigated in detail. The XP spectra measured at the carbon 1s edge are shown in Figure 5.

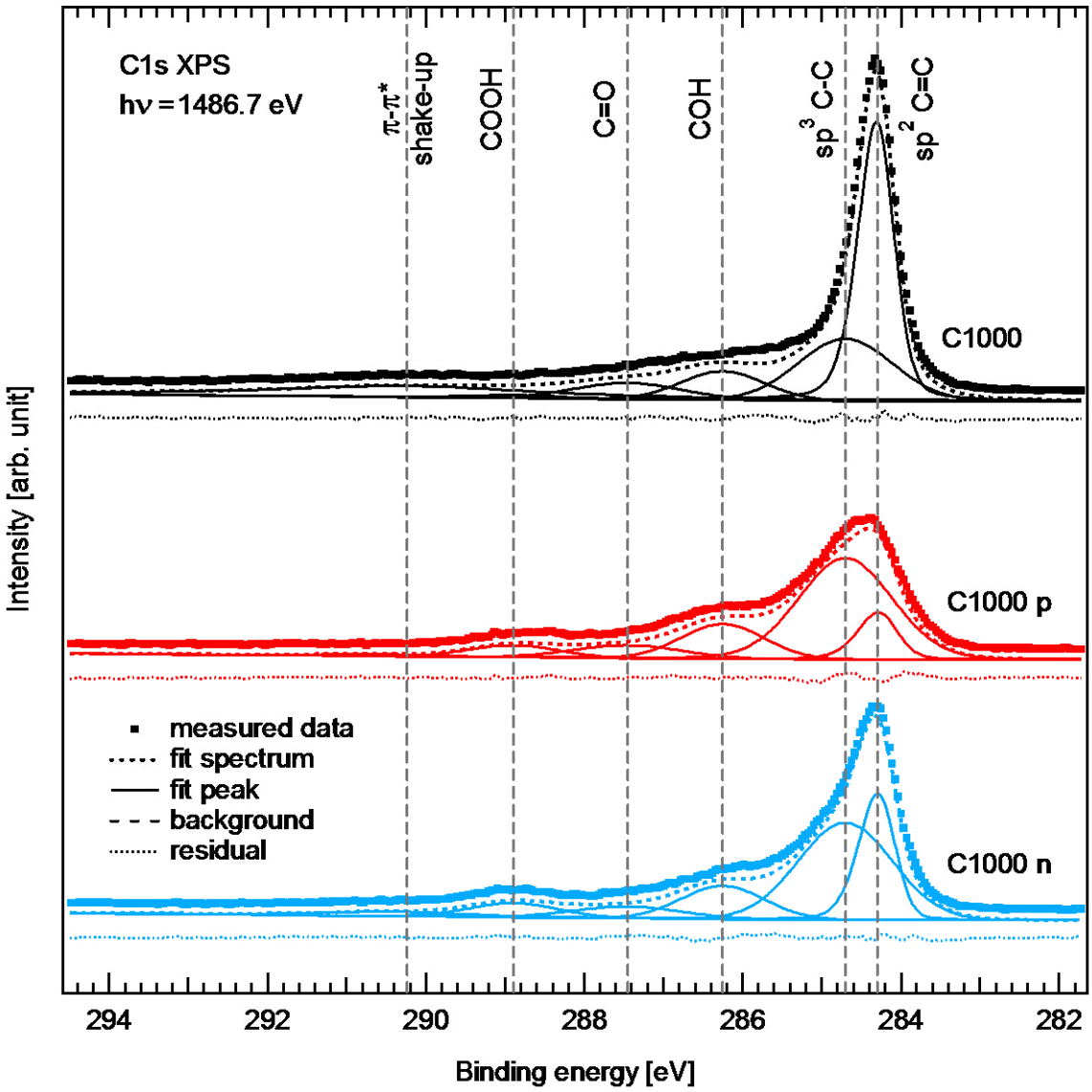

Figure 5. XP spectra of the carbon 1s region as measured for three carbon felts. From top to bottom the pristine sample felt after annealing (C1000), the felt from the positive (C1000 p), and from the negative half-cell (C1000 n). The spectra were decomposed into individual Tougaard-type backgrounds and the same chemically shifted carbon species indicated by dashed vertical lines. For the samples C1000 p and C1000 n the decrease of the low binding-energy peak assigned to sp^2 (C=C) carbon was accompanied by an increase of the sp^3 (C–C) carbon component. The high binding-energy peak assigned to the intrinsic π-π* shake-up process decreases along with the one assigned to sp^2 (C=C) carbon. The areas under the curves are smaller in C1000 p and C1000 n than in C1000. Graphs were given vertical offsets for clarity.

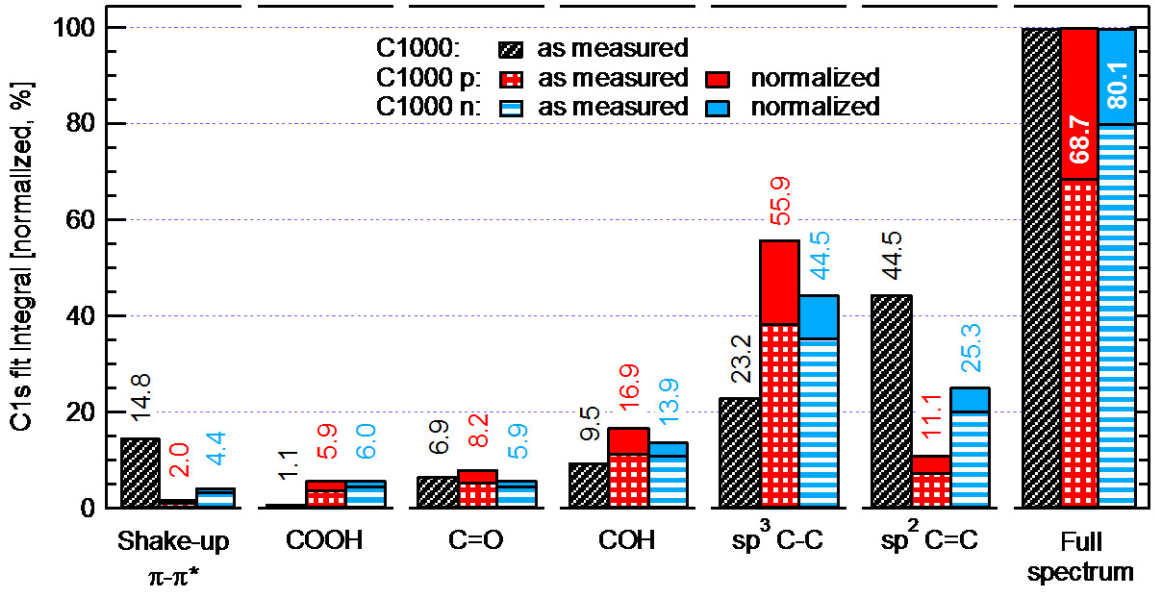

Figure 6. Bar diagram comparing the carbon 1s component fit integrals (cf. Figure 5). Components of the three samples are listed from left to right in order of decreasing binding energy. Numbers are given as percentages of the integral areas of the respective full spectra shown on the right. Patterned bars give the integrals from the spectra as measured, solid bars indicate the integrals after normalization to the full spectrum of C1000.

In the carbon XP spectrum of C1000 the main feature originates from conducting sp^2-hybridized species. Towards higher binding energies there is an ensuing tail of spectral features from sp^3-hybridized carbon material, oxidized carbon species – alcohols up to carboxylic acids –, and intrinsic π-π* shake-up processes taking place in the sp^2-hybridized carbon manifold [31]. These spectral components were all found in the spectra of C1000 p and C1000 n as well, but with different intensities leading to changes of the overall shapes of the spectra. The evaluation of the sample compositions are summarized in Figure 6. It is immediately apparent that the ratio between the sp^2 and sp^3 components has changed in both chemically aged electrode felts in favour of the latter. In case of C1000 p the sp^3 signal had clearly become the main feature, in C1000 n this effect is less pronounced. With the concomitant declines of the relative sp^2 peak areas in C1000 p and C1000 n to a quarter or ca. half that in C1000, respectively, also the π-π* shake-up features decreased compared to C1000. The hydroxyl (COH) and the carbonyl species (C=O) change more subtly, most prominently in roughly a doubling of the hydroxyl peak of C1000 p. The largest relative increase occurred for the peak assigned to carboxyl groups (COOH) which increased by nearly a factor of six in both cases. The measured total C 1s integral areas for the three samples were found to be not the same: Compared to C1000, the integral of the full fit spectrum of C1000 p was decreased to 68.7% and of C1000 n to 80.1%. In Figure 6 the peak integral areas are therefore depicted twice, as measured and also normalized to the full spectrum of C1000.

The oxygen 1s XP spectrum of C1000 in Figure 7 a)**Fehler! Verweisquelle konnte nicht gefunden werden.** is interpreted as a combination of two contributions, namely from singly (O–C) and doubly bonded (O=C) carbon-oxygen compounds. These components were much more prominently observed in C1000 p and C1000 n, with the carbonyl-oxygen (O=C) peak being most intense in C1000 p. For both chemically aged felts, weaker additional spectral intensities on the low-binding-energy side of the spectra were found. These additional signals are attributed to sulfur-oxide and vanadium-oxide species originating from the electrolyte. The component ratios for all the samples have been evaluated and are shown in Figure 7 a).

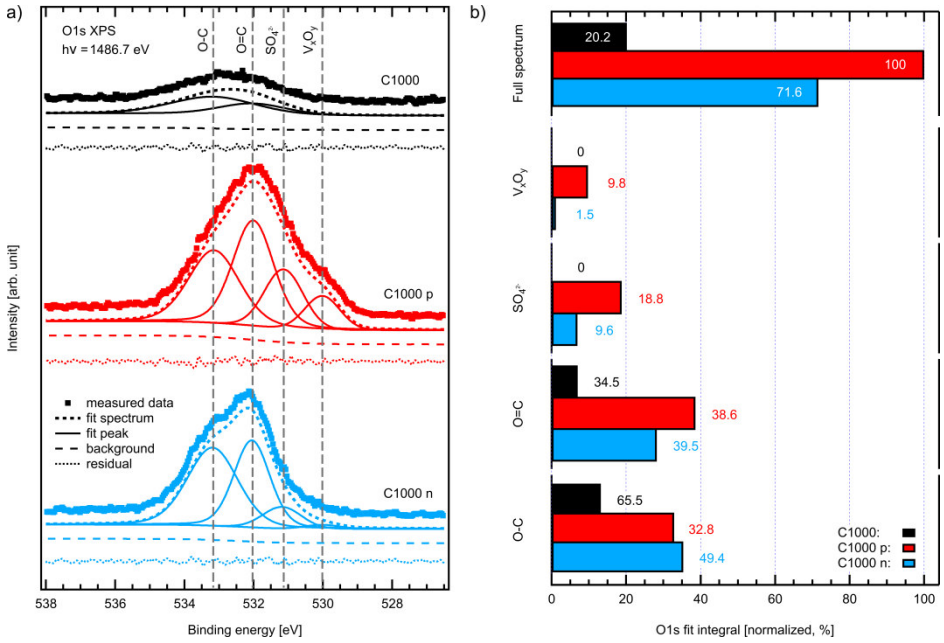

Figure 7: XP spectra of the oxygen 1s region as measured for all three samples.

- **a) From top to bottom the pristine felt after annealing (C1000), the felt from the positive (C1000 p), and from the negative half-cell (C1000 n). The spectra were decomposed into individual Shirley-type backgrounds and the chemically shifted oxygen species indicated by the dashed vertical lines. The peaks assigned to species containing vanadium and sulfur were only found in the samples C1000 p and C1000 n. Graphs were given vertical offsets for clarity**
- **b) Bar diagram comparing the oxygen 1s component fit integrals and the total spectral intensities (cf. Figure 7 a)), all normalized to the total integral of C1000 p. Components of the three samples are listed in order of increasing binding energy. The pristine felt (C1000) does not contain any measurable amounts of species containing sulfur or vanadium. Numbers for the spectral components are given as percentages of the integral areas of the respective full spectra shown at the top; in case of the full spectra, numbers represent the spectral areas relative to C1000 p as percentages.**

The carbon XP spectra revealed two concurrent effects of chemical aging: The sp^2-carbon content was decreased and the hydrocarbons in the felt material were oxidized. The observed strong increase of the carboxylic acid C 1s peak intensity in C1000 p and C1000 n is in agreement with the observations from the O 1s spectra. In Figure 8 the combined spectral intensity changes for the carbon-oxygen species in C 1s and O 1s XP spectra are compared with each other. For convenience the amounts have all been normalized to the pristine felt C1000. The increases in intensity are all expressed as multiples of the initial C1000 C 1s and O 1s intensities. Apparently for both, C1000 p and C1000 n, the increase in the O 1s spectra is roughly double that of the C 1s spectra: For C1000 p we find factors of ca. 1.8 and 3.5, for C1000 n of 1.5 and 3.2, respectively. This indicates that indeed the relative increase is mainly due to the full oxidation of carbon species to form carboxyl groups that contain one carbon atom and two oxygen atoms each. The relative changes for the other singly (COH) and doubly bonded (C=O) carbon oxygen species, are minor compared to this. Still also the observation of a larger relative C 1s increase of the carbonyl compounds (C=O) compared to the singly-bonded carbon-oxygen species (COH) in C1000 p in Figure 6 is in agreement with the observed larger increase of the O 1s carbonyl-oxygen peak (O=C) in Figure 7 b).

The overall decrease of intensity in the C 1s XP spectra of C1000 p and C1000 n could in part be due to a reduction of the sample material's volumetric mass density. A stronger influence, however, should have the formation of a hydrocarbon oxide layer covering the felts. This surface oxide layer, caused by the chemical aging, then additionally attenuates photoelectrons coming from deeper

inside the bulk of the felt material. Thus, the normalization of the C 1s spectral intensities to that of the pristine sample C1000, as shown in Figure 6, might well overestimate all the carbon-oxygen species. That is why instead of an evaluation of absolute amounts, a comparative evaluation of the relative intensities was chosen for the analysis.

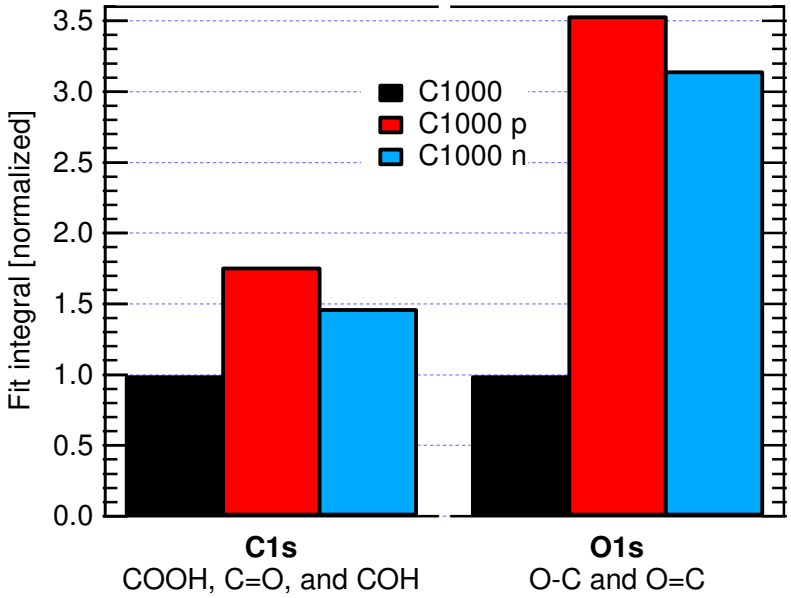

Figure 8. Bar-graph comparison of the summed-up carbon and oxygen 1s integral peak areas assigned to the carbon-oxygen moieties (cf. Figure 5 and Figure 7 a)). The integral areas were normalized to the respective spectra of the pristine felt (C1000) for easier comparison; for C1s the normalized areas from Figure 6 were used. The combined oxygen integrals increased each by about twice the factor of the combined carbon integrals for the felt samples from both half-cells.

XPS shows that in the felts from the positive and negative half-cells a large amount of the sp^2-hybridized carbon material has reacted to sp^3-hybridized carbon (cf. Figure 7 a)). The oxidation of a C=C bond can either result in two C-O bonds or one C-O and one C-H bond. This means that the increase of sp^3-hybridized carbon should never exceed the collective increase of oxygen functional groups on the carbon surface. Our results show that sp^3-hybridized carbon became the dominant species after the chemical aging experiment. One explanation could be the evolution of CO and CO_2, , which would decrease the oxygen signal in relation to the sp^3-hybridized carbon. The accumulation of sp^3-hybridized carbon would lead to an insulating, inactive surface and therefore to a loss of ECSA. The loss of carbon surface is supported by the results of the double layer capacity measurements in Figure 3 a) and Figure 4 b).

An important factor for the activity towards vanadium conversion in the negative half-cell is the concentration of carbonyl groups on the carbon surface because they are expected to catalyze the presumptive inner-sphere reaction.[32,33] The observed small decrease in carbonyl groups for C1000 n and the additional hydroxyl groups and carboxyl groups on the felt surface therefore inhibit the reactivity. The reaction in the positive half-cell on the other hand is considered to be an outer-sphere reaction, which is why it is not influenced by additional oxygen functional groups on the carbon surface [17].

Conclusion

Electroless chemical aging experiments show that the negative half-cell was strongly affected by mere contact with electrolyte. The experiments in pure sulfuric acid demonstrated, that the decrease of the double layer capacitance is not only dependent on the temperature, but also follows two rate constants. During the first 5 days the double layer capacitance decreased much stronger compared to the remaining 7-23 days. The inverse behavior was observed for the charge transfer resistances in diluted and concentrated V(III) electrolyte with 2 M sulfuric acid. The measurements in pure sulfuric acid and diluted V(III) electrolyte showed a temperature dependence indicating a chemical reaction of the sulfuric acid with the carbon felt surface. The measurements in concentrated V(III) electrolyte resulted in the highest aging rates, which were observed at room temperature indicating an interaction of vanadium with the carbon surface. The results from the 3-electrode beaker experiment were confirmed in a flow cell under realistic conditions for a VRFB. The absolute values for the double layer capacitance and the charge transfer resistance varied compared to the first experiments, but the observed aging rates were almost identical for the first 4-5 days.

The electrolyte-induced oxidation of the felts in both half-cells occurred as a pure chemical reaction because no significant potential was applied. XPS measurements revealed that both felts underwent similar changes of their surface. The oxygen functional groups increased by factors of 1.5 to 1.8 while the amounts of sp^2-hybridized carbon decreased to half or even a quarter. The concurrent disproportional increase of sp^3-hybridized carbon can be explained by CO and CO_2 evolution. The amount of carbonyl groups remained nearly constant in comparison to hydroxyl and carboxyl groups, which increased by factors of up to two and six, respectively.

Even though the positive electrode was much stronger oxidized during the chemical aging experiment, the positive half-cell did not show any significant loss of performance. This supports an outer-sphere mechanism for the positive half-cell. The performance of the negative half-cell on the other hand was strongly affected by the oxidation of the felt. This indicates an inner-sphere mechanism in the negative-half cell, as the cell reaction was either inhibited by the additional functional groups or simply became slower due to the loss of electrochemically active surface area. Therefore, the oxidation of the negative electrode needs to be prevented in order to maintain the performance. Improving the electrode material for the negative half-cell would thus be one of the most important tasks.

Acknowledgement

Support by the Deutsche Forschungsgemeinschaft, through collaborative research center Sonderforschungsbereich 658 - "Elementarprozesse in molekularen Schaltern an Oberflächen", is gratefully appreciated.

References

[1] G. Oriji, Y. Katayama, T. Miura, Investigation on V(IV)/V(V) species in a vanadium redox flow battery, Electrochimica Acta. 49 (2004) 3091–3095. doi:10.1016/j.electacta.2004.02.020.

[2] B. Sun, M. Skyllas-Kazacos, Modification of graphite electrode materials for vanadium redox flow battery application—I. Thermal treatment, Electrochimica Acta. 37 (1992) 1253–1260. doi:10.1016/0013-4686(92)85064-R.
[3] B. Sun, M. Skyllas-Kazacos, Chemical modification of graphite electrode materials for vanadium redox flow battery application—part II. Acid treatments, Electrochimica Acta. 37 (1992) 2459–2465. doi:10.1016/0013-4686(92)87084-D.
[4] X. Huang, Fabrication and Properties of Carbon Fibers, Materials. 2 (2009) 2369–2403. doi:10.3390/ma2042369.
[5] L. Joerissen, J. Garche, C. Fabjan, G. Tomazic, Possible use of vanadium redox-flow batteries for energy storage in small grids and stand-alone photovoltaic systems, J. Power Sources. 127 (2004) 98–104. doi:10.1016/j.jpowsour.2003.09.066.
[6] A.A. Shah, H. Al-Fetlawi, F.C. Walsh, Dynamic modelling of hydrogen evolution effects in the all-vanadium redox flow battery, Electrochimica Acta. 55 (2010) 1125–1139. doi:10.1016/j.electacta.2009.10.022.
[7] C.-N. Sun, F.M. Delnick, L. Baggetto, G.M. Veith, T.A. Zawodzinski, Hydrogen evolution at the negative electrode of the all-vanadium redox flow batteries, J. Power Sources. 248 (2014) 560–564. doi:10.1016/j.jpowsour.2013.09.125.
[8] I. Derr, M. Bruns, J. Langner, A. Fetyan, J. Melke, C. Roth, Degradation of all-vanadium redox flow batteries (VRFB) investigated by electrochemical impedance and X-ray photoelectron spectroscopy: Part 2 electrochemical degradation, J. Power Sources. 325 (2016) 351–359. doi:10.1016/j.jpowsour.2016.06.040.
[9] A.M. Pezeshki, R.L. Sacci, G.M. Veith, T.A. Zawodzinski, M.M. Mench, The Cell-in-Series Method: A Technique for Accelerated Electrode Degradation in Redox Flow Batteries, J. Electrochem. Soc. 163 (2016) A5202–A5210. doi:10.1149/2.0251601jes.
[10] P. Han, H. Wang, Z. Liu, X. Chen, W. Ma, J. Yao, Y. Zhu, G. Cui, Graphene oxide nanoplatelets as excellent electrochemical active materials for VO2+/ and V2+/V3+ redox couples for a vanadium redox flow battery, Carbon. 49 (2011) 693–700. doi:10.1016/j.carbon.2010.10.022.
[11] J. Melke, P. Jakes, J. Langner, L. Riekehr, U. Kunz, Z. Zhao-Karger, A. Nefedov, H. Sezen, C. Wöll, H. Ehrenberg, C. Roth, Carbon materials for the positive electrode in all-vanadium redox flow batteries, Carbon. 78 (2014) 220–230. doi:10.1016/j.carbon.2014.06.075.
[12] C.-N. Sun, F.M. Delnick, D.S. Aaron, A.B. Papandrew, M.M. Mench, T.A. Zawodzinski, Probing Electrode Losses in All-Vanadium Redox Flow Batteries with Impedance Spectroscopy, ECS Electrochem. Lett. 2 (2013) A43–A45. doi:10.1149/2.001305eel.
[13] J. Langner, J. Melke, H. Ehrenberg, C. Roth, Determination of Overpotentials in All Vanadium Redox Flow Batteries, ECS Trans. 58 (2014) 1–7. doi:10.1149/05837.0001ecst.
[14] T.-C. Chang, J.-P. Zhang, Y.-K. Fuh, Electrical, mechanical and morphological properties of compressed carbon felt electrodes in vanadium redox flow battery, J. Power Sources. 245 (2014) 66–75. doi:10.1016/j.jpowsour.2013.06.018.
[15] S.-K. Park, J. Shim, J.H. Yang, C.-S. Jin, B.S. Lee, Y.-S. Lee, K.-H. Shin, J.-D. Jeon, The influence of compressed carbon felt electrodes on the performance of a vanadium redox flow battery, Electrochimica Acta. 116 (2014) 447–452. doi:10.1016/j.electacta.2013.11.073.
[16] T. Sukkar, M. Skyllas-Kazacos, Water transfer behaviour across cation exchange membranes in the vanadium redox battery, J. Membr. Sci. 222 (2003) 235–247. doi:10.1016/S0376-7388(03)00309-0.
[17] H. Fink, J. Friedl, U. Stimming, Composition of the Electrode Determines Which Half-Cell's Rate Constant is Higher in a Vanadium Flow Battery, J. Phys. Chem. C. 120 (2016) 15893–15901. doi:10.1021/acs.jpcc.5b12098.
[18] B. Hirschorn, M.E. Orazem, B. Tribollet, V. Vivier, I. Frateur, M. Musiani, Determination of effective capacitance and film thickness from constant-phase-element parameters, Electrochimica Acta. 55 (2010) 6218–6227. doi:10.1016/j.electacta.2009.10.065.

[19] M.P. Seah, I.S. Gilmore, G. Beamson, XPS: binding energy calibration of electron spectrometers 5—re-evaluation of the reference energies, Surf. Interface Anal. 26 (1998) 642–649. doi:10.1002/(SICI)1096-9918(199808)26:9<642::AID-SIA408>3.0.CO;2-3.
[20] D.A. Shirley, High-Resolution X-Ray Photoemission Spectrum of the Valence Bands of Gold, Phys. Rev. B. 5 (1972) 4709–4714. doi:10.1103/PhysRevB.5.4709.
[21] S. Tougaard, Quantitative analysis of the inelastic background in surface electron spectroscopy, Surf. Interface Anal. 11 (1988) 453–472. doi:10.1002/sia.740110902.
[22] M. Repoux, Comparison of background removal methods for XPS, Surf. Interface Anal. 18 (1992) 567–570. doi:10.1002/sia.740180719.
[23] M. Schmid, H.-P. Steinrück, J.M. Gottfried, A new asymmetric Pseudo-Voigt function for more efficient fitting of XPS lines, Surf. Interface Anal. 46 (2014) 505–511. doi:10.1002/sia.5521.
[24] B. Satola, C.N. Kirchner, L. Komsiyska, G. Wittstock, Chemical Stability of Graphite-Polypropylene Bipolar Plates for the Vanadium Redox Flow Battery at Resting State, J. Electrochem. Soc. 163 (2016) A2318–A2325. doi:10.1149/2.0841610jes.
[25] H. Gerischer, An interpretation of the double layer capacity of graphite electrodes in relation to the density of states at the Fermi level, J. Phys. Chem. 89 (1985) 4249–4251. doi:10.1021/j100266a020.
[26] H. Gerischer, R. McIntyre, D. Scherson, W. Storck, Density of the electronic states of graphite: derivation from differential capacitance measurements, J. Phys. Chem. 91 (1987) 1930–1935. doi:10.1021/j100291a049.
[27] I.-T. Kim, M. Egashira, N. Yoshimoto, M. Morita, Effects of electrolytic composition on the electric double-layer capacitance at smooth-surface carbon electrodes in organic media, Electrochimica Acta. 55 (2010) 6632–6638. doi:10.1016/j.electacta.2010.06.011.
[28] M.A. Pope, I.A. Aksay, Four-Fold Increase in the Intrinsic Capacitance of Graphene through Functionalization and Lattice Disorder, J. Phys. Chem. C. 119 (2015) 20369–20378. doi:10.1021/acs.jpcc.5b07521.
[29] C.-T. Hsieh, H. Teng, Influence of oxygen treatment on electric double-layer capacitance of activated carbon fabrics, Carbon. 40 (2002) 667–674. doi:10.1016/S0008-6223(01)00182-8.
[30] J. Friedl, C.M. Bauer, A. Rinaldi, U. Stimming, Electron transfer kinetics of the – Reaction on multi-walled carbon nanotubes, Carbon. 63 (2013) 228–239. doi:10.1016/j.carbon.2013.06.076.
[31] M. Filippi, L. Calliari, Measuring the energy of the graphite π + σ plasmon peak, Surf. Interface Anal. 38 (2006) 595–598. doi:10.1002/sia.2221.
[32] P. Chen, M.A. Fryling, R.L. McCreery, Electron Transfer Kinetics at Modified Carbon Electrode Surfaces: The Role of Specific Surface Sites, Anal. Chem. 67 (1995) 3115–3122. doi:10.1021/ac00114a004.
[33] R.L.M. Peihong Chen, Control of Electron Transfer Kinetics at Glassy Carbon Electrodes by Specific Surface Modification, Anal. Chem. 68 (1996). doi:10.1021/ac960492r.
[34] C.D. Wagner, L.E. Davis, M.V. Zeller, J.A. Taylor, R.H. Raymond, L.H. Gale, Empirical atomic sensitivity factors for quantitative analysis by electron spectroscopy for chemical analysis, Surf. Interface Anal. 3 (1981) 211–225. doi:10.1002/sia.740030506.

Supporting Online Material

Detailed measurements for C1000 p and C1000 n of the sulfur 2p region revealed (cf. Figure 9) weak spin-orbit split doublets shifted to higher binding energy compared to elemental sulfur. C1000 p contains more than double the amount of sulfur found for C1000 n; in the pristine C1000 no sulfur has been observed.

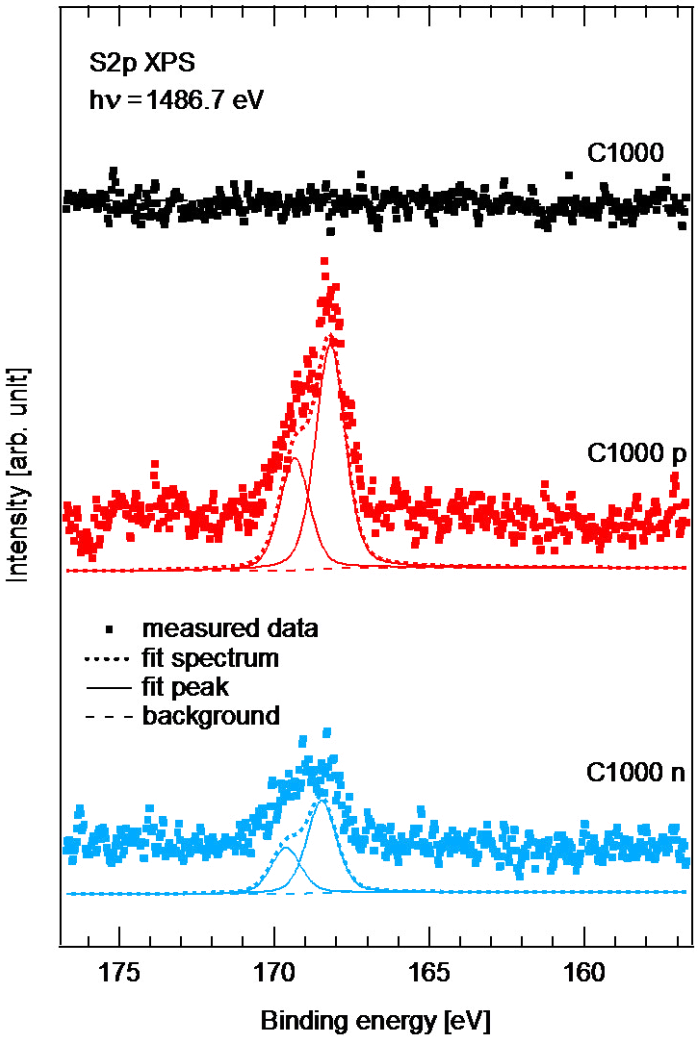

Figure 9. XP spectra of the sulfur 2p region measured for all three samples, from top to bottom the pristine felt after annealing (C1000), the felt from the positive (C1000 p), and from the negative half-cell (CAp n). The intensities are very low (cf. survey spectra in Figure 11). There is no signal intensity in the region of elementary sulfur (ca. 163 eV to 165 eV) in case of the pristine felt there is no sulfur signal observed at all.

The comparison of the absolute sulfur 2p XP spectra with the oxygen 1s peaks assigned to sulfur oxides (cf. Figure 10) suggests that the sulfur oxide species observed in both, C1000 p and C1000 n, contains ca. four times as much oxygen as sulfur and therefore is due to sulfate (SO_4^-) ions from the sulfuric acid electrolyte solution.

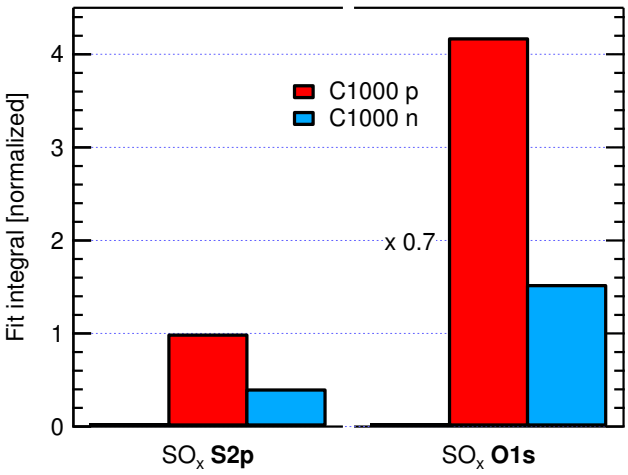

Figure 10. Comparison of XPS fit-peak integrals for the sulfur 2p region and of the spectral component ascribed to SO_x in the oxygen 1s region. The integrals are all normalized on the C1000 p S 2p integral. In addition the O 1s integrals have been multiplied by 0.7, the ratio of tabulated relative sensitivity factors (RSF) of sulfur and oxygen [34], rounded to one decimal digit (to account for instrumental discrepancies[1]).

[1] Instrumental discrepancies are on the order of 12% and 11% for 1s and 2p spectra, respectively [34]

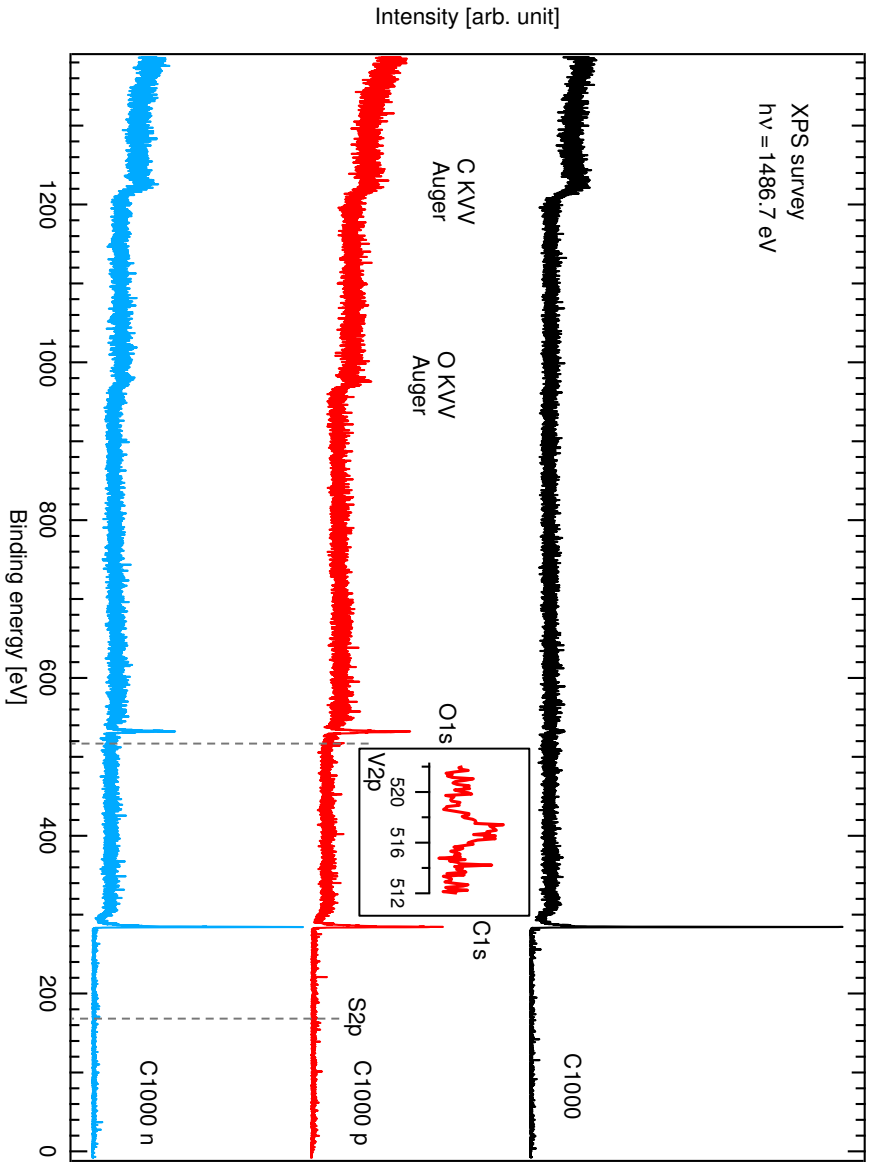

Figure 11. XP survey spectra measured for three carbon felts, from top to bottom the pristine sample after annealing (C1000), the felt from the positive (C1000 p), and from the negative half-cell (CAp n). The very weak signals due to the vanadium and sulfur 2p levels are indicated by dashed lines. Additional lines for these species were too weak to be observed. No further elemental species have been found.

Electrochemical analysis of the performance loss in all vanadium redox flow batteries using different cut-off voltages

Abstract

The performance loss observed in vanadium redox flow batteries over time strongly depends on the material and the cycling conditions. We have chosen 1.65 V and 1.8 V as the cut-off voltages in order to compare the performance loss and the risk of evolving hydrogen on the negative side and CO_2 on the positive side. The 1.8 V experiment was expected to show stronger degradation because of the higher risk of hydrogen and CO_2 evolution due to the higher maximum half-cell potentials. To address this issue we implemented a reference electrode at the inlet of the negative half-cell of a 10 cm^2 test cell. The discharge process on the negative half-cell was assumed to be the process with the highest overpotential after running 50 charge and discharge cycles. After 50 cycles the reduction of V(II) remained the favored reaction compared to the HER in the negative side, even though the overpotentials for both reactions increased significantly. As for the positive half-cell, the risk of CO_2 evolution increased with increasing cut-off voltage. The higher cut-off voltage led to a higher rate of degradation, but it also showed a better overall performance. The potentials in the half-cells were changing dynamically with each cycle depending on the degradation rate of the electrode and the state of the electrolyte. An imbalance of the electrolyte could be observed by measuring the half-cell open circuit potential after each charge and discharge process. The obtained results can be used for the diagnostics and optimization of VRFB systems in order to achieve maximum system output at reasonable risks of parasitic reactions and degradation.

Reference:

I. Derr, A. Fetyan, K. Schutjajew, C. Roth, Electrochemical analysis of the performance loss in all vanadium redox flow batteries using different cut-off voltages, Electrochim. Acta 224 (2017) 9–16, doi:10.1016/j.electacta.2016.12.043.

https://doi.org/10.1016/j.electacta.2016.12.043